comptes rendus palevol

2026 • 25 • 12

New associated postcranial remains from the Shungura Formation (Lower Omo Valley, Ethiopia) provide insights on behaviors and ecology of early *Homo*

Alicia BLASI-TOCCACCELI, Guillaume DAVER, Tiphaine BRUSSE, Tea JASHASHVILI, Jean-Luc VOISIN, Laurent PALLAS, Mathieu DOMALAIN, Jérôme SURAULT, Blade Engda REDAE & Jean-Renaud BOISSERIE

GLIMPSES OF A PLIO-PLEISTOCENE AFRICAN ECOSYSTEM: THE LOWER OMO VALLEY, ETHIOPIA

Edited by Jean-Renaud BOISSERIE, Aurélien MOUNIER, Blade Engda REDAE & Mathieu SCHUSTER

art. 25 (12) — Published on 8 July 2026
www.cr-palevol.fr

PUBLICATIONS SCIENTIFIQUES

MUSÉUM NAL HIST NATURELLE

Couverture / Cover :
Made from the Figures of the article.

Comptes Rendus Palevol est indexé dans / Comptes Rendus Palevol *is indexed by:*
– Cambridge Scientific Abstracts
– Current Contents® Physical
– Chemical, and Earth Sciences®
– ISI Alerting Services®
– Geoabstracts, Geobase, Georef, Inspec, Pascal
– Science Citation Index®, Science Citation Index Expanded®
– Scopus®.

Les articles ainsi que les nouveautés nomenclaturales publiés dans *Comptes Rendus Palevol* sont référencés par / *Articles and nomenclatural novelties published in* Comptes Rendus Palevol *are registered on:*
– ZooBank® (http://zoobank.org)

Comptes Rendus Palevol est une revue en flux continu publiée par les Publications scientifiques du Muséum, Paris et l'Académie des sciences, Paris
Comptes Rendus Palevol *is a fast track journal published by the Museum Science Press, Paris and the Académie des sciences, Paris*

Les Publications scientifiques du Muséum publient aussi / *The Museum Science Press also publish:*
Adansonia, ***Geodiversitas***, ***Zoosystema***, ***Anthropozoologica***, ***European Journal of Taxonomy***, ***Naturae***, ***Cryptogamie*** **sous-sections** ***Algologie***, ***Bryologie***, ***Mycologie***.

L'Académie des sciences publie aussi / *The Académie des sciences also publishes:*
Comptes Rendus Mathématique, Comptes Rendus Physique, Comptes Rendus Mécanique, Comptes Rendus Chimie, Comptes Rendus Géoscience, Comptes Rendus Biologies.

Diffusion – Publications scientifiques Muséum national d'Histoire naturelle
CP 41 – 57 rue Cuvier F-75231 Paris cedex 05 (France)
Tél. : 33 (0)1 40 79 48 05 / Fax : 33 (0)1 40 79 38 40
diff.pub@mnhn.fr / https://sciencepress.mnhn.fr

Académie des sciences, Institut de France, 23 quai de Conti, 75006 Paris.

ISSN (imprimé / *print*) : 1631-0683/ ISSN (électronique / *electronic*) : 1777-571X

New associated postcranial remains from the Shungura Formation (Lower Omo Valley, Ethiopia) provide insights on behaviors and ecology of early *Homo*

Alicia BLASI-TOCCACCELI
Laboratoire Paléontologie Evolution Paléoécosystèmes Paléoprimatologie (PALEVOPRIM),
Université de Poitiers & CNRS, 6 rue Michel Brunet, 86000 Poitiers (France)
and Department of Anatomy, Midwestern University,
Glendale, 19555 N 59th Ave, Glendale, AZ 85308 (United States)
aliciablasit@gmail.com (corresponding author)

Guillaume DAVER
Tiphaine BRUSSE
Laboratoire Paléontologie Evolution Paléoécosystèmes Paléoprimatologie (PALEVOPRIM),
Université de Poitiers & CNRS, 6 rue Michel Brunet, 86000 Poitiers (France)
guillaume.daver@univ-poitiers.fr

Tea JASHASHVILI
Division of Integrative Anatomical Sciences and Department of Radiology,
Keck School of Medicine, University of Southern California,
1975 Zonal Ave, Los Angeles, CA 90033 (United States)
and Department of Geology and Paleontology,
Georgian National Museum, 3 Shota Rustaveli Ave,
Tbilisi 0105 (Georgia)
tea.jashashvili@usc.edu

Jean-Luc VOISIN
Aix Marseille Université, CNRS, EFS, ADES,
58 Boulevard Charles Livon, 13007 Marseille (France)
jeanlucvoisin2004@yahoo.fr

Laurent PALLAS
Laboratoire Paléontologie Evolution Paléoécosystèmes Paléoprimatologie (PALEVOPRIM),
Université de Poitiers & CNRS, 6 rue Michel Brunet, 86000 Poitiers (France)
and Kyoto University, Graduate School of Science, Laboratory of Physical Anthropology,
Yoshidahonmachi, Sakyo Ward, Kyoto 606-8501 (Japan)
and Histoire Naturelle des Humanités Préhistoriques (HNHP), MNHN/CNRS/UPVD,
17 Place du Trocadéro et du 11 Novembre, 75116 Paris (France)
laurent.pallas@mnhn.fr

Mathieu DOMALAIN
Institut PPrime CNRS, École Normale Supérieure de Mécanique et Aérotechnique (ENSMA),
Université de Poitiers, 2 Boulevard des Frères Lumière,
86360 Chasseneuil-du-Poitou (France)
mathieu.domalain@creps-poitiers.sports.gouv.fr

Jérôme SURAULT
Laboratoire Paléontologie Evolution Paléoécosystèmes Paléoprimatologie (PALEVOPRIM),
Université de Poitiers & CNRS, 6 rue Michel Brunet, 86000 Poitiers (France)
jerome.surault@univ-poitiers.fr

Blade Engda REDAE
Institute of Human Origin, School of Human Evolution and Social Change, Arizona State University, 900 S Cady Mall, Tempe, AZ 85281 (United States)
and Laboratoire Paléontologie Evolution Paléoécosystèmes Paléoprimatologie (PALEVOPRIM), Université de Poitiers & CNRS, 6 rue Michel Brunet, 86000 Poitiers (France)
and French Center for Ethiopian Studies, CNRS, Ministry of Europe and Foreign Affairs, Addis Ababa, PO BOX 5554 (Ethiopia)
bredae@asu.edu

Jean-Renaud BOISSERIE
French Center for Ethiopian Studies, CNRS, Ministry of Europe and Foreign Affairs, Addis Ababa, PO BOX 5554 (Ethiopia)
and Laboratoire Paléontologie Evolution Paléoécosystèmes Paléoprimatologie (PALEVOPRIM), CNRS & Université de Poitiers, 6 rue Michel Brunet, 86000 Poitiers (France)
jean.renaud.boisserie@univ-poitiers.fr

Submitted on 2 February 2026 | Accepted on 2 March 2026 | Published on 8 July 2026

urn:lsid:zoobank.org:pub:6542A9B5-DD38-4729-98CB-81C6A167B2B7

Blasi-Toccacceli A., Daver G., Brusse T., Jashashvili T., Voisin J.-L., Pallas L., Domalain M., Surault J., Redae B. E. & Boisserie J.-R. 2026. — New associated postcranial remains from the Shungura Formation (Lower Omo Valley, Ethiopia) provide insights on behaviors and ecology of early *Homo*, *in* Boisserie J.-R., Mounier A., Redae B. E. & Schuster M. (eds), Glimpses of a Plio-Pleistocene African ecosystem: the Lower Omo Valley, Ethiopia. *Comptes Rendus Palevol* 25 (12): 207-247. https://doi.org/10.5852/cr-palevol2026v25a12

ABSTRACT
The genus *Homo* is hypothesized to have ecologically diverged from australopiths (*Australopithecus* and *Paranthropus*) between 2.8 and 1.9 Ma. Compared to australopiths, the behavioral repertoire of *Homo* would be characterized by long distance walking and endurance running, but also by a significant reduction or complete absence of arboreal locomotion and an increase of dexterous activities (throwing, manipulation, load carrying). However, testing these two last hypotheses has been largely constrained by the scarcity of associated fossil remains with varying preservation and different ontogenetic stages. This study presents new adult postcranial remains assigned to a single individual OMO VE 3-10063 from the Shungura Formation (Lower Omo Valley, Ethiopia) and dated to about 1.84 Ma. These remains comprise a subcomplete shoulder and arm, and two vertebral and one rib fragments. Comparative analyses with extant non-human apes, extant humans and Plio-Pleistocene hominins using linear and angular measurements, and geometric morphometrics indicate that OMO VE 3-10063 is taxonomically and functionally closer to *Homo* than to australopiths. It makes this shoulder complex the oldest and best-preserved reliably assigned to this genus. This partial skeleton indicates that *Homo* had already reduced functions of the forelimb related to arboreal locomotion as early as 1.8 Ma, notably with a glenoid surface of the scapula less cranially-oriented than in African apes, an elbow with a shallow trochlear notch, and a clavicle suggesting that loads applied on the forelimb of the individual were similar to those of extant humans. Furthermore, we propose that the morphology observed in OMO VE 3-10063 is consistent with habitual terrestrial bipedalism and increased dexterous activities relative to australopiths.

KEY WORDS
Plio-Pleistocene,
shoulder,
locomotion,
dexterity,
ecological divergence.

RÉSUMÉ
Nouveaux restes postcrâniens associés de la formation de Shungura (basse vallée de l'Omo, Éthiopie) : indices sur les comportements et l'écologie des premiers représentants du genre Homo.
Le genre *Homo* aurait divergé écologiquement des australopithèques (*Australopithecus* et *Paranthropus*) entre 2,8 et 1,9 Ma. En comparaison des australopithèques, le répertoire comportemental d'*Homo* serait caractérisé non seulement par de la marche bipède sur longues distances et de la course d'endurance, mais également par une réduction, voire une absence, de la locomotion arboricole et une augmentation des activités de dextérité (lancer, manipulation, porté de charge). Toutefois, tester ces deux dernières hypothèses restait jusqu'à présent difficile en raison de la rareté des restes associés, de la variabilité de leurs états de préservation et des différences de stade ontogénétique. Cette étude présente de nouveaux restes postcrâniens assignés à l'individu adulte OMO VE 3-10063 provenant de la Formation de Shungura (basse vallée de l'Omo, Éthiopie) et datés à environ 1,84 Ma.

Ces restes comprennent une épaule et un bras subcomplets, ainsi que les fragments de deux vertèbres et d'une côte. Les comparaisons avec des grands singes non-humans actuels, d'humains actuels et des homininés fossiles Plio-Pléistocène en utilisant des mesures linéaires et angulaires et la morphométrie géométrique montrent que OMO VE 3-10063 est taxonomiquement et fonctionnellement plus proche d'*Homo* que des australopithèques. Cela en fait ainsi l'épaule la plus ancienne et la mieux préservée attribuée à ce genre. Ce squelette partiel indique que les représentants du genre *Homo* présentaient dès 1.8 Ma des aptitudes locomotrices arboricoles limitées, notamment avec une surface glénoïde de la scapula moins crânialement orientée que chez les grands singes africains, un coude avec trochlée peu profonde et une morphologie de la clavicule qui suggère que les forces qui se sont exercées sur le membre supérieur de cet individu étaient similaires à celles des humains actuels. Finalement, nous formulons l'hypothèse que les nouveaux restes postcrâniens d'OMO VE 3 sont cohérents avec la pratique d'activités de dextérité accrues et d'une bipédie terrestre habituelle par rapport aux australopithèques.

MOTS CLÉS
Plio-Pléistocène,
épaule,
locomotion,
dextérité,
divergence écologique.

INTRODUCTION

The anatomical divergence of *Homo* Linnaeus, 1758 from australopiths (*Australopithecus* Dart, 1925 and *Paranthropus* Broom, 1938) is estimated to have occurred between 2.8 Ma and 1.9 Ma in Africa (Kimbel *et al.* 1996; Bramble & Lieberman 2004; Prat *et al.* 2005; Lordkipanidze *et al.* 2007; Pontzer *et al.* 2010; Roach *et al.* 2013; Villmoare *et al.* 2015; Yegian *et al.* 2021; Hammond *et al.* 2021). This divergence could be explained by ecological settings (Wood & Strait 2004; Wood & Constantino 2007; Balter *et al.* 2012; Martin *et al.* 2020). The postcranial morphology in *Homo,* especially that of its earliest representatives, would be adapted for long-distance walking and endurance running as compared to other fossil hominins (Bramble & Lieberman 2004; Yegian *et al.* 2021). *Homo erectus* is defined here following Rightmire (2001), who proposed lumping *H. ergaster*, the specimens from Dmanisi (defined later as *H. georgicus*), and eastern Asian *H. erectus.* The early members of *Homo* also appear to have abilities for different dexterous behaviors. Dexterous behaviors refer here to all the non-positional behaviors (Prost 1965), which include throwing or high-speed throwing (Fifer 1987; Roach *et al.* 2013), refined manipulatory abilities e.g., precision grasping (Karakostis *et al.* 2021), and load carrying (Wang & Crompton 2004). However, the extent to which each of these behaviors is a critical component of the ecological niche of *Homo* is still a matter of debate (Larson 2007; Skinner *et al.* 2015; Pobiner 2020; Karakostis *et al.* 2021), notably because of lack of consensus regarding the functional morphology of the forelimb in the earliest members of *Homo*.

Indeed, the human fossil record between 2.8 and 1.9 Ma shows taxonomic diversity (*Australopithecus*, *Paranthropus* and *Homo*) accompanied by contrasting morphologies of the forelimb (Walker & Leakey 1993; Larson 2007, 2009, 2013; Lordkipanidze *et al.* 2007; Harmon 2013; Churchill *et al.* 2013; Ward 2015; Roach & Richmond 2015; Richmond *et al.* 2020). However, these observations are supported by a limited number of individuals with varying preservation and ontogenetic stages. Among the three earliest subcomplete shoulders and forelimbs assigned to *Homo*, only one is attributed to an adult individual (Lordkipanidze *et al.* 2007). These remains were found in Dmanisi, Georgia (i.e., one adult individual and one subadult individual, represented by the specimens D4166/D4162/D4161/D4507), dated to approximately 1.77 Ma (Lordkipanidze *et al.* 2007; McDougall *et al.* 2012), and were described as mostly primitive (i.e., closer to the australopith condition than to the *Homo* condition; Lordkipanidze *et al.* 2007). The early African *H. erectus* represented by only one subadult individual (KNM-WT 15000; Walker & Leakey 1993), dated to around 1.47 Ma (McDougall *et al.* 2012), and described as having more derived shoulder morphology relative to that of the Dmanisi specimens (Larson 2007). In particular, fossil specimens of *Homo* from Africa and Europe, along with extant *Homo*, exhibit humeral trochleae that are less prominently keeled compared to those of australopiths, as well as increased scapular-neck breadths (Green *et al.* 2018). Early *Homo* and australopiths are also united by their lower degrees of humeral torsion compared to extant *Homo* (Larson 2007). Finally, australopiths and the *Homo* specimen from Dmanisi share more cranially oriented scapular glenoid fossae, in contrast to African *H. erectus* and extant *Homo*, which present more horizontally oriented glenoid fossae. Based on the morphology of subadult African *H. erectus* and other isolated specimens, increased frequency of activities involving manipulation such as stone tool manufacture and use could explain the morphological differences between australopiths and early *H. erectus* (Larson 2007). Alternatively, some authors hypothesized that long-distance walking, endurance running and high-speed throwing capabilities emerged in Africa at around 2 Ma and may have facilitated the dispersal of *Homo* to Eurasia (Bramble & Lieberman 2004; Roach *et al.* 2013). Nonetheless, despite being characterized by a derived lower limb adapted for long-distance walking and running (Lordkipanidze *et al.* 2007; Pontzer *et al.* 2010), the primitive forelimbs of the Dmanisi specimens contrasts with the configuration associated with high-speed throwing capabilities (Lordkipanidze *et al.* 2007). In addition, the proposed high-speed throwing capabilities of early African *H. erectus* have been questioned, particularly due to indications that the clavicle may have been too short (Larson 2007). Therefore, the morphology of early *Homo* and its functional interpretation are still unclear due to a lack of associated adult fossil shoulder and forelimb remains.

Here we describe new associated postcranial remains from the locality OMO VE 3, Member H of the Shungura Formation (Lower Omo Valley, southwestern Ethiopia) discovered by the Omo Group Research Expedition (OGRE). The individual is radiochronologically dated to 1.843 ± 0.023 Ma (McDougall & Brown 2006; see Appendices 1; 2). OMO VE 3-10063 preserves a relatively complete right humerus, a partial right scapula, a partial right clavicle, two cervical vertebrae, most probably C6 and C7, and one rib of uncertain position (Fig. 1; the details of the description of each element can be found in Appendix 1(see "Description of OMO VE 3-10063") and linear measurements in Appendix 3). We compared the morphology of this new individual with extant hominids and Plio-Pleistocene hominins using linear distances, angles, and geometric morphometrics with two objectives: 1) propose a taxonomic attribution; and 2) make a functional analysis of the shoulder. Based on the dating and location of OMO VE 3-10063, we expected the specimen to be attributable to either *Homo* or *Paranthropus*. The morphology of the distal humeral cross-section is particularly informative for taxonomic distinction between *Homo* and *Paranthropus* (Lague 2015), whereas additional features of the shoulder and forelimb were used either to corroborate the taxonomic inference or to explore the functional implications for the upper limb of the OMO VE 3 individual.

MATERIAL AND METHODS

OMO VE 3-10063

The geological context and complete descriptions of each specimen from OMO VE 3-10063 are available in Appendix 1 (see "Description of OMO VE 3-10063"). The humerus (OMO VE 3-10063a) is essentially complete, although it is preserved in three refitting fragments and the humeral head is significantly eroded. This fossil represents the best-preserved hominin humerus older than the Middle Pleistocene. The scapula (OMO VE 3-10063b) consists mostly of the lateral part, including the glenoid fossa, the lateralmost portion of the spine and acromion, the coracoid process, and part of the axillary border. The acromial part of the clavicle (OMO VE 3-10063c) is mostly preserved, although it consists of four fragments and its distal end is eroded. The two vertebral fragments (OMO VE 3-10063d and e) consist of an incomplete neural arc and a centrum of two cervical vertebrae. The rib fragment (OMO VE 3-10063f) consists of three refitting elements. The shoulder will be the focus of this study due to its exceptional preservation. OMO VE 3-10063 is curated at the Ethiopian Heritage Authority (EHA) in Addis Ababa, Ethiopia.

Comparative samples

Comparative samples acquired for this study consist of extant hominoids (*Homo sapiens*, *Pan troglodytes, Pan paniscus, Gorilla beringei ,* and *Pongo abelii*; Appendix 4), and fossil hominins ranging from the Pliocene to the Pleistocene, including *Australopithecus* spp., *Paranthropus* spp., and *Homo* spp. (Appendix 5). For the analysis of the outline shape of the distal humeral diaphysis, the distal trochlear angle of the humerus, and the glenoid shape analysis, we acquired three-dimensional (3D)-data on original material or used available 3D-models for extant hominoids and fossil hominins (details in Appendices 4; 5). For the other analyses, we used published linear and angular data when available. We did not consider KNM-ER 47000A for the pillar-glenoid angle because the specimen is fragmented and, according to Green *et al.* (2018: 182) only "conjoin at a small contact area" (Green *et al.* 2018), leading to uncertainty when measuring this angle (see "Material and Methods" section, subheading "Angular measurements"). The comparative sample of extant humeri and scapulae comes from adult individuals (i.e., with fused epiphyses) with no external sign of pathology. For *H. sapiens*, we favored protohistoric populations from a broad geographic range including North America, Europe, Africa, and North Asia. Regarding non-human hominids, wild-caught individuals were preferred.

For the analysis of the outline shape of the distal humerus, comparative sections were taken from 3D-models from $n = 71$ extant specimens, including *H. sapiens* ($n = 15$), *P. troglodytes* ($n = 15$), *P. paniscus* ($n = 10$), *G. beringei* ($n = 15$), and *P. abelii* ($n = 14$), and $n = 14$ fossil hominins (Appendices 4; 5). Fossil specimens with missing parts were not included in the analysis to ensure that all landmarks could be placed.

Comparative values for the distal trochlear angle of the humerus were measured on 3D-models of $n = 51$ extant specimens that include *H. sapiens* ($n = 12$), *P. troglodytes* ($n = 15$), *G. beringei* ($n = 10$), and *P. abelii* ($n = 14$; Appendix 4), and $n = 18$ fossil hominins (Appendix 5). Some fossil specimens were excluded from the analysis due to their preservation.

For the glenoid shape analysis, the extant comparative sample consisted of n = 86 hominoids, including *H. sapiens* (n = 20), *P. troglodytes* (n = 20), *P. paniscus* (n = 13), *Gorilla* spp. Geoffroy, 1852 (n = 19 *G. beringei* and n = 1 *G. gorilla* Savage, 1847), and *P. pygmaeus* Linnaeus, 1760 (n = 13; Appendix 4). The fossil comparative sample included Plio-Pleistocene specimens (n = 6; Appendix 5). Fossil specimens with missing parts were not included in the analysis to ensure that all landmarks could be placed. KNM-ER 47000 was not included because we were unable to access the specimen. While the glenoid of Sts 7 exhibits erosion along its dorsal border, we included the specimen in the analysis without reconstruction, as it does not appear to significantly impact its distinctive narrow shape (Senut 1981).

As for the humeral torsion angles, pillar-glenoid angles, scapular neck breadths, coracoid lengths, clavicle lengths, and clavicle curvatures, values were mainly taken from the literature for extant and fossil specimens (see Appendices 4; 5). We measured the humeral torsion only for MH2, KNM-ER 739 and KNM-WT 15000 on 3D-humeral models.

3D-acquisition

Micro-CT scans of the original fossil material OMO VE 3-10063 were performed by Tomohiko Sasaki and Gen Suwa with X-ray microtomography, SkyScan 1173, at 130 kV, 40 µA, with a voxel size of 100 µm (University of Tokyo Museum, Tokyo, Japan).

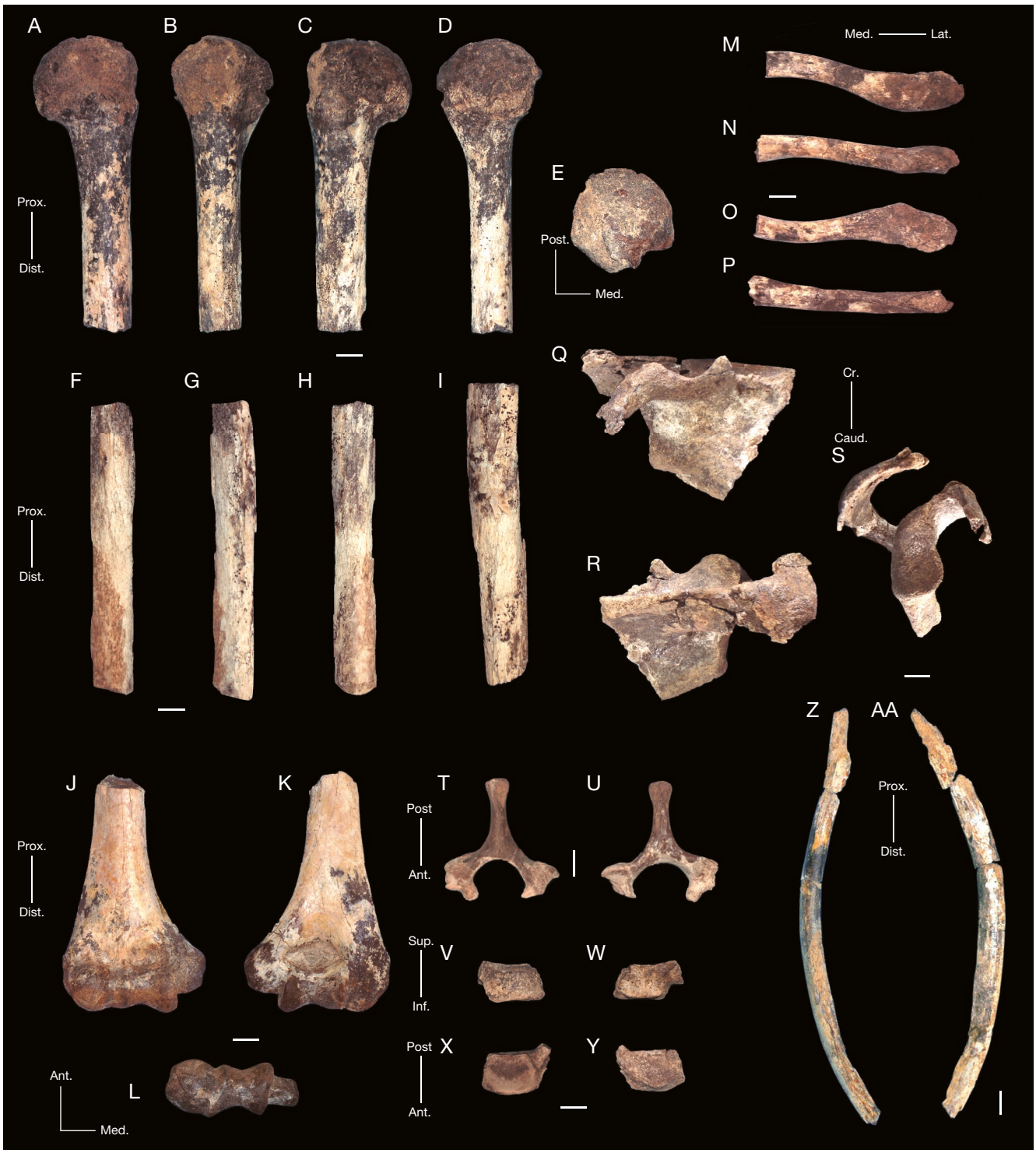

FIG. 1. — Views of OMO VE 3-10063: **A**-**E**, humerus OMO VE 3-10063a, proximal portion: **A**, lateral; **B**, anterior; **C**, medial, **D**, posterior; **E**, proximal; **F**-**I**, humerus OMO VE 3-10063a, diaphysis: **F**, lateral; **G**, anterior; **H**, medial; **I**, posterior; **J**-**L**, humerus OMO VE 3-10063a, distal portion: **J**, anterior; **K**, posterior; **L**, distal; **M**-**P**, clavicle OMO VE 3-10063c: **M**, proximal; **N**, posterior; **O**, distal; **P**, anterior; **Q**-**S**, scapula OMO-VE 3-10063b: **Q**, anterior; **R**, posterior; **S**, lateral; **T**, **U**, cervical neural arch OMO VE 3-10063d: **T**, superior; **U**, inferior; **V**-**Y**, cervical body OMO VE 3-10063e: **V**, anterior; **W**, posterior; **X**, inferior; **Y**, superior; **Z**, **AA**, rib OMO VE 3-10063f: **Z**, superior; **AA**, inferior. See the detailed description of the individual in the Appendices 1 ("Description of OMO VE 3-10063"]; 3. Abbreviations: **Ant.**, anterior; **Dist.**, distal; **Lat.**, lateral; **Med.**, medial; **Post.**, posterior; **Prox.**, proximal. Scale bars: 10 mm.

3D-surfaces were generated using Avizo Standard Edition v7.0 (Thermo Fischer Scientific). The three fragments of the humerus of OMO VE 3-10063 were reassembled. After extracting surfaces with Avizo, the 3D-models were decimated, realigned, and manually repositioned relative to each other using Geomagic (Geomagic Wrap 2021, 3D Systems).

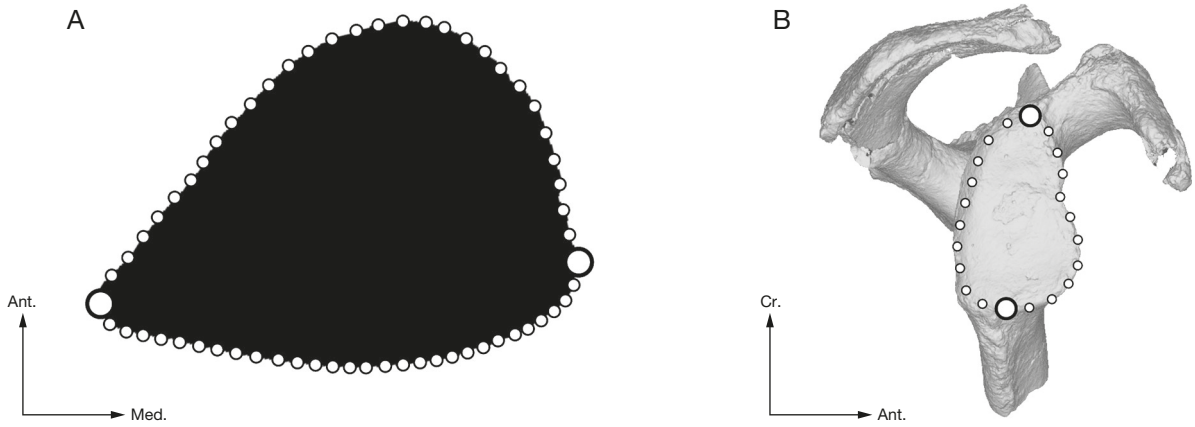

Fig. 2. — Landmark sets for the geometric morphometrics analyses: **A**, cranial view of the cross-section of the distal humerus at about 19% of the total length of the humerus of OMO VE 3-10063. The two **bigger dots** are the type II landmarks on the most medial and lateral points of the section. The **smaller dots** are the sliding semilandmarks, n = 29 on the anterior border and n = 29 on the posterior border; **B**, lateral view of the scapula of OMO VE 3-10063. The two **bigger dots** are the type II landmarks on the most cranial and caudal points of the glenoid outline. The **smaller dots** are the sliding semilandmarks, n = 20 on the glenoid outline. Abbreviations: **Ant.**, anterior; **Cr.**: cranial; **Med.**: medial.

For the fossil comparative sample, information about their origin is summarized in Appendix 5. For the extant sample, surface scans of *H. sapiens* humeri were collected with an Artec Space Spider structured light scanner (Artec Inc., Luxembourg). Surface models for non-human apes were generated from CT scans provided by E. Gillissen from the Musée Royal d'Afrique Centrale. For the 3D-geometric morphometric analysis of the glenoid of the scapula, surface scans of scapulae of extant hominoids were collected with an Artec Spider structured light scanner (Artec Inc.). To facilitate comparison with the right scapula of all fossil hominins, right scapulae of extant hominoids were preferred and left scapulae were mirrored using Meshlab 2022.02 (Cignoni *et al.* 2008).

Two-dimensional (2D)-shape analysis of the distal humeral diaphyseal contour

Cross-sectional contours of the distal humeral diaphysis are useful for taxonomic identification of fossil and extant hominins (Senut 1981; Susman *et al.* 2001; Lague 2015; Lague *et al.* 2019). Ruff *et al.* (2006) showed that long bone cross-sectional shapes respond, to some extent, to mechanical loadings during life history, whereas Ibáñez-Gimeno *et al.* (2013) did not find the same to be true for the distal humeral diaphyseal contour in humans. Instead, the distal humeral cross-section as a whole seems more genetically constrained in mice (Wallace *et al.* 2010), making such an indicator particularly useful for investigating evolutionary adaptations. First, to be able to identify and extract the same section of the distal humerus (located at *c.* 19% of the total length of the humerus, measured from the distal end; Lague 2015) in all the comparative sample, all incomplete fossil specimens were scaled to a humerus of *Homo sapiens* based on the width of their trochlea. Then, following Lague (2015), n = 60 2D-landmarks were collected from the surface outline of the transverse section of the distal diaphysis for each specimen with tpsDIG 2.32 software (Rohlf, New York). Of these n = 60 landmarks, n = 2 were type II landmarks corresponding to the most medial and lateral points of the section, n = 29 sliding semilandmarks were defined on the anterior portion of the contour and kept equidistant from each other, and n = 29 sliding semilandmarks were defined on the posterior portion of the contour and kept equidistant from each other (Fig. 2A). Specimens lacking complete landmark set were excluded from the analysis, therefore, no method to account for missing landmarks was implemented. To assess the repeatability of acquisition of the transverse section located at *c.* 19% on fragmented fossil humeri and adequate placement of landmarks, this protocol was performed by two operators on four specimens, and we adapted the method described by Melillo (2016) to calculate the inter-operator error. The average of the Procrustes distance between the four specimens acquired by the first and second operators was calculated. Then, we estimated the intra-specific variation by calculating the average pairwise distance among individuals within extant species (*H. sapiens*, *P. troglodytes, P. paniscus*, *G. beringei*, and *P. abelii*). We then calculated an overall average intra-specific variation by calculating the average of the intra-specific variation of all the extant species. The Procrustes distance between the trials of the two operators on the fossil specimens was on average less than 48% of the overall average intra-specific range of variation. Also, when plotting the repeated specimens on a Principal Component Analysis bi-plot (cf. *Statistical Analyses* of this *Material and Methods* section to read about the method), their positions were judged close enough to each other, and the overall structure of the bi-plot was respected. Thus, the protocol of extraction of the transverse sections and placement of landmarks was therefore considered sufficiently repeatable for this study.

R v.4.0.3 (R Core Team 2022) was used to run a Generalized Procrustes Analysis (Gower 1975) to superimpose landmark configurations of each specimen, using the criterion of Procrustes distance to optimize the position of semilandmarks (Andresen *et al.* 2000; Sheets *et al.* 2004; function gpagen from the geomorph package; Adams *et al.* 2022).

3D-shape analysis of the glenoid contour

We performed a 3D-geometric morphometrics analysis to explore the pattern of glenoid shape variation within fossil and extant samples. We collected a total of n = 22 landmarks with MorphoDig v.1.6.8. Of these n = 22 landmarks, n = 2 type II landmarks were positioned on the caudal- and cranial-most points of maximum curvature of the glenoid outline along with n = 20 sliding semilandmarks on the glenoid outline that were kept equidistant. (Fig. 2B). The landmark set was adjusted to include the maximum number of fossils, while excluding those specimens on which all landmarks could not be reliably placed. Therefore, no method to account for missing landmarks was implemented. R v.4.0.3 (R Core Team 2022) was used to run the geometric morphometrics procedure. We slid semilandmarks along curve tangents to optimize the placement of semilandmarks by minimizing bending energy (function slider3d from Morpho package). A Generalized Procrustes Analysis (Gower 1975) was performed to superimpose landmark configurations of each specimen using the criterion of minimization of the Procrustes distances (Andresen *et al.* 2000; Sheets *et al.* 2004) using the function gpagen from the geomorph package (Adams *et al.* 2022). This procedure removes differences due to translation, rotation, and scale between specimens to extract comparable shape variables (Bookstein 1991).

Angular measurements

Angular measurements for the scapula and the humerus were taken with the software ImageJ 1.54g (Schneider *et al.* 2012). These measurements have been widely used in the literature to investigate morphological and functional aspects associated with the different characters of the glenohumeral and humeroulnar joints (Martin 1957; Ashton *et al.* 1965; Senut 1981; Rose 1988; Melillo 2016; Selby & Lovejoy 2017; Arias-Martorell 2019). The distal trochlear angle is formed by the medial and lateral sides of the trochlear crests in anterior view (Zylstra 2000). It quantifies the depth of the trochlear central sulcus and mainly discriminates between arboreal suspensors and taxa that do not habitually load the humeroulnar joint significantly (Drapeau 2008).

Humeral torsion is measured using the angle formed by the greatest axes of the humeral head and the trochlea, both projected onto a transverse plane (Martin 1957). In proximal view, the axis of the head corresponds to its parasagittal diameter. The trochlear axis, in distal view, corresponds to a mediolateral axis with the same orientation as the long axis of the trochlea. A low level of torsion (80-120°) is characteristic of fossil hominins and corresponds to a posteriorly oriented humeral head, whereas a higher torsion (above 120°) is characteristic of extant non-human apes and humans and corresponds to a more medially oriented humeral head (Feuerriegel *et al.* 2017). The torsion angle of the OMO VE 3-10063a specimen was measured from superimposed sections of the distal epiphysis and humeral head obtained using Meshlab 2022.02 (Cignoni *et al.* 2008).

The pillar-glenoid angle is formed by the ventral bar and the long axis of the glenoid cavity (Stern & Susman 1983). The pillar-glenoid angle determines the orientation of the glenoid cavity (Stern & Susman 1983) and differentiates primates that regularly raise their arms above the head from primates frequently using their arm for non-locomotor tasks (keeping their arms below the shoulder level) (Ashton & Oxnard 1964; Ashton *et al.* 1965; Melillo 2016; Selby & Lovejoy 2017). The lower the value of this angle, the more cranially oriented the glenoid cavity is. Three experienced operators measured this angle on OMO VE 3-10063b and found a maximum difference of 7°. This relatively significant difference between operators is due to an insufficiently preserved ventral bar, resulting in variation in axis position along the ventral bar.

Linear measurements and indices

Linear measurements and their definitions for OMO VE 3-10063 are provided in Appendix 3. Measurements were taken on the 3D-digital model of OMO VE 3-10063 using Geomagic software (Geomagic Wrap 2021, 3D-Systems). We used the scapular neck breadth index to estimate the relative breadth of the scapular neck. This index is represented as the scapular neck breadth divided by glenoid size (square root of the product of the anteroposterior breadth of the glenoid and its superoinferior height) following Green *et al.* (2018).

Length estimate of the clavicle

We estimated the length of the clavicle of OMO VE 3-10063 using the ordinary least squares regression: maximum length = 38.1713 + 9.3131 * midshaft size, published by Taylor *et al.* (2024). This equation uses *Gorilla*, *Pan*, and *H. sapiens* individuals as a reference sample. Midshaft size is calculated as $\sqrt{(\text{minimum midshaft width} \times \text{perpendicular measurement})}$ following Melillo (2016) and Taylor *et al.* (2024). While it may seem difficult to locate the midshaft of the clavicle OMO VE 3-10063c with precision due to its incompleteness, the dimensions of the cross-section of the medial-most part of OMO VE 3-10063c appear relatively invariant toward the sternal-most end. So, this argument gives us confidence that the midshaft size can be estimated in OMO VE 3-10063c.

Regarding the method provided by Taylor *et al.* (2024), their regression equation to estimate clavicle length is based on a sample that incorporates highly dimorphic non-human apes. In particular, the large-bodied male *Gorilla* individuals plot at one end of the sample and seem to drive the regression equation. To estimate the extent to which our result is primarily influenced by the sample composition, we then ran four regression analyses using: 1) the complete sample used by Taylor *et al.* (2024); 2) their sample excluding male *Gorilla*; 3) their sample excluding male and female *Gorilla*; and 4) their sample excluding all *Gorilla* and *Pan*. The midshaft size definition used by Taylor *et al.* (2024) is based on the minimum midshaft width, a measure that has not been made available by the authors. We thus defined the midshaft size differently, based on the other measurements made available by the authors. We defined then the

midshaft size based on the anteroposterior width and the superoinferior height rather than based on the minimum midshaft width. Thus, our midshaft size is defined here as $\sqrt{\text{anteroposterior width} \times \text{superoinferior height}}$. Despite using a different definition of midshaft size than Taylor *et al.* (2024), we expected the regression model to display broadly similar behavior. Specifically, we assumed that the regression equation would vary with sample composition in a comparable manner regardless of whether midshaft size was defined using our metric or that of Taylor *et al.* (2024). We then evaluated how the regression model responded to changes in sample composition. Including the large-bodied male *Gorilla* could overemphasize the strength of the regression and lead to under-estimating the errors on the clavicle length estimation of OMO VE 3-10063. It should be noted that Taylor *et al.* (2024) found a higher coefficient of determination than ours.

Curvature estimate of the clavicle

We assessed the curvature of the clavicle of OMO VE 3-10063 following *Taylor et al.* (2024). To this end, the clavicle was photographed from cranial view in a standardized position with the acromial end set horizontally. The midline curve was drawn by marking the midline at each of 50 anteroposterior thickness measurements across the length of the bone with ImageJ 1.54g (Schneider *et al.* 2012) following Melillo (2016). A curve connecting each point was drawn using Inkscape. As in Taylor *et al.* (2024), two circles were overlaid on the acromial curvature and on the sternal curvature of the clavicle using the circle tool in Inkscape, which automatically provides their radii. We used the function *ggplot* from the package *ggplot2* in R 4.0.2 for the bivariate plots.

Statistical analyses

For the 2D-shape analysis of the distal humeral diaphyseal contour, R v.4.0.3 (R Core Team 2022) was used to run a Principal Component Analysis (PCA) to assess the morphometric affinities of OMO VE 3-10063 (function *gm.prcomp* from *geomorph* package; Adams *et al.* 2022).

As for the 3D-glenoid shape, R v.4.4.0 (R Core Team 2024) was used to run the statistical analyses. A PCA was used to assess the morphometric affinities of OMO VE 3-10063 (function *gm.prcomp* from the *geomorph* package and function *PCA* from the *FactoMineR* package; Adams *et al.*, 2022). Only Principal Components (PCs) showing clear differentiation between taxa are shown in the results section. For visualization, the extreme shapes on the first two PCs of the PCA were extracted (function *tps3d* from the *Morpho* package).

We explored overall morphological affinities among OMO VE 3-10063 and the comparative sample using hierarchical agglomerative clustering in JMP® 19 Pro (SAS Institute Inc., Cary, NC, United States). Ward's minimum-variance method with Euclidean distances was applied to log-transformed and z-standardized versions of 21 postcranial characters (Appendix 6; Ward 1963; Murtagh & Legendre 2014). Missing values (27 entries, restricted to *H. habilis* and *Paranthropus*) were imputed using the Singular Value Decomposition (SVD) option in JMP's Explore Missing Values platform (JMP® 19 Documentation, "Explore Missing Values"), which implements an iterated low-rank SVD matrix-completion approach to estimate missing entries from the multivariate structure of the complete variables (Troyanskaya *et al.* 2001; Joss & Husson 2016). The resulting dendrogram and constellation plot were used as descriptive summaries of overall morphological affinities.

To assess the influence of missing data and to quantify cluster separation, we repeated the Ward clustering on the subset of taxa with complete data (OMO VE 3-10063, *H. erectus*, *H. sapiens*, *Australopithecus*, *P. troglodytes*). From this analysis, we saved the Euclidean distance matrix and calculated, for the cluster containing OMO VE 3-10063 and the comparative *Homo* specimens, the mean pairwise distance among members of the cluster and the mean pairwise distance between this cluster and the remaining taxa. The ratio of between- to within-cluster distances is reported as a simple distance-based index of cluster separation (Thrun 2021), where values > 1 indicate that the cluster is more distant from other taxa than it is internally, with larger ratios corresponding to greater separation.

Abbreviations

Anatomy

m.	*musculus.*

Institutional and curatorial acronyms

A.L.	Afar Locality;
D	Dmanisi;
EHA	Ethiopian Heritage Authority;
ER	East Rudolf;
IB	Gombore I;
KNM	Kenya National Museums;
KP	Kanapoi;
KSD	Korsi Dora;
MH	Malapa Hominin;
NME	National Museum of Ethiopia;
OGRE	Omo Group Research Expedition;
OH	Olduvai Hominid;
OMO	Shungura Formation locality prefix;
SK	Swartkrans;
SKX	Swartkrans;
Sts	Sterkfontein Type locality;
StW	Sterkfontein;
TM	Kromdraai;
U.W.	University of Witwatersrand;
VE	*Vierge à l'enfant* (virgin and child) locality group secondary prefix;
VP	Vertebrate Paleontology;
WT	West Turkana.

Methodology

2D	Two-dimensional;
3D	Three-dimensional;
PC	Principal Components;
PCA	Principal Component Analysis;
SVD	Singular Value Decomposition.

Other

cf.	*confer*;
spp.	species plural.

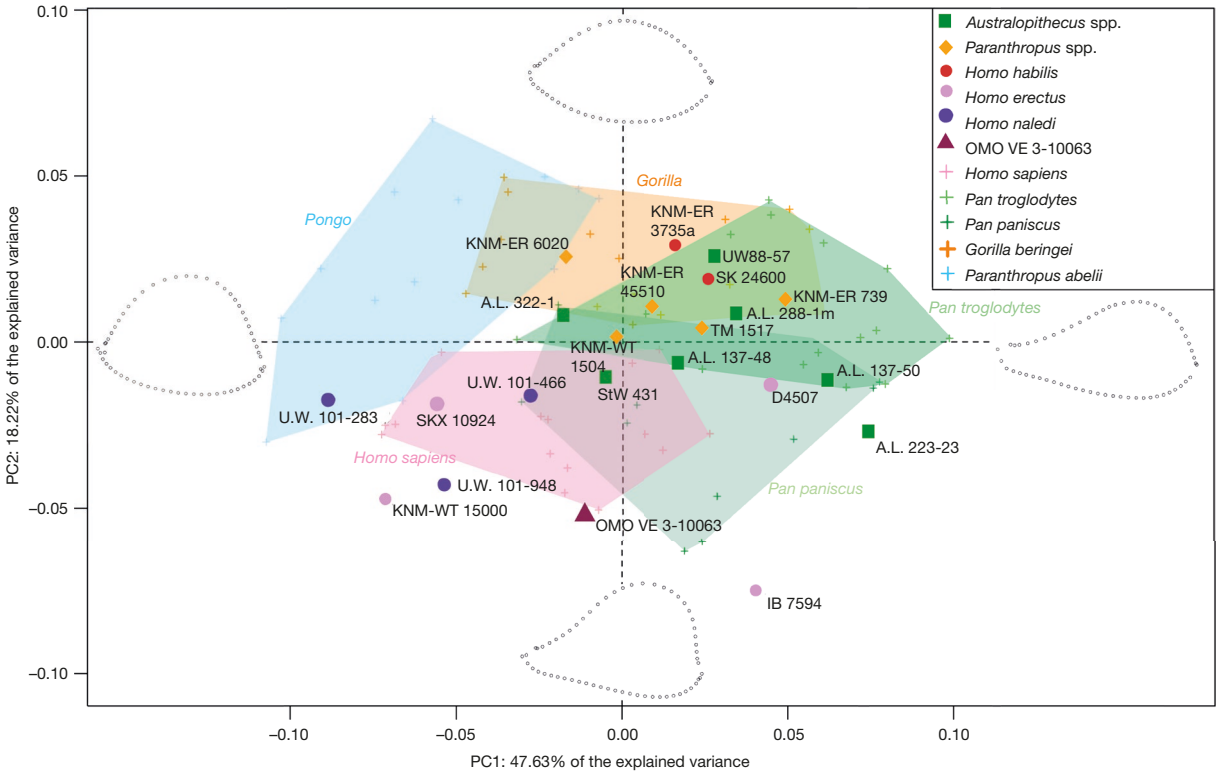

Fig. 3. — 2D-shape analysis of the distal humeral diaphyseal outline. Biplot of Principal Component (PC)1 and PC2 scores of Procrustes landmarks coordinates taken on the distal humeral diaphysis cross-section of extant and extinct hominoids.

RESULTS

Humerus

Humeral characters allowing discrimination of hominin morphotypes were qualitatively and quantitatively assessed in OMO VE 3-10063 (Figs 2; 3A, B; Appendices 6; 7A). Qualitatively, the humerus OMO VE 3-10063a shares phenetic similarities with fossils assigned to *Homo* (Appendices 6; 7A) such as a shallow bicipital groove. At approximately 339 mm, the humerus of OMO VE 3-10063 falls near the upper end of the length range estimated for *Paranthropus* and early *Homo* (e.g., KNM-ER 739 = 329 mm; KNM-WT 15000 = 319 mm; D4507 = 295 mm; Richmond *et al.* 2020; Lordkipanidze *et al.* 2007), noting that these values are estimates and that none of the comparative specimens is preserved in full.

Quantitatively, the PC1-PC2 biplot of the distal humerus cross-sectional outlines accounts for more than 65% of the variance and shows good taxonomic separation with moderate overlap between extant taxa (Fig. 3). In this pattern of variation, OMO VE 3-10063 occupies negative PC1 and PC2 scores with extant and fossil *Homo,* except for two specimens assigned to *H. habilis*. OMO VE 3-10063 is notably outside the range of variation of australopiths and the two specimens assigned to *H. habilis* (Fig. 3). On PC1 (47.63% of variance), increasing positive scores reflect an accentuation of the lateral supracondylar ridges and a mediolateral expansion of the diaphysis (Fig. 3). *Pan troglodytes* has positive scores on PC1 and differs from the negative scores of *Pongo*. *Gorilla* has more intermediate scores on average but overlaps the ranges of both *Pongo* and *Pan*. In contrast, fossil *Homo* scatter all along PC1. OMO VE 3-10063 is characterized by a faint lateral supracondylar ridge, a moderate mediolateral compression of the diaphysis, and is within the ranges of variation for *H. sapiens* and African apes, and within the lower values of australopiths. PC1 also shows that early members of the genus *Homo* (D4507, IB 7594, KNM-WT 15000, SKX 10924) show a range of variation for the lateral supracondylar ridge that exceeds that of australopiths on PC1. On PC2 (18.22% of the observed variance), increasing positive scores illustrate cross-sections that range from a subtriangular shape (the posterior margin of the diaphysis being planar) to an elliptical shape (the posterior margin of the diaphysis being convex). The range of *H. sapiens* overlaps with that of *P. paniscus* (negative scores). Both variation ranges differ from those of *Gorilla* and *P. troglodytes* (mostly positive scores). The range of *Pongo* mostly overlaps that of all other groups, except that of *P. paniscus* and the lowest values for *Homo.* With the lowest scores along PC2, fossil specimens of *Homo* and OMO VE 3-10063 are characterized by a subtriangular diaphyseal shape and differ from most specimens putatively assigned to *Paranthropus* and *Australopithecus* (higher values).

Trochlear depth is deemed to contribute to the mediolateral stability of the elbow during arboreal and terrestrial locomotion in primates with elbow stability reflected by the acute distal trochlear angle (Senut 1981; Morrey & An

1983; Drapeau 2008). The obtuse distal trochlear angle of OMO VE 3-10063 (136°; Fig. 4A) depicts a shallow trochlear central sulcus within the range of variation of *H.sapiens* (120°-155°) and outside that of extant non-human apes (98°-133°) which mostly features a deeper sulcus. OMO VE 3-10063 is also within the range of *H. erectus* (134°-147°), close to values measured for most species of *Australopithecus* (i.e., *H. sediba*, *A. afarensis*, and *A. africanus*), and contrasts with the condition reflected by *H. habilis*, *Paranthropus* spp. and *A. anamensis* (Fig. 4A). Overall, OMO VE 3-10063 does not deviate from the condition seen in *H. erectus* and some species of *Australopithecus* and is clearly outside the range displayed by all specimens assigned to *Paranthropus*. OMO VE 3-10063 would thus be characterized by a humeroulnar joint that is mediolaterally less stable than those of non-human apes that use their forelimbs in postural and locomotor behaviors. This interpretation suggests that transverse loads on the humeroulnar joint of the individual from Shungura were likely weaker and suggests a weaker musculature of the forearm compared to non-human apes (Drapeau 2008; Lague *et al.* 2019). Hence, the individual OMO VE 3-10063, like extant *Homo* and *H. erectus* and some *Australopithecus* species, was less able to use its elbow for locomotor purposes than extant non-human apes and *Paranthropus*.

Humeral torsion represents humeral head orientation relative to the bicondylar axis (Krahl 1947) and is supposed to be related to the range of internal and external rotation of the humerus in *H. sapiens* (Roach *et al.* 2012). With a value of 110°, OMO VE 3-10063 is below the ranges of *H. sapiens* (125°-172°) and African apes (121°-168°) and is at the lower limit observed for *Pongo* (110°-147°; Fig. 4B). The humeral torsion of OMO VE 3-10063 falls within the observed ranges for *H. erectus* and *H. naledi,* and is close to the value of 111° ± 6° estimated for *P. boisei* (KNM-ER 739; Larson 1996). OMO VE 3-10063 falls below all torsion values reported for *Australopithecus* (Fig. 4B). No data are available for *H. habilis*. This angle shows that fossil hominins all display a posterior orientation of the humeral head (despite some variations) contrasting with the medial orientation seen in extant non-human apes and *H. sapiens*. Nonetheless, the function of low humeral torsion is unclear: it seems to be associated with an extended range of external rotation of the glenohumeral joint (Roach *et al.* 2012). Some authors have suggested that low humeral torsion facilitates high-speed throwing and could have been an exaptation in *Homo* (Roach *et al.* 2013). Low torsion could also be related to a more anterior position of the scapula on the thorax (Larson 1988, 2007). While all fossil hominins (including *Ardipithecus ramidus*; Lovejoy *et al.* 2009; not depicted in Figure 4A) tend to display low values for this angle, such a trait is particularly well-expressed on the fossil *Homo* specimens. The torsion of the humerus from OMO VE 3 falls within the variation of fossil *Homo* (excluding *H. habilis* that has no humerus to estimate such an angle) and in the lower part of the variation of other fossil hominins. More studies are needed to definitely determine the functional significance of this character.

Scapula

In qualitative terms, the scapula OMO VE 3-10063b displays a weak ventral bar and a glenoid notch on the anterior margin of the glenoid cavity (Appendices 6; 7B, C). Like other *Homo* fossils, OMO VE 3-10063 seems to have a reduced subacromial space, indicated by a cranial spine insertion on the shoulder blade (Appendices 6; 7C), which contrasts with the specimens of *Paranthropus*, *Australopithecus*, and *P. troglodytes*. The reduction of the subacromial space seems related to rotator cuff weaknesses during elevation of the arm (Voisin *et al.* 2014; Lee *et al.* 2020; MacLean & Dickerson 2020). Hence, this non-articular scapular morphology of OMO VE 3-10063 likely reflects low abilities for arm elevation and could indicate low propensities for habitual climbing and suspension. The overall morphology and estimated lengths of the coracoid process of OMO VE 3-10063 are more similar to those of *H. sapiens* than those of non-human apes. Although the coracoid process lacks its most distal extremity, the width is constant along its entire length, as in *H. sapiens*, whereas *Pan* displays a distal part substantially wider than the central part (Appendices 7D; 8A). In addition, the absolute length of the coracoid process of OMO VE 3-10063 is within the ranges of variation of *H. sapiens* and *Pan* (Appendix 8B). We can thus infer that this individual may have had a body size intermediate between these two extant species. The relative length of the coracoid process of OMO VE 3-10063 is within the low ranges of variation of *H. sapiens*, *P. paniscus*, and *Gorilla* spp. (Appendix 8C).

Quantitatively, the orientation of the glenohumeral joint in primates is commonly assumed to reflect the propensity for using the forelimb in elevated positions, such as in climbing and suspensory activities, and the position, low to high, of the scapula on the thorax (Stern & Susman 1983). High and narrow shoulders have been interpreted as advantageous for suspension to reduce mechanical demands during elevation of the arm (Ashton & Oxnard 1964). On the contrary, low and wide shoulders are hypothesized to be advantageous for endurance running to generate a counter-rotation of the trunk against the hip during running (Bramble & Lieberman 2004) and for high-speed throwing to set the *m. pectoralis major* in a favorable condition to perform internal rotation of the arm (Roach *et al.* 2013). To evaluate the glenohumeral joint orientation of OMO VE 3-10063, we estimated the pillar (bar)-glenoid angle (Stern & Susman 1983). With a value estimated between 129° and 136° (inter-observer variability due to lack of the axillary border; Fig. 4C), OMO VE 3-10063 fits within the upper range of variation observed in extant non-human apes (*P. troglodytes,* 122°-134°; *G. gorilla*, 124°-137°; *P. pygmaeus,* 116°-134°) and *Australopithecus* spp. (124°-134°), all displaying a cranial orientation of the glenohumeral joint, and the lower variation range of *H. sapiens* (135°-149°), all characterized by a lateral orientation of the glenohumeral joint. The orientation of the glenohumeral joint of OMO VE 3-10063 (Fig. 4C) is intermediate between that of *H. sapiens*, *Australopithecus* and *P. troglodytes* and is lower than the values reported for the early *H. erectus* individuals KNM-WT 15000 (138°) and D4166 (146°). No data is reported for *H. habilis* or *Paranthropus*.

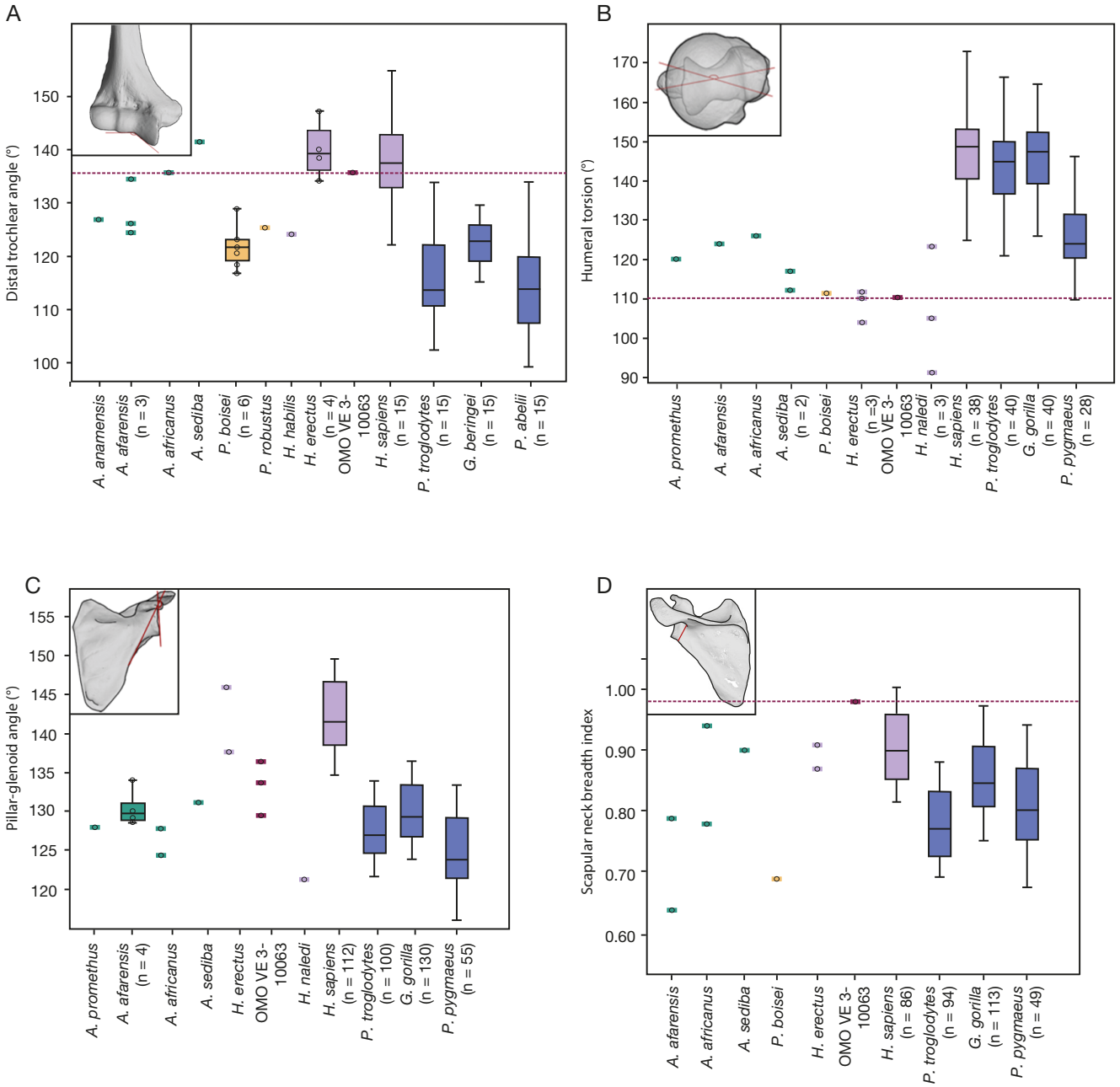

FIG. 4. — Quantitative comparisons. Boxplots for selected morphometric indices, with all boxplots indicating the median as well as first and third quartile. The horizontal dashed line corresponds to OMO VE 3-10063: **A**, distal trochlear angle. The humerus is represented in anterior view. Values for *Paranthropus boisei* and *Homo erectus* (except for KNM-WT 15000 and SKX 10924) were taken from the literature (Lague *et al.* 2019). *Australopithecus anamensis*is represented by KNM-KP 271; *A. afarensis* by A.L. 137-48, A.L. 288-1, and A.L. 322-1; *A. africanus* by Stw 431; *A. sediba* by MH2; *P. boisei* by KNM-ER 739, KNM-ER 6020, KNM-ER 47000, KNM-ER 1504, KNM-ER 1591, and KNM-ER 45510; *P. robustus* by TM 1517; *H. habilis* by SK 24600; *H. erectus* by D4507, IB 7594, KNM-WT 15000, and SKX 10924; **B**, humeral torsion. The humerus is represented in cranial view. Extant and extinct specimen values were taken from the literature (Larson 1996, 2007, 2013; Lordkipanidze *et al.* 2007; Roach *et al.* 2013; Feuerriegel *et al.* 2017, 2019; Heaton *et al.* 2019). *Australopithecus prometheus* is represented by StW 573; *A. afarensis* by A.L. 288-1; *A. africanus* by Sts7; *A. sediba* by MH1 and MH2; *P. boisei* by KNM-ER 739; *H. erectus* by KNM-WT 15000, D4507 and D2680; and *H. nalediby* U.W. 101-283, U.W. 102a-257, and U.W. 101-948; **C**, pillar glenoid angle. The scapula is represented in ventral view. Extant and extinct specimen values (except for D4166) were taken from the literature (Stern & Susman 1983; Larson *et al.* 2009; Haile-Selassie *et al.* 2010; Green & Alemseged 2012; Feuerriegel *et al.* 2017; Churchill *et al.* 2018; Green *et al.* 2018; Carlson *et al.* 2021). *Australopithecus prometheus* is represented by StW 573; *A. afarensis* by A.L. 288-1, DIK 1-1 (right and left scapula), and KSD-VP 1/1; *A. africanus* by Sts7 and StW 162; *A. sediba* by MH2; *H. erectus* by KNM-WT 15000 and D4166; and *H. naledi* by U.W. 101-1301. Three measurements taken by three operators are represented for OMO VE 3-10063 highlighting the measurement error for this angle; **D**, scapular neck breadth relative to glenoid size. The scapula is represented in dorsal view. Extant and extinct values (except for D4166) were taken from literature (Green *et al.* 2018). The cranial and caudal borders of the glenoid of D4166 are eroded, resulting in a possible underestimation of the craniocaudal height of the glenoid of the specimen. As such, the index indicated here is a minimal estimation for D4166. *A. afarensis* is represented by A.L. 288-1 and KSD-VP-1/1; *A. africanus* by Sts7 and StW 162; *A. sediba* by MH2; *P. boisei* by KNM-ER 47000; and *H. erectus* by KNM-WT 15000.

The intermediate angular estimates for OMO VE 3-10063 indicate a shoulder positioned neither high nor low on the thorax, and we thus argue here that it does not confer an advantage for suspension or climbing behaviors, as seen in *P. troglodytes*.

In suspensory primates, a large scapular neck breadth is traditionally associated with a powerful *m. infraspinatus*, which is important for glenohumeral lateral rotation and for stabilizing the glenohumeral joint during abduction (Larson 1995). Among primates, hominoids generally have large scapular necks, and *H. sapiens* display overall a larger neck than other extant hominoids. Nevertheless, this is likely a primitive trait particularly variable in hominoids, thus caution should be used when interpreting hominin morphology (Green 2013; Green *et al.* 2018). In *H. sapiens*, the large neck breadth would allow the *m. infraspinatus* to pass posteriorly to the glenohumeral joint. This characteristic would be advantageous in controlling the axial rotation of this joint for a pendant arm used for dextrous activities, especially when carrying an object (Gagey 1985; Larson 1995). With a scapular neck breadth index estimated at 0.98 (Fig. 4D), OMO VE 3-10063 fits within the upper part of the range of variation for *H. sapiens* (0.82-1.00) and is slightly above the upper ranges of variation for *G. gorilla* (0.75-0.97) and *P. pygmaeus* (0.66-0.95) and is outside the observed range of variation of *P. troglodytes* (0.69-0.88). The scapular neck of OMO VE 3-10063 is broader than those of A.L. 288-1 (0.79), KSD-VP-1/1 (0.64), KNM-ER 47000 (0.69), and Sts 7 (0.79), close to StW 162 (0.94), MH2 (0.90), D4161 (0.91), and KNM-WT 15000 (0.87). Hence, the broad scapular neck of OMO VE 3-10063 is distinct from those of the specimens attributed to *Paranthropus* and *A. afarensis*, close to *Australopithecus* specimens from South Africa and is consistent with the morphology of extant and fossil *Homo*. Data are not available for *H. habilis,* however.

Due to its three degrees of freedom, the glenohumeral joint is primarily responsible for forelimb mobility in primates (Arias-Martorell 2019). The shape of the glenoid has been used in discriminating hominin species (Di Vincenzo *et al.* 2012; Macias & Churchill 2015; Arias-Martorell *et al.* 2015), but its functional interpretation has raised debate (Lee *et al.* 2023; Raventós-Izard *et al.* 2023). Here, we ran a PCA to explore its pattern of morphological variation. Overall, PC1-PC2 biplot accounts for more than 50% of the variance (Fig. 5). On PC1 (34.3% of variance), increasing positive scores reflect narrowing of the glenoid in lateral view (craniocaudal length longer than dorsoventral width) with an accentuation of the craniocaudal curvature in dorsal view (Fig. 5). *Pongo* has mostly positive scores, *Gorilla* is restricted to the center of the biplot, while *P. paniscus*, *P. troglodytes*, and *H. sapiens* expand largely into both negative and positive scores. On PC2 (16.9% of variance), increasing positive scores reflect a glenoid with a straight dorsal border reflecting an overall triangular shape. In contrast, decreasing negative scores illustrate a glenoid with a convex dorsal border. The glenoid slightly deepens from negative to positive values. All extant taxa greatly overlap on PC2, *H. sapiens* and *Pongo* having mostly positive values, while negative and positive scores are seen for *P. troglodytes, P. paniscus,* and *Gorilla*. On PC1, fossil hominins have positive scores except for D4166, which is negative. OMO VE 3-10063 falls within the highest scores of *H. sapiens, P. paniscus*, and *P. troglodytes* and within the intermediate values of *Pongo*. KNM-WT 15000, A.L. 288-1, and KSD-VP-1/1 are within the values of all extant taxa. D4166 is within the variation ranges of *H. sapiens*, *P. paniscus*, *P. troglodytes*, and *Gorilla.* U.W. 88-56 and Sts 7 are within the variation ranges of *Pongo* only, and close to the highest values of *H. sapiens*, *P. paniscus*, and *P. troglodytes*. On PC2, all fossil hominins are distributed along the axis. OMO VE 3-10063, D4166 have positive values and are within the variation ranges of *H. sapiens* and *Pongo.* A.L. 288-1 and KSD-VP-1/1 have positive values and are within the ranges of variation of all extant taxa. KNM-WT 15000 has a negative value and is within the lowest scores of *P. paniscus* and *P. troglodytes*. U.W. 88-56 and Sts 7 have negative values and are near the lowest scores of *P. troglodytes*. Considering PC1 and PC2 scores, D4166 and OMO VE 3-10063 fit within the ranges of variation of *H. sapiens* only, the latter being near the ranges of *Pongo*. KNM-WT 15000 falls in the range of variation of *P. troglodytes.* KSD-VP-1/1 and A.L. 288-1, close to each other, are within the ranges of variation of *H. sapiens, Pongo,* and *Gorilla,* and close to *P. paniscus.* U.W. 88-56 and Sts 7 are outside the range of variation of any extant taxa. It should be noted that the dorsal margin of the glenoid of Sts 7 is likely damaged, and that without this damage its position would shift toward lower PC1 scores and higher PC2 scores, although no substantial alteration of its overall shape is anticipated. Specifically, OMO VE 3-10063 is characterized by a narrow glenoid, a slightly concave ventral border with a glenoid notch and convex dorsal border, similar to *Pongo* and *H. sapiens* morphology. Overall, the glenoid morphology of OMO VE 3-10063 is distinct from those of *Australopithecus* and its comparison highlights its morphological affinities with *Homo*. It should be noted that no specimens for *H. habilis* nor *Paranthropus* were included in glenoid shape assessment as none were available for study or documented in the fossil record. This analysis would particularly benefit from the inclusion of KNM-ER 47000, attributed to *P. boisei*. In functional terms, our results suggest that glenoid morphology could reflect the predominant direction and magnitude of shear forces acting on the glenohumeral joint. We could argue that these forces are oriented inferiorly during bipedal posture (the primary locomotor behavior in *Homo sapiens*), anteriorly during knuckle-walking (in *Gorilla* and *Pan*), and superiorly during suspensory behaviors (in *Pongo*). Nevertheless, the forces acting on the glenohumeral joint have received little attention to date (Thompson *et al.* 2018), and this hypothesis warrants further investigation. Nonetheless, recent insights into the potential roles of the glenoid labrum (Raventós-Izard *et al.* 2023) provide grounds for a more nuanced interpretation of the functional role of the glenoid morphology.

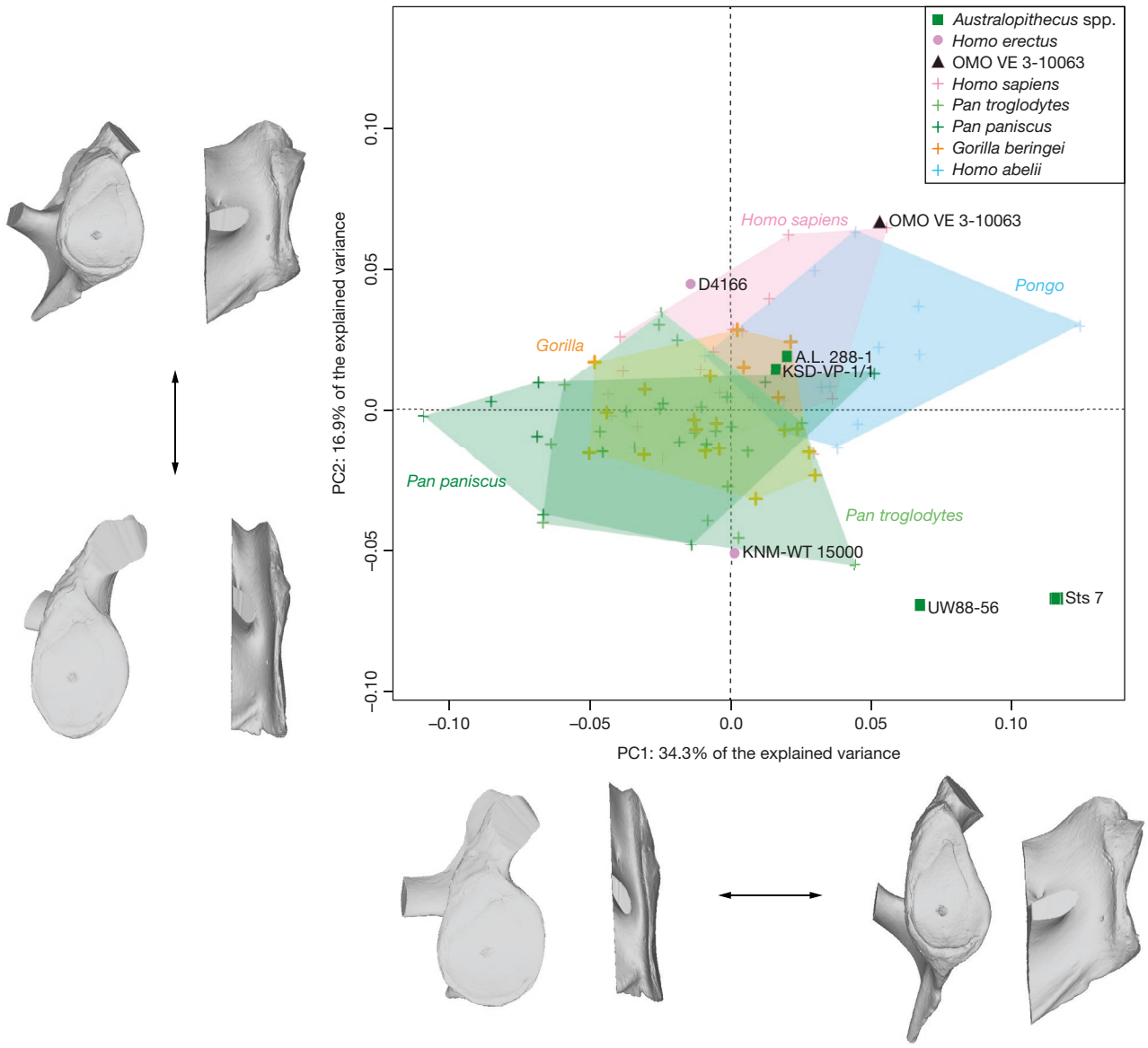

Fig. 5. — 3D-shape analysis of the glenoid of the scapula. Bivariate plot of the first two components of the Principal Component (PC) Analysis on the glenoid shape. Glenoid shape changes are shown at the extreme ends of each axis in lateral and dorsal views.

Clavicle

The overall shape of the clavicle of OMO VE 3-10063 is closer to that of *H. sapiens* and early *Homo* than to *Australopithecus* and *P. troglodytes*, especially because of its weak conoid tubercle (Appendix 7E). The orientation of the shaft of the clavicle has been often related to the superoinferior position of the scapula on the thorax (Voisin 2006; Larson 2007; Churchill *et al.* 2013). Nevertheless, a recent study demonstrated that this relationship is not verified in *H. sapiens* (Melillo *et al.* 2019). Thus, this character may only have taxonomic significance here. OMO VE 3-10063 displays a horizontal clavicular shaft when its acromial end set horizontally. This condition is like that of *H. sapiens* and early *H. erectus,* and different from that of *Australopithecus* and *P. troglodytes* (Appendices 6; 7E). The groove of the *m. subclavius* is slightly pronounced in OMO VE 3-10063 and although this muscle is present in all hominoids, the frequency of the *m. subclavius* groove on the clavicle is much higher in *H. sapiens* (80%) than in any other hominoids (<40%; Appendix 9; Feuerriegel *et al.* 2019). Thus, the presence of this groove in OMO VE 3-10063 is consistent with this clavicle belonging to *Homo*.

Given the importance of clavicle length for maintaining the position of the shoulder girdle (Larson 2007; Kagaya *et al.* 2010; Roach & Richmond 2014; Melillo *et al.* 2019) and for estimation of shoulder breadth (Melillo *et al.* 2019), we estimated clavicle length of OMO VE 3-10063 based on the protocol and regression equation published by Taylor *et al.* (2024). We found that the midshaft size of OMO VE 3-10063 is 11.1 mm, leading to an estimate for the maximum length of the clavicle of 141.4 +/- 1.9 mm. This estimate falls within the range of variation of *H. sapiens*, is within the highest values for *Pan* and falls in the range of fossil hominins (Fig. 6).

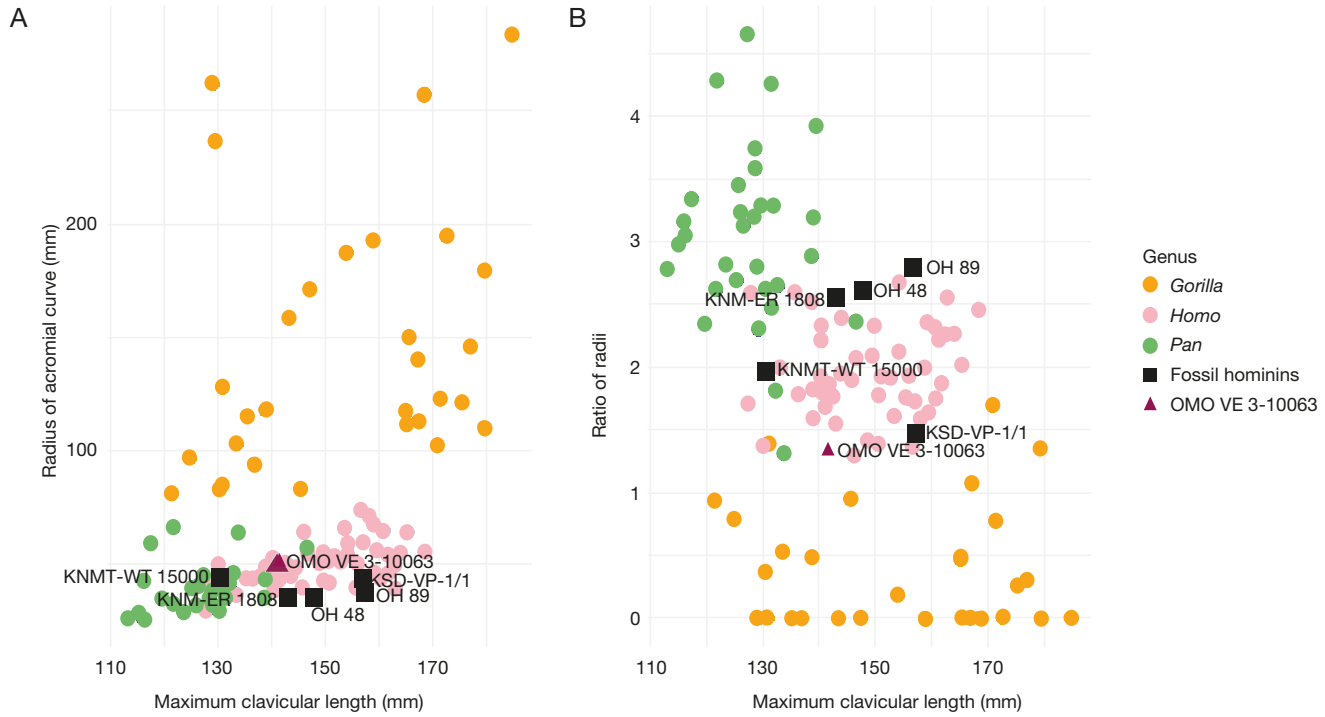

FIG. 6. — Bivariate plots of clavicular curvature on clavicular maximum length (data after Taylor *et al.* 2024): **A**, radius of acromial curve against maximum clavicular length; **B**, ratio of radii (radius of sternal curve/radius of acromial curve) against maximum clavicular length. The specimen OMO VE 3-10063 was added to the results from (Taylor *et al.* 2024).

Our length estimate would indicate that the shoulder breadth of OMO VE 3-10063 would have been similar to an average *H. sapiens*. However, this clavicle length estimation relies on regression equations influenced by *Gorilla* outliers. Thus, we evaluated further the reliability of this result by performing four regression analyses on clavicle length using different reference samples. Results show that removing male *Gorilla* from the sample strongly decreases the coefficient of determination R^2 and gives longer estimates (about 1 mm; Appendix 10). Hence, uncertainties on our estimate may be higher than the bracket provided here and the estimated maximum length of the clavicle could be longer.

Curvatures of the clavicle in cranial view may also give insights into the function of the forelimbs when interpreted along with its length and general morphology. Especially, the internal curvature may give more mobility to the shoulder and a mechanical advantage for *m. deltoideus* and *m. pectoralis major* in suspensory primates (Squyres & DeLeon 2015). However, this morphology would provide a weak resistance to stresses exerted during terrestrial quadrupedal locomotion (Voisin 2006). On another note, *A. afarensis* clavicular morphology has been interpreted as evidence of increased dextrous function of the forelimb (Melillo 2016). Here, we estimated the curvatures of the clavicle of OMO VE 3-10063 based on the protocol of Taylor *et al.* (2024). We found an acromial radius of 49.9 mm and a sternal radius of 71.8 mm. We then added OMO VE 3-10063 to the data provided by Taylor *et al.* (2024), and we generated the same plots. OMO VE 3-10063 falls within the variation of *H. sapiens* and *Pan* in acromial curvature, outside the variation of *Gorilla*, and is close to other fossil hominins attributed to *A. afarensis*, *H. habilis*, and *H. erectus* (no specimens for *Paranthropus*; Fig. 6A). *Gorilla* fall far from the rest of the hominoids with a longer acromial radius, that may be the results of a size-effect. Considering the ratio of radii, OMO VE 3-10063 plots in the lower range of *Homo* and *Pan*, in the upper range of *Gorilla*, and is close to KSD-VP-1/1 and KNM-WT 15000 (Fig. 6B). Again, *Gorilla* fall low compared to other hominoids, meaning that their sternal radius is mostly shorter than their acromial radius. Some specimens even display no sternal curvature and thus fall on the zero-line. Overall, the clavicle shape, length and curvatures of OMO VE 3-10063 are within the range of variation of *H. sapiens* and suggest that the biomechanical forces acting on the shoulder of this individual were partly similar to those of *H. sapiens*, i.e., reduced use of the forelimb for locomotion.

VERTEBRAE

OMO-VE3-10063 also includes two fragments of the 6th and 7th cervical vertebrae. Although both specimens display some key diagnostic features, their state of preservation limits further quantitative comparisons. In dorsal view, the spinous process of OMO VE 3-10063 is robust and slightly caudally inclined as in hominins, which contrasts with the horizontally oriented and blade-shaped process of the cervical vertebrae of *P. troglodytes*. The end of the spinous process of OMO VE 3-10063 is more expanded mediolaterally than craniocaudally, as on the C7 vertebrae of *H. sapiens* and *H. erectus* (KNM-WT 15000) and differs from that of *P. troglodytes* and *A. sediba* (U.W. 88-09; Appendix 7F). In ventral view,

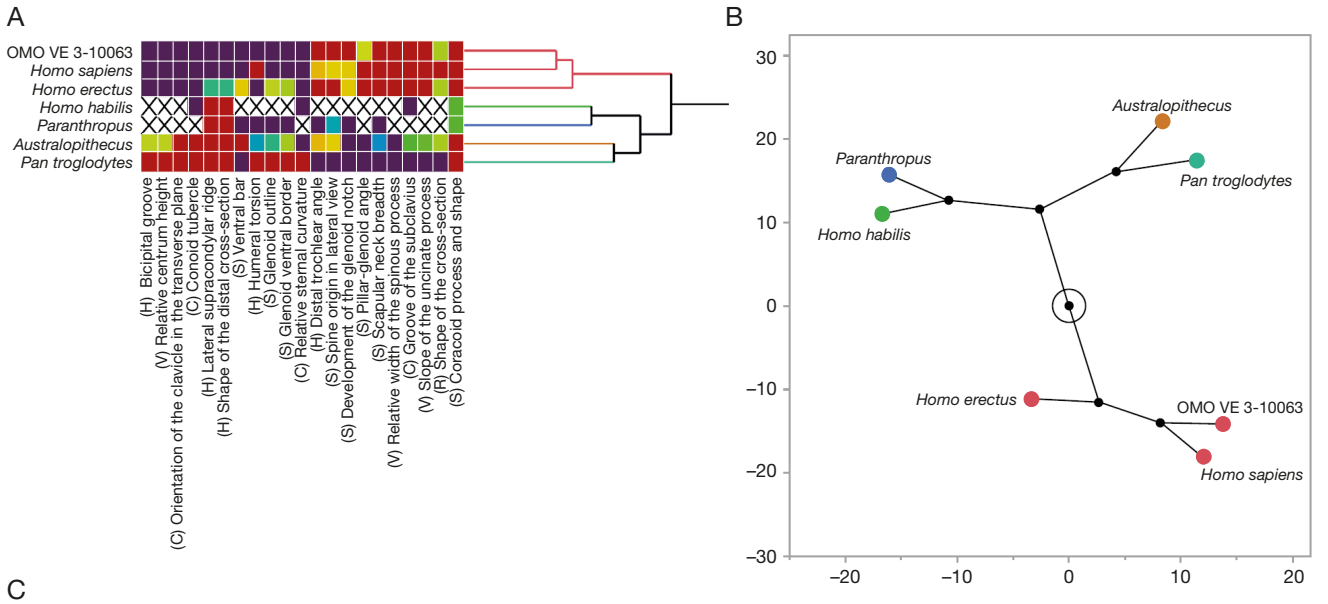

C

Clustering history			
Number of clusters	**Distance**	**Leader**	**Joiner**
6	2.157349568	OMO VE 3-10063	*Homo sapiens*
5	2.546226697	OMO VE 3-10063	*Homo erectus*
4	2.695547438	*Homo habilis*	*Paranthropus*
3	3.879510930	*Australopithecus*	*Pan troglodytes*
2	4.710161766	*Homo habilis*	*Australopithecus*
1	8.388108700	OMO VE 3-10063	*Homo habilis*

FIG. 7. — Hierarchical clustering of postcranial morphology: **A**, heat map of the 21 postcranial characters used in the cluster analysis (columns; see Appendix 6) for OMO VE 3-10063 and the comparative taxa (**rows**). Different colors indicate discrete character states; white cells with **black crosses mark** missing values. The dendrogram to the right shows Ward's hierarchical clustering based on Euclidean distances of log-transformed, z-standardized characters. Colored branches indicate the three clusters discussed in the text. Note that missing values are restricted to *Homo habilis* and *Paranthropus*; **B**, constellation plot of the same clustering. Points are colored by genus (**red**, *Homo*; **blue**, *Paranthropus*; **orange**, *Australopithecus*; **green**, *Pan*), and the connecting lines reproduce the hierarchical relationships from panel A. OMO VE 3-10063 falls within the *Homo* cluster; **C,** clustering history showing distance between clusters.

the vertebral body of OMO VE 3-10063 is relatively short craniocaudally, a condition shared by *H. sapiens* and *Australopithecus* and differing from that of *P. troglodytes*. Despite a slight erosion of its cranial end, the preserved portion of the uncinate process of OMO VE 3-10063 is obliquely oriented, a condition variable in *A. afarensis*, but shared with *Homo* and different from that of *P. troglodytes* (Appendices 6; 7G).

Rib

Given the extremely poor state of preservation of this right 6th-9th rib, little can be said about its morphology and its use for estimating the thoracic shape is impossible in the absence of its dorsal-most portion. The oval-shaped cross section of the rib of OMO VE 3-10063 differs both from the rounded contour typical of African apes and from the internal-to-externally flattened aspect of the homologous ribs of *H. sapiens.* This oval shape resembles the condition commonly described in australopiths and archaic humans (Appendix 6).

Overall assessment

The Ward hierarchical clustering of all seven taxa (Fig. 7A) groups OMO VE 3-10063 with *H. erectus* and *H. sapiens*, while *Australopithecus* and *P. troglodytes* form a separate branch, and *H. habilis* clusters with *Paranthropus*. OMO VE 3-10063 and the comparative *Homo*, *Australopithecus*, and *Pan* specimens are complete for all 21 characters, so the distances underlying these relationships are based entirely on observed data. In contrast, *H. habilis* and *Paranthropus* each lack more than half of the characters, and their placement relies on SVD imputed values (Fig. 7A; Appendix 11). We therefore consider the small node linking *H. habilis* and *Paranthropus* to be less reliable than the relationships among the fully scored taxa and interpret it with caution. When *H. habilis* and *Paranthropus* are removed, and the clustering is repeated on the five fully observed taxa, OMO VE 3-10063 again clusters with *H. erectus* and *H. sapiens*, whereas *Australopithecus* and *P. troglodytes* remain distinct (Appendix 12). For this reduced dataset, the mean within-cluster Euclidean distance among OMO VE 3-10063, *H. erectus*, and *H. sapiens* is 3.22 (Appendix 13), whereas the mean distance between this "OMO-*Homo*" cluster and *Australopithecus* and *P. troglodytes* is 7.39 (between/within ratio = 2.30). This ratio, being greater than 1, indicates that the cluster is compact internally and well separated from the other taxa. We therefore regard the cluster analysis and associated constellation plot (Fig. 7B) as an exploratory visual summary that is fully consistent with the attribution of OMO VE 3-10063 to *Homo* established by the primary analyses above.

DISCUSSION

We demonstrated here that the associated elements of OMO VE 3-10063 dated to 1.84 Ma share taxonomic and functional traits with early Pleistocene *Homo*. Our study supports the interpretation that OMO VE 3-10063 provides the oldest and best-preserved shoulder and arm bones attributable to *Homo* and is therefore significant for understanding the evolution of our genus. More specifically, OMO VE 3-10063 shares with *H. erectus* a distal humeral diaphysis with a subtriangular cross section due to a reduced lateral supracondylar ridge, a character relevant for taxonomic attribution (Lague 2015). OMO VE 3-10063 contrasts with the condition observed in the penecontemporaneous specimens assigned to *Paranthropus*, which display a prominent supracondylar ridge, and *H. habilis*, with an elliptical distal diaphysis. OMO VE 3-10063 also contrasts with the morphology observed in *Australopithecus* spp., which were no longer present in Africa by 1.84 Ma. The humerus of OMO VE 3-10063 also shows a trochlea clearly shallower than that of *Paranthropus* and the specimen of *H. habilis* and similar to that of *H. erectus*, while its diaphyseal torsion is typical of early hominins, including *Australopithecus*, *Paranthropus*, and early *Homo*, but noting that no humerus is complete enough to estimate this character for *H. habilis*. As for characters on the scapula, there are no specimens attributed to *H. habilis*, and only one to *Paranthropus*. Thus, despite the fact that OMO VE 3-10063 scapular traits (i.e., bar-glenoid angle, scapular neck breadth, and glenoid shape) are within the expected range of variation for early *H. erectus*, we cannot rule out that these traits could have been close to their ranges in *H. habilis* or *Paranthropus*, with the exception of scapular neck breadth of OMO VE 3-10063 that seems distinct from the breadth measured in *Paranthropus*. Finally, the curvatures of the clavicle of OMO VE 3-10063 are in the ranges of variation observed in all fossil hominins so this character was not discriminatory for taxonomic analysis. Thus, although the morphology of the distal humerus – specifically the trochlea and the sectional outline, for which comparative data are available for taxa that could have been penecontemporaneous in eastern Africa at around 1.8 Ma (*H. erectus*, *H. habilis*, and *Paranthropus*) – is consistent with an attribution to *H. erectus*, the limited early *Homo* (and especially *H. habilis*) record, the potential for individual variation, and no associated craniodental elements lead us to adopt the more conservative designation *H.* cf. *erectus* for OMO VE 3-10063. Thus, the discovery of OMO VE 3-10063 is a significant contribution to the fossil record of postcranial remains for early *Homo* considering that only five fossil localities dated between 2.3 and 1.44 Ma yielded other comparable shoulder and forelimb remains. These localities are represented by eight individuals, including two individuals (one adult and one subadult) from Dmanisi (1.81-1.77 Ma, Georgia; Lordkipanidze *et al.* 2007; Mgeladze *et al.* 2011), the subadult individual KNM-WT 15000 (*c.* 1.5-1.44 Ma, Nariokotome, Kenya; Walker & Leakey 1993; McDougall *et al.* 2012), and the damaged partial skeleton KNM-ER 3735 (1.9 Ma, Koobi Fora, Kenya), which comprises only a fragment of the clavicle, a fragment of the scapular spine and a damaged distal humerus (Leakey & Walker 1985). This inventory also includes isolated fragments of a clavicle, OH 48 (1.87-1.75 Ma, Olduvai, Tanzania; Leakey *et al.* 1964), a humeral diaphysis, OH 62 (1.8 Ma, Olduvai, Tanzania; Johanson *et al.* 1987), and two distal humeral epiphyses SKX 24600 (1.7 Ma, Swartkrans, South Africa) and SK 2598 (2.3-1.7 Ma, Swartkrans, South Africa; Susman *et al.* 2001). Unfortunately, these isolated specimens are poorly preserved, drastically limiting taxonomic and functional interpretations. Accordingly, the present study demonstrates that OMO VE 3-10063 preserves the oldest shoulder attributable to *Homo*, is slightly older than, but broadly contemporary with the Eurasian material from Dmanisi, and is the most complete adult shoulder of early *Homo* from Africa. Given these previous lines of evidence, OMO VE 3-10063 is therefore a key specimen for estimating habitual functional and behavioral abilities of earliest *Homo*.OMO VE 3-10063, like other early *Homo* included here, displays extremely low humeral torsion, and an elbow mediolaterally less stable than in non-human apes and the specimens putatively assigned to *Paranthropus*. The curvatures of the clavicle OMO VE 3-10063c, as well as the presence of a slight subclavian groove, contrast with the morphology of *Pan* and resemble the morphology seen in *Australopithecus* and *Homo* (no clavicle is attributed to *Paranthropus*), suggesting that the loads applied on the shoulder girdle of OMO VE 3-10063 were partly similar to those of *H. sapiens* and different from those of non-human apes. This further suggests that OMO VE 3-10063 did not extensively use its forelimb for arboreal locomotor activities. Despite the orientation of the glenoid surface of the scapula being intermediate between australopiths and *H. sapiens,* the pectoral girdle of OMO VE 3-10063 shares more similarities with *Homo* than with other hominins. Specifically, OMO VE 3-10063 displays a more horizontally oriented shaft of the clavicle, a reduced subacromial space of the scapula, a larger scapular neck, a more modern human-like shape and length of the coracoid process, and a glenoid surface closer in shape to *H. sapiens* rather than to *P. troglodytes* or most australopiths. Overall, OMO VE 3-10063 displays a modern human-like shoulder architecture associated with low mechanical advantages for (arboreal) locomotion. Despite the forelimb of the Dmanisi specimens being described as primitive (Lordkipanidze *et al.* 2007), our results suggest that most of the traits quantified here are similar to those of OMO VE 3-10063, suggesting that these specimens may be more derived than previously suggested. Overall, our results support the idea that by 1.8 Ma in Africa *Homo* reduced the use of its forelimbs in arboreal locomotion. This finding would be consistent with an increase in the amount of bipedal locomotion in its locomotor repertoire but remains to be tested. While some would consider the shoulder morphology of OMO VE 3-10063 to be consistent with enhanced abilities for dextrous behaviors particularly high-speed throwing, which is thought to have emerged in *Homo c.* 2 Ma ago in Africa and to have facilitated dispersion in Eurasia (Roach *et al.* 2013), further analyses are still needed to assess more conclusively the validity of this hypothesis.

OMO VE 3-10063, like other early *Homo* included here, displays extremely low humeral torsion, and an elbow mediolaterally less stable than in non-human apes and the specimens putatively assigned to *Paranthropus*. The curvatures of the clavicle OMO VE 3-10063c, as well as the presence of a slight subclavian groove, contrast with the morphology of Pan and resemble the morphology seen in *Australopithecus* and *Homo* (no clavicle is attributed to *Paranthropus*), suggesting that the loads applied on the shoulder girdle of OMO VE 3-10063 were partly similar to those of *H. sapiens* and different from those of non-human apes. This further suggests that OMO VE 3-10063 did not extensively use its forelimb for arboreal locomotor activities. Despite the orientation of the glenoid surface of the scapula being intermediate between australopiths and *H. sapiens*, the pectoral girdle of OMO VE 3-10063 shares more similarities with *Homo* than with other hominins. Specifically, OMO VE 3-10063 displays a more horizontally oriented shaft of the clavicle, a reduced subacromial space of the scapula, a larger scapular neck, a more modern human-like shape and length of the coracoid process, and a glenoid surface closer in shape to *H. sapiens* rather than to *P. troglodytes* or most australopiths. Overall, OMO VE 3-10063 displays a modern human-like shoulder architecture associated with low mechanical advantages for (arboreal) locomotion. Despite the forelimb of the Dmanisi specimens being described as primitive (Lordkipanidze *et al.* 2007), our results suggest that most of the traits quantified here are similar to those of OMO VE 3-10063, suggesting that these specimens may be more derived than previously suggested. Overall, our results support the idea that by 1.8 Ma in Africa *Homo* reduced the use of its forelimbs in arboreal locomotion. This finding would be consistent with an increase in the amount of bipedal locomotion in its locomotor repertoire but remains to be tested. While some would consider the shoulder morphology of OMO VE 3-10063 to be consistent with enhanced abilities for dextrous behaviors particularly high-speed throwing, which is thought to have emerged in *Homo c.* 2 Ma ago in Africa and to have facilitated dispersion in Eurasia (Roach *et al.* 2013), further analyses are still needed to assess more conclusively the validity of this hypothesis.

This study provides new arguments supporting distinct ecological niches between early *Homo* and australopiths by highlighting morphological characteristics of the shoulder and forelimb that could be functionally associated with reduced performance for arboreal locomotion in early African *H. erectus* (Richmond *et al.* 2020; Patterson *et al.* 2022). Despite the substantial intra-specific variation observed in hominoids in general, and in hominins in particular (as confirmed by our study), our results nonetheless demonstrate the presence of two distinct morphotypes. Our results especially support the interpretation that the shoulder morphology of early *H. erectus* could have hindered arboreal locomotor activities, which is consistent with previous results reporting fore- and hind-limb adaptations for long-range terrestrial bipedalism (Lordkipanidze *et al.* 2007; Pontzer *et al.* 2010) or even endurance running (Bramble & Lieberman 2004) for this species. In contrast, fore- and hind-limbs of *Paranthropus* have been described as facilitating arboreal climbing (Domínguez-Rodrigo *et al.* 2013; Daver *et al.* 2018; Lague *et al.* 2019; Richmond *et al.* 2020) in combination with a form of bipedalism slightly different from that used by *Homo* (Susman & Brain 1988; Ryan *et al.* 2018; DeSilva & Grabowski 2020; Georgiou *et al.* 2020). Although the fossil record between 2.8-2.0 Ma is sparse and poorly preserved, the previous evidence also supports a behavioral divergence between *Homo* and australopiths, which perhaps reflects broader niche partitioning (O'Brien *et al.* 2023). Despite the scarce evidence supporting a strict association between lithic assemblages and *Paranthropus* (Leakey *et al.* 1964; Leakey 1971; Coppens *et al.* 1973; Prat *et al.* 2003; Pickering *et al.* 2008, 2019; Plummer *et al.* 2023), the occurrences of early *H. erectus* as a whole are concomitant with the intensification and diversification of stone tool use and making, which possibly suggests natural selection for this behavior (Leakey 1971; Asfaw *et al.* 1992; Bar-Yosef & Goren-Inbar 1993; Semaw *et al.* 1997; Kuman & Clarke 2000; Morgan *et al.* 2012; Stammers *et al.* 2018). When integrated into research on hominin evolutionary trajectories, OMO VE 3-10063, with its modern shoulder morphology, is distinct from the more primitive morphotype seen in *Australopithecus*, which seems consistent with a slow, progressive loss of arboreality accompanied by increased tool use throughout hominin evolution (Young *et al.* 2015). Thus, we propose the hypothesis here that the shoulder and forelimb morphology of the *c.* 1.84 Ma OMO VE 3-10063 individual would have also provided improved abilities for lithic tool production and use, although this remains a hypothesis that needs to be tested. Furthermore, isotopic and micro-wear analyses support that the divergence of *Homo* from australopiths seems contemporaneous with a dietary shift involving increased meat consumption in early *H. erectus* (between 2-1.65 Ma; Ungar *et al.* 2006; Balter *et al.* 2012; Cerling *et al.* 2013; Patterson *et al.* 2019; Martin *et al.* 2020), whereas evidences support that *Paranthropus* could have had a plant-based diet (Sponheimer *et al.* 2006; Ungar *et al.* 2008; Lüdecke *et al.* 2018; Martin *et al.* 2020; Wynn *et al.* 2020). Therefore, when integrated with the various morphological, behavioral, and ecological data presented above, our results on OMO VE 3-10063 support the general hypothesis that *Homo* differed ecologically from *Paranthropus*.

Acknowledgements
We are grateful to the National Museum of Ethiopia/Ethiopian Heritage Authority (ex-ARCCH, Ministry of Tourism) for allowing access to collections and to perform research. We deeply thank the NME/EHA staff (M. Endalamaw, Y. Assefa, and T. Leta) for guidance and support with the collection study. We are deeply indebted to the hundreds of people who participated to the fieldwork missions of the International Omo Research Expedition, the OGRE, and other research programs, who managed collections and databases, who prepared specimens, who contributed to their study, who provided financial support, who helped with

administrative processes, and who provided advice and moral support. The OGRE is a joint program of PALEVOPRIM, the CFEE and the EHA principally funded by the Ministry of Europe and Foreign Affairs, the National Research Agency, the Région Nouvelle-Aquitaine, CNRS INEE, PALEVOPRIM, and the Fyssen Foundation. The OGRE is extremely grateful to the EHA, the SNNPR, the South Omo Zone, the Nyangatom and Dassanetch Weredas and their people for their help and hospitality. This work also benefits from the HOMTECH grant from the National Research Agency (ANR-17-CE27-0005-02) and from the LocHoSim project from the Région Nouvelle Aquitaine (AAPR2020 2020 8624210). We are also grateful to the École Doctorale Théodore Monod (Université de Poitiers) for providing financial support. We are also grateful to the curators and staff of the following institutions: the National Museum of Ethiopia (Addis Ababa), National Museums of Kenya (Nairobi) and the Government of Kenya, the Ditsong National Museum of Natural History, South Africa (Pretoria) and the Evolutionary Studies Institute, University of the Witwatersrand, South Africa (Johannesburg). We would like to thank Dr. Gen Suwa for allowing us to use their equipment (X-ray microtomography, SkyScan 1173, at 130 kV, 40 µA, with a voxel size of 100 µm at University of Tokyo Museum, Tokyo, Japan). We would like to acknowledge and thank Y. Haile-Selassie for providing surface scans of the KSD-VP-1/1 scapula and clavicle. We thank Amélie Beaudet for scanning and providing the surface scan of KNM-WT 15000R, Emmanuel Ndiema and the curatorial staff of the National Museums of Kenya for collection access, and the National Research Foundation of South Africa (Research Development Grants for Y-Rated Researchers, grant number 129336) for funding. We would like to express our gratitude to the Musée Royal d'Afrique Centrale in Tervuren, Museum für Naturkunde in Berlin, Musée de l'Homme in Paris, and Smithonian Museum of Natural History in New-York for permission to gather the comparative data of extant non-human apes and humans. Creation of datasets accessed on MorphoSource was made possible by Lee Berger et Rebecca Cook for U.W. 88-56 and U.W. 88-57. We thank the Smithsonian Institution for providing online access to surface scans for U.W. 101-283, U.W. 101-466, and U.W. 101-948. We are grateful to Africanfossils.org for access to the surface scan of KNM KP 271. Finally, this article was peer-reviewed by PCI Paleontology (https://doi.org/10.24072/pci.paleo.100405) and we are grateful to the recommender S. Frost, the reviewer D. Green, and the two anonymous reviewers, and the associate editor, Aurélien Mounier, for their time and their helpful comments on the manuscript.

Funding

National Research Agency grant HOMTECH ANR-17-CE27-0005-02 (GD).
Région Nouvelle Aquitaine grant LOCHOSIM AAPR2020 2020 8624210 (GD).
Ministry of Europe and Foreign *Affairs Mission Paléoanthropologique dans l'Omo* (JRB).
National Research Agency project OLD (JRB).
Région Nouvelle-Aquitaine ECCE-Omo (JRB).
CNRS Écologie & Environnement International Research Project OGRE (JRB).
PALEVOPRIM support to OGRE (JRB).
Fyssen Foundation project OGRE (JRB).
École doctorale Théodore Monod – Université de Poitiers (ABT).

Author contributions

Fieldwork and authorizations to perform study: OGRE (JRB).
Design of the study: ABT, GD.
Supervision: GD.
Data collection: ABT, GD, JLV, JRB, TB, ABT, JS.
Analyses: ABT, TB, TJ, GD, JLV.
Interpretations: ABT, GD, JLV, JRB, LP, TJ.
Writing, original draft: ABT.
Writing, review and editing: ABT, GD, JRB, LP, JLV, BER, MD, TB, TJ.
Leading the OGRE: JRB, BER.

Data, script and code availability

Once published, access to the original material can be obtained by sending a request to the Ethiopian Heritage Authority, final repository of the fossil specimens collected by the Omo Group Research Expedition. The codes for statistical analysis are uploaded here: https://doi.org/10.5281/zenodo.15644796

REFERENCES

Adams D. C., Collyer M. L., Kaliontzopoulou A. & Baken E. 2022. — Geomorph: Software for geometric morphometric analyses. R package version 4.0.4.

Alemseged Z. 2003. — An integerated approach to taphonomy and faunal change in the Shungeura Formation (Ethiopia) and its implication for hominid evolution. *Journal of Human Evolution* 44 (4): 451-478. https://doi.org/10.1016/S0047-2484(03)00012-5

Alemseged Z., Spoor F., Kimbel W. H., Bobe R., Geraads D., Reed D. & Wynn J. G. 2006. — A juvenile early hominin skeleton from Dikika, Ethiopia. *Nature* 443 (7109): 296-301. https://doi.org/10.1038/nature05047

Andresen P. R., Bookstein F. L., Couradsen K., Ersboll B. K., Marsh J. L. & Kreiborg S. 2000. — Surface-bounded growth modeling applied to human mandibles. *IEEE Transactions on Medical Imaging* 19 (11): 1053-1063. https://doi.org/10.1109/42.896780

Arias-Martorell J. 2019. — The morphology and evolutionary history of the glenohumeral joint of hominoids: a review. *Ecology and Evolution* 9 (1): 703-722. https://doi.org/10.1002/ece3.4392

Arias-Martorell J., Potau J. M., Bello-Hellegouarch G. & Pérez-Pérez A. 2015. — Like father, like son: assessment of the morphological affinities of A.L. 288–1 (*A. afarensis*), Sts 7 (*A. africanus*) and Omo 119–73–2718 (*Australopithecus* sp.) through a three-dimensional shape analysis of the shoulder joint, *in* Bondioli L. (ed.). *PLOS ONE* 10 (2): e0117408. https://doi.org/10.1371/journal.pone.0117408

Asfaw B., Beyene Y., Suwa G., Walter R. C., White T. D., WoldeGabriel G. & Yemane T. 1992. — The earliest Acheulean from Konso-Gardula. *Nature* 360 (6406): 732-735. https://doi.org/10.1038/360732a0

Ashton E. H. & Oxnard C. E. 1964. — Functional adaptation in the primate shoulder girdle. *Proceedings of the Zoological Society of London* 142 (1): 49-66. https://doi.org/10.1111/j.1469-7998.1964.tb05153.x

Ashton E. H., Healy M. J. R., Oxnard C. E. & Spence T. F. 1965. — The combination of locomotor features of the primate shoulder girdle by canonical analysis. *Proceedings of the Zoological Society of London* 147 (4): 406-429. https://doi.org/10.1111/j.1469-7998.1966.tb02908.x

Balter V., Braga J., Télouk P. & Thackeray J. F. 2012. — Evidence for dietary change but not landscape use in South African early hominins. *Nature* 489 (7417): 558-560. https://doi.org/10.1038/nature11349

Bar-Yosef O. & Goren-Inbar N. (eds) 1993. — *The lithic assemblages of 'Ubeidiya: a lower palaeolithic site in the Jordan Valley*. Institute of Archaeology, Hebrew University of Jerusalem, Qedem, Jerusalem, 280 p.

Boisserie J.-R., Guy F., Delagnes A., Hlukso L. J., Bibi F., Beyene Y. & Guillemot C. 2008. — New palaeoanthropological research in the Plio-Pleistocene Omo Group, Lower Omo Valley, SNNPR (Southern Nations, Nationalities and People Regions), Ethiopia. *Comptes Rendus Palevol* 7 (7): 429-439. https://doi.org/10.1016/j.crpv.2008.07.010

Bookstein F. L. 1991. — *Morphometric tools for landmark data: geometry and biology [Orange book]*. Cambridge New York, Cambridge University Press.

Braga J., Thackeray J. F. & Zipfel B. 2022. — The Kromdraai early hominin-bearing site. A review of recent findings. *L'Anthropologie* 126 (4): 103054. https://doi.org/10.1016/j.anthro.2022.103054

Bramble D. M. & Lieberman D. E. 2004. — Endurance running and the evolution of *Homo*. *Nature* 432 (7015): 345-352. https://doi.org/10.1038/nature03052

Campisano C. J. & Feibel C. S. 2008. — Depositional environments and stratigraphic summary of the Pliocene Hadar Formation at Hadar, Afar Depression, Ethiopia, *in* Quade J. & Wynn J. G. (eds), *The Geology of Early Humans in the Horn of Africa*. Geological Society of America, Boulder, Colorado: 179-201. https://doi.org/10.1130/2008.2446(08)

Carlson K. J., Green D. J., Jashashvili T., Pickering T. R., Heaton J. L., Beaudet A., Stratford D., Crompton R., Kuman K., Bruxelles L. & Clarke R. J. 2021. — The pectoral girdle of StW 573 ('Little Foot') and its implications for shoulder evolution in the Hominina. *Journal of Human Evolution* 158: 102983. https://doi.org/10.1016/j.jhevol.2021.102983

Carretero J. M., Arsuaga J. L. & Lorenzo C. 1997. — Clavicles, scapulae and humeri from the Sima de los Huesos site (Sierra de Atapuerca, Spain). *Journal of Human Evolution* 33 (2-3): 357-408. https://doi.org/10.1006/jhev.1997.0128

Cerling T. E., Manthi F. K., Mbua E. N., Leakey L. N., Leakey M. G., Leakey R. E., Brown F. H., Grine F. E., Hart J. A., Kalem P., Roche H., Uno K. T. & Wood B. A. 2013. — Stable isotope-based diet reconstructions of Turkana Basin hominins. *Proceedings of the National Academy of Sciences* 110 (26): 10501-10506. https://doi.org/10.1073/pnas.1222568110

Churchill S. E., Holliday T. W., Carlson K. J., Jashashvili T., Macias M. E., Mathews S., Sparling T. L., Schmid P., De Ruiter D. J. & Berger L. R. 2013. — The Upper Limb of *Australopithecus sediba*. *Science* 340 (6129). https://doi.org/10.1126/science.1233477

Churchill S. E., Green D. J., Feuerriegel E. M., Macias M. E., Mathews S., Carlson K. J., Schmid P. & Berger L. 2018. — The Shoulder, Arm, and Forearm of *Australopithecus sediba*. *PaleoAnthropology*: 234-281

Cignoni P., Callieri M., Corsini M., Dellepiane M., Ganovelli F. & Ranzuglia G. 2008. — MeshLab: an Open-Source Mesh Processing Tool, *in* Scarano V., De Chiara R. & Erra U. (eds), *Eurographics Italian Chapter Conference*. The Eurographics Association: 129-136.

Coppens Y., Chavaillon J. & Beden M. 1973. — Résultats de la nouvelle mission de l'Omo (campagne 1972). Découverte de restes d'Hominidés et d'une industrie sur éclats. *Comptes Rendus de l'Académie des Sciences, Paris* 276: 161-164.

Corruccini R.S. & Ciochon R.L. 1976. — Morphometric affinities of the human shoulder. *American Journal of Physical Anthropology* 45 (1): 19-37. https://doi.org/10.1002/ajpa.1330450104

Cunningham C. B., Scheuer L. & Black S. 2016. — The vertebral colomn, *in* Cunningham C., Scheuer L. & Black S. (eds), *Developmental Juvenile Osteology*. Second Edition. Chap. 7. Academic Press, London: 177-223.

Daver G., Berillon G., Jacquier C., Ardagna Y., Yadeta M., Maurin T., Souron A., Blondel C., Coppens Y. & Boisserie J.-R. 2018. — New hominin postcranial remains from locality OMO 323, Shungura Formation, Lower Omo Valley, southwestern Ethiopia. *Journal of Human Evolution* 122: 23-32. https://doi.org/10.1016/j.jhevol.2018.03.011

DeSilva J. M. & Grabowski M. 2020. — Femur, *in* Zipfel B., Richmond B. G. & Ward C. V. (eds), *Hominin Postcranial Remains from Sterkfontein, South Africa, 1936-1995*. Ch. 12. Oxford University Press, New-York: 210-229.

Di Vincenzo F., Churchill S. E. & Manzi G. 2012. — The Vindija Neanderthal scapular glenoid fossa: comparative shape analysis suggests evo-devo changes among Neanderthals. *Journal of Human Evolution* 62 (2): 274-285. https://doi.org/10.1016/j.jhevol.2011.11.010

Dirks P. H. G. M., Kibii J. M., Kuhn B. F., Steininger C., Churchill S. E., Kramers J. D., Pickering R., Farber D. L., Mériaux A.-S., Herries A. I. R., King G. C. P. & Berger L. R. 2010. — Geological Setting and Age of *Australopithecus sediba from Southern Africa. Science* 328 (5975): 205-208. https://doi.org/10.1126/science.1184950

Dirks P. H., Roberts E. M., Hilbert-Wolf H., Kramers J. D., Hawks J., Dosseto A., Duval M., Elliott M., Evans M., Grün R., Hellstrom J., Herries A. I., Joannes-Boyau R., Makhubela T. V., Placzek C. J., Robbins J., Spandler C., Wiersma J., Woodhead J. & Berger L. R. 2017. — The age of *Homo naledi* and associated sediments in the Rising Star Cave, South Africa. *eLife* 6: e24231. https://doi.org/10.7554/eLife.24231

Domínguez-Rodrigo M., Pickering T. R., Baquedano E., Mabulla A., Mark D. F., Musiba C., Bunn H. T., Uribelarrea D., Smith V., Diez-Martin F., Pérez-González A., Sánchez P., Santonja M., Barboni D., Gidna A., Ashley G., Yravedra J., Heaton J. L. & Arriaza M. C. 2013. — First partial skeleton of a 1.34-million-year-old *Paranthropus boisei* from Bed II, Olduvai Gorge, Tanzania, *in* Curnoe D. (ed.). *PLoS ONE* 8 (12): e80347. https://doi.org/10.1371/journal.pone.0080347

Drapeau M. S. M. 2008. — Articular morphology of the proximal ulna in extant and fossil hominoids and hominins. *Journal of Human Evolution* 55 (1): 86-102. https://doi.org/10.1016/j.jhevol.2008.01.005

Drapeau M. S. M., Ward C. V., Kimbel W. H., Johanson D. C. & Rak Y. 2005. — Associated cranial and forelimb remains attributed to *Australopithecus afarensis* from Hadar, Ethiopia. *Journal of Human Evolution* 48 (6): 593-642. https://doi.org/10.1016/j.jhevol.2005.02.005

Dwight T. 1905. — The size of the articular surfaces of the long bones as characteristic of sex; an anthropological study. *American Journal of Anatomy* 4 (1): 19-31. https://doi.org/10.1002/aja.1000040103

Feibel C. S., Brown F. H. & McDougall I. 1989. — Stratigraphic context of fossil hominids from the Omo group deposits: Northern Turkana Basin, Kenya and Ethiopia. *American Journal of Physical Anthropology* 78 (4): 595-622. https://doi.org/10.1002/ajpa.1330780412

Feuerriegel E. M., Green D. J., Walker C. S., Schmid P., Hawks J., Berger L. R. & Churchill S. E. 2017. — The upper limb of *Homo naledi*. *Journal of Human Evolution* 104: 155-173. https://doi.org/10.1016/j.jhevol.2016.09.013

Feuerriegel E. M., Voisin J.-L., Churchill S. E., Haeusler M., Mathews S. & Schmid P. 2019. — Upper limb fossils of *Homo naledi* from the Lesedi Chamber, rising star system, South Africa. *Paleoanthropology* 2019: 311-349

Fifer F. C. 1987. — The adoption of bipedalism by the hominids: a new hypothesis. *Human Evolution* 2 (2): 135-147. https://doi.org/10.1007/BF02436402

Gagey O. 1985. — Etude de l'élévation du membre supérieur. Rôle des ligaments articulaires et des muscles fléchisseurs de l'articulation scapulo-humérale. *Laboratoire d'Anatomie de la Faculté de Médecine de Paris*.

Georgiou L., Dunmore C. J., Bardo A., Buck L. T., Hublin J.-J., Pahr D. H., Stratford D., Synek A., Kivell T. L. & Skinner M. M. 2020. — Evidence for habitual climbing in a Pleistocene hominin in South Africa. *Proceedings of the National Academy of Sciences* 117 (15): 8416-8423. https://doi.org/10.1073/pnas.1914481117

Gibbon R. J., Pickering T. R., Sutton M. B., Heaton J. L., Kuman K., Clarke R. J., Brain C. K. & Granger D. E. 2014. — Cosmogenic nuclide burial dating of hominin-bearing Pleistocene cave deposits at Swartkrans, South Africa. *Quaternary Geochronology* 24: 10-15. https://doi.org/10.1016/j.quageo.2014.07.004

Gower J. C. 1975. — Generalized procrustes analysis. *Psychometrika* 40 (1): 33-51. https://doi.org/10.1007/BF02291478

Granger D. E., Gibbon R. J., Kuman K., Clarke R. J., Bruxelles L. & Caffee M. W. 2015. — New cosmogenic burial ages for Sterkfontein Member 2 *Australopithecus* and Member 5 Oldowan. *Nature* 522 (7554): 85-88. https://doi.org/10.1038/nature14268

Granger D. E., Stratford D., Bruxelles L., Gibbon R. J., Clarke R. J. & Kuman K. 2022. — Cosmogenic nuclide dating of *Australopithecus* at Sterkfontein, South Africa. *Proceedings of the National Academy of Sciences* 119 (27): e2123516119. https://doi.org/10.1073/pnas.2123516119

Green D. J. 2013. — Ontogeny of the hominoid scapula: the influence of locomotion on morphology: ontogeny of hominoid scapular morphology and locomotion. *American Journal of Physical Anthropology* 152 (2): 239-260. https://doi.org/10.1002/ajpa.22353

Green D. J. & Alemseged Z. 2012. — *Australopithecus afarensis* scapular ontogeny, function, and the role of climbing in Human Evolution. *Science* 338 (6106): 514-517. https://doi.org/10.1126/science.1227123

Green D. J., Chirchir H., Mbua E., Harris J. W. K., Braun D. R., Griffin N. L. & Richmond B. G. 2018. — Scapular anatomy of *Paranthropus boisei* from Ileret, Kenya. *Journal of Human Evolution* 125: 181-192. https://doi.org/10.1016/j.jhevol.2017.06.013

Haile-Selassie Y., Latimer B. M., Alene M., Deino A. L., Gibert L., Melillo S. M., Saylor B. Z., Scott G. R. & Lovejoy C. O. 2010. — An early *Australopithecus afarensis* postcranium from Woranso-Mille, Ethiopia. *Proceedings of the National Academy of Sciences* 107 (27): 12121-12126. https://doi.org/10.1073/pnas.1004527107

Hammond A. S., Mavuso S. S., Biernat M., Braun D. R., Jinnah Z., Kuo S., Melaku S., Wemanya S. N., Ndiema E. K., Patterson D. B., Uno K. T. & Palcu D. V. 2021. — New hominin remains and revised context from the earliest *Homo erectus* locality in East Turkana, Kenya. *Nature Communications* 12 (1): 1-12. https://doi.org/10.1038/s41467-021-22208-x

Harmon E. H. 2013. — Age and Sex Differences in the Locomotor Skeleton of *Australopithecus*, *in* Reed K. E., Fleagle J. G. & Leakey R. E. (eds), *The Paleobiology of Australopithecus*. Springer (Vertebrate Paleobiology and Paleoanthropology; 18), Dordrecht: 263-272. https://doi.org/10.1007/978-94-007-5919-0_18

Heaton J. L., Pickering T. R., Carlson K. J., Crompton R. H., Jashashvili T., Beaudet A., Bruxelles L., Kuman K., Heile A. J., Stratford D. & Clarke R. J. 2019. — The long limb bones of the StW 573 *Australopithecus* Skeleton from Sterkfontein Member 2: Descriptions and Proportions. *Journal of Human Evolution* 133: 167-197. https://doi.org/10.1016/j.jhevol.2019.05.015

Heinzelin J. 1983. — *The Omo Group: Archives of the International Omo Research Expedition.* Musée royal de l'Afrique centrale. (Annalen; vol. 1), Tervuren, 365 p.

Hrdlička A. 1920. — Anthropometry. *American Journal of Physical Anthropology* 3 (1): 147-173. https://doi.org/10.1002/ajpa.1330030108

Ibáñez-Gimeno P., De Esteban-Trivigno S., Jordana X., Manyosa J., Malgosa A. & Galtés I. 2013. — Functional plasticity of the human humerus: shape, rigidity, and muscular entheses. *American Journal of Physical Anthropology* 150 (4): 609-617. https://doi.org/10.1002/ajpa.22234

Johanson D. C., Masao F. T., Eck G. G., White T. D., Walter R. C., Kimbel W. H., Asfaw B., Manega P., Ndessokia P. & Suwa G. 1987. — New partial skeleton of *Homo habilis* from Olduvai Gorge, Tanzania. *Nature* 327: 205-209. https://doi.org/10.1038/327205a0

Joss J. & Husson F. 2016. — missMDA: A package for handling missing values in multivariate data analysis. *Journal of Statistical Software* 70 (1): 1-31. https://doi.org/10.18637/jss.v070.i01

Kagaya M., Ogihara N. & Nakatsukasa M. 2010. — Is the clavicle of apes long? An investigation of clavicular length in relation to body mass and upper thoracic width. *International Journal of Primatology* 31 (2): 209-217. https://doi.org/10.1007/s10764-010-9402-x

Karakostis F. A., Haeufle D., Anastopoulou I., Moraitis K., Hotz G., Tourloukis V. & Harvati K. 2021. — Biomechanics of the human thumb and the evolution of dexterity. *Current Biology* 31 (6): 1317-1325. https://doi.org/10.1016/j.cub.2020.12.041

Kimbel W. H., Walter R. C., Johanson D. C., Reed K. E., Aronson J. L., Assefa Z., Marean C. W., Eck G. G., Bobe R., Hovers E., Rak Y., Vondra C., Yemane T., York D., Chen Y., Evensen N. M. & Smith P. E. 1996. — Late Pliocene *Homo* and Oldowan Tools from the Hadar Formation (Kada Hadar Member), Ethiopia. *Journal of Human Evolution* 31 (6): 549-561. https://doi.org/10.1006/jhev.1996.0079

Krahl V. E. 1947. — The torsion of the humerus: its localization, cause and duration in man. *American Journal of Anatomy* 80 (3): 275-319. https://doi.org/10.1002/aja.1000800302

Kuman K. & Clarke R. J. 2000. — Stratigraphy, artefact industries and hominid associations for Sterkfontein, Member 5. *Journal of Human Evolution* 38 (6): 827-847. https://doi.org/10.1006/jhev.1999.0392

Lague M. R. 2015. — Taxonomic identification of Lower Pleistocene fossil hominins based on distal humeral diaphyseal cross-sectional shape. *PeerJ* 3: e1084. https://doi.org/10.7717/peerj.1084

Lague M. R. 2019. — Another massive distal humerus of *Paranthropus boisei* from Koobi Fora, Kenya. *American Journal of Physical Anthropology* 168: 134-135.

Lague M. R., Chirchir H., Green D. J., Mbua E., Harris J. W. K., Braun D. R., Griffin N. L. & Richmond B. G. 2019. — Humeral anatomy of the KNM-ER 47000 upper limb skeleton from Ileret, Kenya: Implications for taxonomic identification. *Journal of Human Evolution* 126: 24-38. https://doi.org/10.1016/j.jhevol.2018.06.011

LARSON S. G. 1988. — Subscapularis function in gibbons and chimpanzees: Implications for interpretation of humeral head torsion in hominoids. *American Journal of Physical Anthropology* 76 (4): 449-462. https://doi.org/10.1002/ajpa.1330760405

LARSON S. G. 1995. — New characters for the functional interpretation of primate scapulae and proximal humeri. *American Journal of Physical Anthropology* 98 (1): 13-35. https://doi.org/10.1002/ajpa.1330980103

LARSON S. G. 1996. — Estimating humeral torsion on incomplete fossil anthropoid humeri. *Journal of Human Evolution* 31 (3): 239-257. https://doi.org/10.1006/jhev.1996.0059

LARSON S. G. 2007. — Evolutionary transformation of the hominin shoulder. *Evolutionary Anthropology: Issues, News, and Reviews* 16 (5): 172-187. https://doi.org/10.1002/evan.20149

LARSON S. G. 2009. — Evolution of the Hominin Shoulder: Early *Homo*, *in* GRINE F. E., FLEAGLE J. G. & LEAKEY R. E. (eds), *The First Humans – Origin and Early Evolution of the Genus* Homo. *Vertebrate Paleobiology and Paleoanthropology.* Springer, Dordrecht: 65-75. https://doi.org/10.1007/978-1-4020-9980-9_7

LARSON S. G. 2013. — Shoulder Morphology in Early Hominin Evolution, *in* REED K. E., FLEAGLE J. G. & LEAKEY R. E. (eds), *The Paleobiology of Australopithecus. Vertebrate Paleobiology and Paleoanthropology*. Springer Netherlands, Dordrecht: 247-261. https://doi.org/10.1007/978-94-007-5919-0_17

LARSON S. G., JUNGERS W. L., TOCHERI M. W., ORR C. M., MORWOOD M. J., SUTIKNA T., AWE R. D. & DJUBIANTONO T. 2009. — Descriptions of the upper limb skeleton of *Homo floresiensis*. *Journal of Human Evolution* 57 (5): 555-570. https://doi.org/10.1016/j.jhevol.2008.06.007

LEAKEY L., TOBIAS P. V. & NAPIER J. R. 1964. — A new species of the genus *Homo* from Olduvai Gorge. *Nature* 202 (4927): 7-9. https://doi.org/10.1038/202007a0

LEAKEY M. D. 1971. — *Olduvai Gorge: Volume 3, Excavations in Beds I and II, 1960-1963*. Cambridge University Press, 378 p.

LEAKEY R. E. F. & WALKER A. C. 1985. — Further hominids from the Plio-Pleistocene of Koobi Fora, Kenya. *American Journal of Physical Anthropology* 67 (2): 135-163. https://doi.org/10.1002/ajpa.1330670209

LEE E. C. S., ROACH N. T., CLOUTHIER A. L., BICKNELL R. T., BEY M. J., YOUNG N. M. & RAINBOW M. J. 2020. — Three-dimensional scapular morphology is associated with rotator cuff tears and alters the abduction moment arm of the supraspinatus. *Clinical Biomechanics* 78: 105091. https://doi.org/10.1016/j.clinbiomech.2020.105091

LEE E. C. S., YOUNG N. M. & RAINBOW M. J. 2023. — A comparative approach for characterizing the relationship among morphology, range-of-motion and locomotor behaviour in the primate shoulder. *Proceedings of the Royal Society B: Biological Sciences* 290: 20231446. https://doi.org/10.1098/rspb.2023.1446

LORDKIPANIDZE D., JASHASHVILI T., VEKUA A., DE LEÓN M. S. P., ZOLLIKOFER C. P. E., RIGHTMIRE G. P., PONTZER H., FERRING R., OMS O., TAPPEN M., BUKHSIANIDZE M., AGUSTI J., KAHLKE R., KILADZE G., MARTINEZ-NAVARRO B., MOUSKHELISHVILI A., NIORADZE M. & ROOK L. 2007. — Postcranial evidence from early *Homo* from Dmanisi, Georgia. *Nature* 449 (7160): 305-310. https://doi.org/10.1038/nature06134

LOVEJOY C. O., SIMPSON S. W., WHITE T. D., ASFAW B. & SUWA G. 2009. — Careful climbing in the Miocene: the forelimbs of *Ardipithecus ramidus* and humans are primitive. *Science* 326 (5949): 70-70e8. https://doi.org/10.1126/science.1175827

LÜDECKE T., KULLMER O., WACKER U., SANDROCK O., FIEBIG J., SCHRENK F. & MULCH A. 2018. — Dietary versatility of Early Pleistocene hominins. *Proceedings of the National Academy of Sciences* 115 (52): 13330-13335. https://doi.org/10.1073/pnas.1809439115

MACIAS M. E. & CHURCHILL S. E. 2015. — Functional morphology of the Neandertal scapular glenoid fossa. *The Anatomical Record* 298 (1): 168-179. https://doi.org/10.1002/ar.23072

MACLEAN K. F. E. & DICKERSON C. R. 2020. — Development of a comparative chimpanzee musculoskeletal glenohumeral model: implications for human function. *The Journal of Experimental Biology* 223 (22): jeb225987. https://doi.org/10.1242/jeb.225987

MARTIN J. E., TACAIL T., BRAGA J., CERLING T. E. & BALTER V. 2020. — Calcium isotopic ecology of Turkana Basin hominins. *Nature Communications* 11 (1): 3587. https://doi.org/10.1038/s41467-020-17427-7

MARTIN R. 1957. — *Lehrbuch der Anthropologie in systematischer Darstellung mit besouderer Berücksichtigung der anthropologischen Methoden.* Vol. 1. G. Fischer (Lehrbuch der Anthropologie in systematischer Darstellung), Stuttgart, 518 p.

MCDOUGALL I. & BROWN F. H. 2006. — Precise $^{40}Ar/^{39}Ar$ geochronology for the upper Koobi Fora Formation, Turkana Basin, northern Kenya. *Journal of the Geological Society* 163 (1): 205-220. https://doi.org/10.1144/0016-764904-166

MCDOUGALL I. & BROWN F. H. 2008. — Geochronology of the pre-KBS tuff sequence, Omo Group, Turkana Basin. *Journal of the Geological Society* 165 (2): 549-562. https://doi.org/10.1144/0016-76492006-170

MCDOUGALL I., BROWN F. H., VASCONCELOS P. M., COHEN B. E., THIEDE D. S. & BUCHANAN M. J. 2012. — New single crystal $^{40}Ar/^{39}Ar$ ages improve time scale for deposition of the Omo Group, Omo–Turkana Basin, East Africa. *Journal of the Geological Society* 169 (2): 213-226. https://doi.org/10.1144/0016-76492010-188

MCHENRY H. M. & CORRUCCINI R. S. 1975. — Distal humerus in hominoid evolution. *Folia Primatologica; International Journal of Primatology* 23 (3): 117-144.

MCHENRY L. J. 2012. — A revised stratigraphic framework for Olduvai Gorge Bed I based on tuff geochemistry, Five Decades after Zinjanthropus and *Homo habilis*: landscape Paleoanthropology of Plio-Pleistocene Olduvai Gorge, Tanzania. *Journal of Human Evolution* 63 (2): 284-299. https://doi.org/10.1016/j.jhevol.2011.04.010

MELILLO S. M. 2016. — The Shoulder Girdle of KSD-VP-1/1, *in* HAILE-SELASSIE Y. & SU D. F. (eds), *The Postcranial Anatomy of* Australopithecus afarensis. *Vertebrate Paleobiology and Paleoanthropology.* Springer Netherlands, Dordrecht: 113-141. https://doi.org/10.1007/978-94-017-7429-1_6

MELILLO S., GUNZ P., COQUEUGNIOT H., RESKE S. & HUBLIN J.-J. 2019. — Structural effects of variation in the human clavicle. *American Journal of Physical Anthropology* 168 (4): 687-704. https://doi.org/10.1002/ajpa.23787

MGELADZE A., LORDKIPANIDZE D., MONCEL M.-H., DESPRIEE J., CHAGELISHVILI R., NIORADZE M. & NIORADZE G. 2011. — Hominin occupations at the Dmanisi site, Georgia, Southern Caucasus: raw materials and technical behaviours of Europe's first hominins. *Journal of Human Evolution* 60 (5): 571-596. https://doi.org/10.1016/j.jhevol.2010.10.008

MORGAN L. E., RENNE P. R., KIEFFER G., PIPERNO M., GALLOTTI R. & RAYNAL J.-P. 2012. — A chronological framework for a long and persistent archaeological record: Melka Kunture, Ethiopia. *Journal of Human Evolution* 62 (1): 104-115. https://doi.org/10.1016/j.jhevol.2011.10.007

MORREY B. F. & AN K.-N. 1983. — Articular and ligamentous contributions to the stability of the elbow joint. *The American Journal of Sports Medicine* 11 (5): 315-319. https://doi.org/10.1177/036354658301100506

MURTAGH F. & LEGENDRE P. 2014. — Ward's hierarchical agglomerative clustering method: clustering criterion and agglomerative algorithm. *Journal of Classification* 31: 274-295. https://doi.org/10.1007/s00357-014-9161-z

O'BRIEN K., HEBDON N. & FAITH J. T. 2023. — Paleoecological evidence for environmental specialization in *Paranthropus boisei* compared to early *Homo*. *Journal of Human Evolution* 177: 103325. https://doi.org/10.1016/j.jhevol.2023.103325

PATTERSON & HOWELLS 1967. — Hominid Humeral Fragment from Early Pleistocene of Northwestern Kenya.

Patterson D. B., Braun D. R., Allen K., Barr W. A., Behrensmeyer A. K., Biernat M., Lehmann S. B., Maddox T., Manthi F. K., Merritt S. R., Morris S. E., O'Brien K., Reeves J. S., Wood B. A. & Bobe R. 2019. — Comparative isotopic evidence from East Turkana supports a dietary shift within the genus *Homo*. *Nature Ecology & Evolution* 3 (7): 1048-1056. https://doi.org/10.1038/s41559-019-0916-0

Patterson D. B., Du A., Faith J. T., Rowan J., Uno K., Behrensmeyer A. K., Braun D. R. & Wood B. A. 2022. — Did vegetation change drive the extinction of *Paranthropus boisei*? *Journal of Human Evolution* 173: 103154. https://doi.org/10.1016/j.jhevol.2022.103154

Pickering T. R., Egeland C. P., Domínguez-Rodrigo M., Brain C. K. & Schnell A. G. 2008. — Testing the "shift in the balance of power" hypothesis at Swartkrans, South Africa: Hominid cave use and subsistence behavior in the Early Pleistocene. *Journal of Anthropological Archaeology* 27 (1): 30-45. https://doi.org/10.1016/j.jaa.2007.07.002

Pickering T. R., Heaton J. L., Clarke R. J. & Stratford D. 2019. — Hominin vertebrae and upper limb bone fossils from Sterkfontein Caves, South Africa (1998-2003 excavations). *American Journal of Physical Anthropology* 168 (3): 459-480. https://doi.org/10.1002/ajpa.23758

Plummer T. W., Oliver J. S., Finestone E. M., Ditchfield P. W., Bishop L. C., Blumenthal S. A., Lemorini C., Caricola I., Bailey S. E., Herries A. I. R., Parkinson J. A., Whitfield E., Hertel F., Kinyanjui R. N., Vincent T. H., Li Y., Louys J., Frost S. R., Braun D. R., Reeves J. S., Early E. D. G., Onyango B., Lamela-Lopez R., Forrest F. L., He H., Lane T. P., Frouin M., Nomade S., Wilson E. P., Bartilol S. K., Rotich N. K. & Potts R. 2023. — Expanded geographic distribution and dietary strategies of the earliest Oldowan hominins and *Paranthropus*. *Science* 379 (6632): 561-566. https://doi.org/10.1126/science.abo7452

Pobiner B. L. 2020. — The zooarchaeology and paleoecology of early hominin scavenging. *Evolutionary Anthropology: Issues, News, and Reviews* 29 (2): 68-82. https://doi.org/10.1002/evan.21824

Pontzer H., Rolian C., Rightmire G. P., Jashashvili T., Ponce de León M. S., Lordkipanidze D. & Zollikofer C. 2010. — Locomotor anatomy and biomechanics of the Dmanisi hominins. *Journal of Human Evolution* 58 (6): 492-504. https://doi.org/10.1016/j.jhevol.2010.03.006

Prat S., Brugal J.-P., Roche H. & Texier P.-J. 2003. — Nouvelles découvertes de dents d'hominidés dans le membre Kaitio de la formation de Nachukui (1,65–1,9 Ma), Ouest du lac Turkana (Kenya). *Comptes Rendus Palevol* 2 (8): 685-693. https://doi.org/10.1016/j.crpv.2003.07.001

Prat S., Brugal J.-P., Tiercelin J.-J., Barrat J.-A., Bohn M., Delagnes A., Harmand S., Kimeu K., Kibunjia M., Texier P.-J. & Roche H. 2005. — First occurrence of early *Homo* in the Nachukui Formation (West Turkana, Kenya) at 2.3-2.4 Myr. *Journal of Human Evolution* 49 (2): 230-240. https://doi.org/10.1016/j.jhevol.2005.03.009

Prost J. H. 1965. — A Definitional System for the Classification of Primate Locomotion. *American Anthropologist* 67 (5): 1198-1214. https://doi.org/10.1525/aa.1965.67.5.02a00060

Raventós-Izard G., Potau J. M., Casado A., Pastor J. F. & Arias-Martorell J. 2023. — The morphofunctional implications of the glenoid *labrum* of the glenohumeral joint in hominoids. *American Journal of Biological Anthropology*181 (2): 195-205. https://doi.org/10.1002/ajpa.24729

Richmond B. G., Green D. J., Lague M. R., Chirchir H., Behrensmeyer A. K., Bobe R., Bamford M. K., Griffin N. L., Gunz P., Mbua E., Merritt S. R., Pobiner B., Kiura P., Kibunjia M., Harris J. W. K. & Braun D. R. 2020. — The upper limb of *Paranthropus boisei* from Ileret, Kenya. *Journal of Human Evolution* 141: 102727. https://doi.org/10.1016/j.jhevol.2019.102727

Rightmire G. P. 2001. — Patterns of hominid evolution and dispersal in the Middle Pleistocene. *Quaternary International* 75 (1): 77-84. https://doi.org/10.1016/S1040-6182(00)00079-3

Roach N. T. & Richmond B. G. 2014. — Clavicle length, throwing performance and the reconstruction of the *Homo erectus* shoulder. *Journal of Human Evolution* 80: 107-113. https://doi.org/10.1016/j.jhevol.2014.09.004

Roach N. T. & Richmond B. G. 2015. — Humeral torsion does not dictate shoulder position, but does influence throwing speed. *Journal of Human Evolution* 85: 206-211. https://doi.org/10.1016/j.jhevol.2015.05.011

Roach N. T., Lieberman D. E., Gill T. J., Palmer W. E. & Gill T. J. 2012. — The effect of humeral torsion on rotational range of motion in the shoulder and throwing performance: Humeral torsion and range of motion in the shoulder. *Journal of Anatomy* 220 (3): 293-301. https://doi.org/10.1111/j.1469-7580.2011.01464.x

Roach N. T., Venkadesan M., Rainbow M. J. & Lieberman D. E. 2013. — Elastic energy storage in the shoulder and the evolution of high-speed throwing in *Homo*. *Nature* 498 (7455): 483-486. https://doi.org/10.1038/nature12267

Rose M. D. 1988. — Another look at the anthropoid elbow. *Journal of Human Evolution* 17 (1-2): 193-224. https://doi.org/10.1016/0047-2484(88)90054-1

Ruff C., Holt B. & Trinkaus E. 2006. — Who's afraid of the big bad Wolff?: "Wolff's law" and bone functional adaptation. *American Journal of Physical Anthropology* 129 (4): 484-498. https://doi.org/10.1002/ajpa.20371

Ryan T. M., Carlson K. J., Gordon A. D., Jablonski N., Shaw C. N. & Stock J. T. 2018. — Human-like hip joint loading in *Australopithecus africanus* and *Paranthropus robustus*. *Journal of Human Evolution* 121: 12-24. https://doi.org/10.1016/j.jhevol.2018.03.008

Schneider C. A., Rasband W. S. & Eliceiri K. W. 2012. — NIH Image to ImageJ: 25 years of image analysis. *Nature Methods* 9 (7): 671-675. https://doi.org/10.1038/nmeth.2089

Selby M. S. & Lovejoy C. O. 2017. — Evolution of the hominoid scapula and its implications for earliest hominid locomotion: Selby and Lovejoy. *American Journal of Physical Anthropology* 162 (4): 682-700. https://doi.org/10.1002/ajpa.23158

Semaw S., Renne P., Harris J. W. K., Feibel, Craig S, Bernor R. L., Fesseha N. & Mowbray K. 1997. — 2.5-million-year-old stone tools from Gona, Ethiopia. *Nature* 385: 333-336. https://doi.org/10.1038/385333a0

Senut B. 1981. — *L'humérus et ses articulations chez les Hominidés plio-pléistocènes*. CNRS Éditions (Cahiers de paléontologie), Paris, 141 p.

Sheets H. D., Kim K. & Mitchell C. E. 2004. — A combined landmark and outline-based approach to ontogenetic shape change in the Ordovician trilobite *Triarthrus becki*, *in* Elewa A. M. T. (ed.), *Morphometrics*. Springer, Berlin, Heidelberg: 67-82. https://doi.org/10.1007/978-3-662-08865-4_6

Skinner M. M., Stephens N. B., Tsegai Z. J., Foote A. C., Nguyen N. H., Gross T., Pahr D. H., Hublin J.-J. & Kivell T. L. 2015. — Human-like hand use in *Australopithecus africanus*. *Science* 347 (6220): 395-399. https://doi.org/10.1126/science.1261735

Sponheimer M., Passey B. H., De Ruiter D. J., Guatelli-Steinberg D., Cerling T. E. & Lee-Thorp J. 2006. — Isotopic Evidence for Dietary Variability in the Early Hominin *Paranthropus robustus*. *Science* 314 (5801): 980-982. https://doi.org/10.1126/science.1133827

Squyres N. & DeLeon V. B. 2015. — Clavicular curvature and locomotion in anthropoid primates: A 3D geometric morphometric analysis. *American Journal of Physical Anthropology* 158 (2): 257-268. https://doi.org/10.1002/ajpa.22785

STAMMERS R. C., CARUANA M. V. & HERRIES A. I. R. 2018. — The first bone tools from Kromdraai and stone tools from Drimolen, and the place of bone tools in the South African Earlier Stone Age. *Quaternary International* 495: 87-101. https://doi.org/10.1016/j.quaint.2018.04.026

STERN J. T. & SUSMAN R. L. 1983. — The locomotor anatomy of *Australopithecus afarensis*. *American Journal of Physical Anthropology* 60 (3): 279-317. https://doi.org/10.1002/ajpa.1330600302

SUSMAN R. L. & BRAIN T. M. 1988. — New first metatarsal (SKX 5017) from Swartkrans and the gait of *Paranthropus robustus*. *American Journal of Physical Anthropology* 77 (1): 7-15. https://doi.org/10.1002/ajpa.1330770103

SUSMAN R. L., DE RUITER D. & BRAIN C. K. 2001. — Recently identified postcranial remains of *Paranthropus* and Early *Homo* from Swartkrans Cave, South Africa. *Journal of Human Evolution* 41 (6): 607-629. https://doi.org/10.1006/jhev.2001.0510

TAYLOR C., MASAO F., NJAU J. K., SONGITA A. V. & HLUSKO L. J. 2024. — OH 89: A newly described ~1.8-million-year-old hominid clavicle from Olduvai Gorge. *Peer Community Journal* 4. https://doi.org/10.1101/2023.02.02.526656

THOMPSON N. E., RUBINSTEIN D., & LARSON S. G. 2018. — Great ape thorax and shoulder configuration - An adaptation for arboreality or knuckle walking? *Journal of Human Evolution* 125: 15-26. https://doi.org/10.1016/j.jhevol.2018.09.005

THRUN M. C. 2021. — Distance-based clustering challenges for unbiased benchmarking studies. *Scientific Reports* 11: 18988. https://doi.org/10.1038/s41598-021-98126-1

TROYANSKAYA O., CANTOR M., SHERLOCK G., BROWN P., HASTIE T., TIBSHIRANI R., BOTSTEIN D. & ALTMAN R. B. 2001. — Missing value estimation methods for DNA microarrays. *Bioinformatics* 17 (6): 520-525. https://doi.org/10.1093/bioinformatics/17.6.520

UNGAR P. S., GRINE F. E. & TEAFORD M. F. 2008. — Dental Microwear and Diet of the Plio-Pleistocene Hominin *Paranthropus boisei*. *PLoS ONE* 3 (5): 10. https://doi.org/10.1371/journal.pone.0002044

UNGAR P. S., GRINE F. E. & TEAFORD M. F. 2006. — Diet in Early *Homo*: a review of the evidence and a new model of adaptive versatility. *Annual Review of Anthropology* 35 (1): 209-228. https://doi.org/10.1146/annurev.anthro.35.081705.123153

VANDERMEERSH B. 1995. — The Postcranial Remains of the Régourdou 1 Neandertal: the shoulder and arm remains. *Journal of Human Evolution* 28 (5): 439-476. https://doi.org/10.1006/jhev.1995.1034

VILLMOARE B., KIMBEL W. H., SEYOUM C., CAMPISANO C. J., DIMAGGIO E. N., ROWAN J., BRAUN D. R., ARROWSMITH J. R. & REED K. E. 2015. — Early *Homo* at 2.8 Ma from Ledi-Geraru, Afar, Ethiopia. *Science* 347 (6228): 1352-1355. https://doi.org/10.1126/science.aaa1343

VOISIN J.-L. 2000. — *L'épaule des hominidés : Aspects architecturaux et fonctionnels, références particulières à la clavicule*. Thèse de doctorat, Muséum national d'histoire naturelle, Paris, 442 p.

VOISIN J.-L. 2006. — Clavicle, a neglected bone: morphology and relation to arm movements and shoulder architecture in primates. *The Anatomical Record Part A: Discoveries in Molecular, Cellular, and Evolutionary Biology* 288A (9): 944-953. https://doi.org/10.1002/ar.a.20354

VOISIN J.-L., ROPARS M. & THOMAZEAU H. 2014. — The human acromion viewed from an evolutionary perspective. *Orthopaedics & Traumatology: Surgery & Research* 100 (8): S355-S360. https://doi.org/10.1016/j.otsr.2014.09.011

WALLACE I. J., MIDDLETON K. M., LUBLINSKY S., KELLY S. A., JUDEX S., GARLAND JR. T. & DEMES B. 2010. — Functional significance of genetic variation underlying limb bone diaphyseal structure. *American Journal of Physical Anthropology* 143 (1): 21-30. https://doi.org/10.1002/ajpa.21286

WALKER A. & LEAKEY R. E. (eds) 1993. — *The Nariokotome* Homo erectus *skeleton*. Springer-Verlag, Berlin, 457 p.

WANG W. J. & CROMPTON R. H. 2004. — The role of load-carrying in the evolution of modern body proportions. *Journal of Anatomy* 204 (5): 417-430. https://doi.org/10.1111/j.0021-8782.2004.00295.x

WARD C. V. 2015. — Postcranial and locomotor adaptations of Hominoids, *in* HENKE W. & TATTERSALL I. (eds), *Handbook of Paleoanthropology*. Springer, Heidelberg, Berlin: 1363-1386.

WARD J. H. 1963. — Hierarchical Grouping to Optimize an Objective Function. *Journal of the American Statistical Association* 58 (301): 236-244. https://doi.org/10.1080/01621459.1963.10500845

WHITE T. D. & FOLKENS P. A. 2005. — Thorax: Sternum and Ribs, *in* WHITE T. D. & FOLKENS P. A. (eds), *The Human Bone Manual.* Ch. 10. Academic Press, Burlington, MA: 153-176.

WOOD B. & CONSTANTINO P. 2007. — *Paranthropus boisei*: Fifty years of evidence and analysis. *American Journal of Physical Anthropology* 134 (S45): 106-132. https://doi.org/10.1002/ajpa.20732

WOOD B. & STRAIT D. 2004. — Patterns of resource use in early *Homo* and *Paranthropus*. *Journal of Human Evolution* 46 (2): 119-162. https://doi.org/10.1016/j.jhevol.2003.11.004

WYNN J. G., ALEMSEGED Z., BOBE R., GRINE F. E., NEGASH E. W. & SPONHEIMER M. 2020. — Isotopic evidence for the timing of the dietary shift toward C4 foods in eastern African *Paranthropus*. *Proceedings of the National Academy of Sciences* 117 (36): 21978-21984. https://doi.org/10.1073/pnas.2006221117

YEGIAN A. K., TUCKER Y., GILLINOV S. & LIEBERMAN D. E. 2021. — Shorter distal forelimbs benefit bipedal walking and running mechanics: implications for hominin forelimb evolution. *American Journal of Physical Anthropology* 175 (3): 589-598. https://doi.org/10.1002/ajpa.24274

YOUNG N. M., CAPELLINI T. D., ROACH N. T. & ALEMSEGED Z. 2015. — Fossil hominin shoulders support an African ape-like last common ancestor of humans and chimpanzees. *Proceedings of the National Academy of Sciences* 112 (38): 11829-11834. https://doi.org/10.1073/pnas.1511220112

ZYLSTRA M. 2000. — *Functional morphology of the hominoid forelimb, implications for knuckle-walking and the origin of hominid bipedalism Thesis*. PhD thesis, University of Toronto, 231 p.

Submitted on 2 February 2026;
accepted on 2 March 2026;
published on 8 July 2026.

APPENDICES

Appendix 1. — Geological context of the associated remains of OMO VE 3-10063.

GEOLOGICAL CONTEXT OF THE ASSOCIATED REMAINS OF OMO VE 3-10063.

OMO VE 3-10063 was found in Member H, Unit H-4 of the Shungura Formation (Ethiopia), in the OMO VE 3 locality (Appendix 2). The specimen is located *c.* 100 m north of the detailed stratigraphic log established by the International Omo Research Expedition (IORE, from 1967 to 1976) for Member H (Heinzelin 1983). H deposits are characterized by alternating sandy to clayey silt deposits of fluvio-deltaic origin, interpreted as mudflats to deltaic and lacustrine facies (Heinzelin 1983). The fauna documented in this member by the IORE is predominantly composed of bovids and hippopotamids, reflecting a humid environment (Alemseged 2003). However, the mammalian fauna collected by the OGRE is more diversified. In this new collection, although Reduncini are still the most abundant taxon (23.5% of the whole sample), followed by Hippopotamidae (15.1%), Equidae (11.4%) and Cercopithecidae (7.4%), they were found nearly ten times and five times more abundant, respectively, than in the IORE collection. Similar results are noted for Carnivora, Aepycerotini, Alcelaphini, Antilopini, and Hominidae. This is partly due to a more selective collection by OGRE, increasing the number of identifiable specimens relative to the total number of collected specimens (notably for bovids). However, it also reflects a different faunal composition; e.g., there were about 37% more cercopithecid remains collected in Member H by the OGRE compared to the IORE, although the latter collected a total number of specimens more than three times greater. These differences could be interpreted as a more complex environmental signal.

In contrast to older members of the Shungura Formation (from 3.75 to 1.9 Ma), only four specimens have been attributed to hominins in Member H, all in the same catchment: a metatarsal III attributed to an undetermined hominid and a tooth attributed to *Homo* cf. *habilis* discovered by the IORE, and, at locality OMO VE 3, a gracile tooth attributed to *Homo* sp., and the presently described set of bones.

Unit H-4 is characterized by silty deposits of primarily lacustrine origin (Appendix 2). The depositional environment is interpreted to be marshier in the last few meters of the unit. The $^{40}Ar/^{39}Ar$ radiometric dating method has resulted in an age estimate of the Tuff H-4, which lies about 2 meters below the discovery area of the remains of OMO VE 3-10063, at 1.843 ± 0.023 Ma (McDougall & Brown 2006).

All OMO VE 3-10063 elements were collected during fieldwork campaigns conducted in 2011 and 2012 by the OGRE (Boisserie *et al.* 2008). The humerus (OMO VE 3-10063a), composed of three fragments, was first found on July 16th, 2011, by Sakir Özkurt on an eroded slope located about 2 m above Tuff H-4 (Appendix 2). The distal fragment was partially in the sediments, in contrast to the two other humeral fragments that were found further down the slope (Appendix 2). The scapula OMO VE 3-10063b was found in situ in a whitish clayey silt layer below the humerus distal fragment. These four bone fragments were found nearly aligned following the slope, and the distance between the uppermost and lowermost fragments (distal and proximal humerus fragments, respectively) was 80 cm. The lag covering the slope was sieved on a surface of *c.* 30 m² (from top to bottom of the slope), resulting in the finding of a few unrelated bone fragments. An excavation was performed at the level of the fragments, but it did not allow for the discovery of other elements. The four fragments of the clavicle OMO VE 3-10063c were discovered during the 2012 fieldwork campaign by sieving the sediment lag filling the channel located at the foot of the slope, about 2 m south of the humerus and scapula. The three refitting fragments of the rib OMO VE 3-10063f were found by scraping the lag again, 2 m south of the clavicular remains. The vertebral fragments were found another 3 m further south from the rib fragments, one by sieving (OMO VE 3-10063d), the other by scraping the lag (OMO VE 3-10063e). More excavation and sieving operations were performed on this surface in 2012 and subsequent years, but did not result in further discoveries.

The single-individual nature of all the shoulder elements found is supported by the restricted area of the outcrop (less than 0.2 m²) in which the scapula and the humeral fragments were discovered in situ or freshly eroded. Moreover, the elements all belong to the right shoulder, and the developmental stage and the size of the different bone elements support the attribution of these remains to the same individual.

DESCRIPTION OF OMO VE 3-10063

OMO VE 3-10063a – RIGHT HUMERUS

Preservation

OMO VE 3-10063a is a complete right humerus that consists of three refitting fragments of equivalent proximodistal length: a proximal fragment that includes the head, the distal part of the bicipital groove and a portion of the shaft; a diaphyseal fragment and a distal fragment in perfect condition, that includes the capitulum, the trochlea, the olecranon fossa, radial and coronoid fossae and both epicondyles.

All fragments are light beige colored and covered with spots of manganese, especially concentrated on the epiphyses. The junction between the fragments can be established with matching broken surfaces, fissures, and regions of preserved cortical bone. A transverse fracture separates the proximal fragment (maximum length of 125.3 mm) from the diaphyseal fragment (maximum length of 124.5 mm). The diaphyseal fragment is separated from the distal fragment (maximum length of 100.6 mm) by an oblique fracture oriented posteroproximally to anterodistally.

Morphology

The humerus has a maximum length of 338.8 mm and a physiological length of 337.1 mm. The humeral head is oriented posteriorly, which indicates a small amount of torsion (110°). The articular surface of the humeral head is almost spherical in proximal view (sagittal diameter = 43.1 mm, transverse diameter = 40.5 mm). Although this humeral portion has undergone significant erosion, these dimensions are valid because they are based on fully preserved portions of cortical bone (Fig. 1). Despite the erosion of the proximal ends of the greater and lesser tubercles, the preserved portion of the bicipital groove indicates that it is shallow and wide (ML width = 14.5 mm). The lateral lip of the bicipital groove is shallow proximally and forms a slight bulge distally, corresponding to the *m. pectoralis major* enthesis. The medial lip of the bicipital groove (*mm. teres major* and *latissimus dorsi* entheses) forms a rounded bulge and extends less distally than the lateral lip.

At the fracture point between the proximal and the diaphyseal fragment, the shaft has a teardrop-shaped transverse cross-section, with its lateral edge constituting the portion of greatest convexity and the medial edge's least rounded portion. The shaft is slightly flattened mediolaterally. The deltoid tuberosity is not discernible.

The lateral supracondylar ridge is faint and forms a slight rounded bulge. Still along the lateral border, a flat, rough surface, delimited by a small ridge, is present on the anterior surface of the humerus, set proximally on the lateral epicondyle and corresponding to the origin of *mm. brachioradialis* and *extensor carpi radialis longus.*

The lateral epicondyle is prominent and just proximal to the capitulum. The maximum projection of the lateral epicondyle, from the groove between the lateral crest of the trochlea and the capitulum, is 29.8 mm. The lateral epicondyle forms a rounded, slightly anteriorly curved bulge. This configuration is accentuated by a deep radial fossa, which has a double concavity and extends widely laterally toward the epicondyle. The common extensor tendon origin (*mm. extensor carpi radialis brevis, extensor digitorum, extensor digiti minimi, extensor carpi ulnaris* and *supinator*) is marked by a slight depression on the lateral border, below the bulge formed by the lateral epicondyle. This depression does not extend posteriorly, but extends distally toward a small bulge, positioned approximately at the same level as the center of the capitulum.

The medial epicondyle is 12.1 mm thick and has a 42.1 mm medial projection from the lateral crest of the trochlea.

The common flexor tendon origin (*mm. pronator teres, flexor carpi radialis, palmaris longus, flexor carpi ulnaris,* and *flexor digitorum superficialis*) is marked by a roughened area on the medial border of the epicondyle, which forms a depression distally and a prominent bulge proximally. In medial view, the epicondyle is slightly deviated anteriorly.

The capitulum is spherical, measuring 17.7 mm in mediolateral diameter and 19.4 mm in superoinferior height. It is proximally domed and flattens on the distal edge of the humerus such that it has an elliptical shape in lateral view. In distal view, the lateral margin of the capitulum forms a prominent and oblique ridge proximolaterally to distomedially. The zona conoidea is wide. The radial fossa is wider (19.2 mm ML) than the coronoid fossa (16.8 mm ML) and also shallower. Both fossae have approximately the same height. The trochlea has a width of 23.7 mm and a diameter of 15.1 mm AP. The lateral ridge of the trochlea has a diameter of 21.0 mm AP. The medial crest has a diameter of 23.2 mm AP and a height of 17.9 mm and is distally projected relative to the lateral crest. The trochlear notch is shallow. In this section, the lateral crest of the trochlea has a relatively smooth edge in its anterior portion and is sharper in its posterior portion. The medial crest of the trochlea has a sharp edge anteriorly and posteriorly. In medial view, it forms a crescent, slightly concave on its medial edge. In posterior view, the two crests are oblique (proximolateral to distomedial). The olecranon fossa is deep (7.4 mm), has a width of 24.5 mm, and is subtriangular in shaped. The fossa is bordered by a medial pillar that is notably narrower (10.8 mm) than its lateral counterpart (17.9 mm).

OMO VE 3-10063b – RIGHT SCAPULAR FRAGMENT

Preservation

Most of the lateral part of the scapula OMO VE 3-10063b is well preserved. It includes the lateral portion of the scapular spine and most of its acromial end, almost the entire coracoid process, and the glenoid cavity, and the proximalmost portion (32.3 mm in length) of the axillary border. The spinal border is entirely missing. The proximal edge of the scapula is fractured obliquely, proximolaterally to distomedially, from a point located just medial to the scapular incision to the spine, 47.8 mm from the base of the acromion. Following this fracture, another oblique fracture proximo-medially to distolaterally, extending from the spine to the axillary margin, is present. The medial and distal parts of the scapula are not preserved past these fractures. The scapular fragment is completely covered with large manganese spots. Most of the scapular blade lacks the superficial cortical layer, likely due to a weathering-induced exfoliation.

The acromion is fractured in three spots proximodistally. A slightly oblique fracture runs along the proximal edge of the acromion from its base and intersects the coronal fractures. Several small portions of the bone are missing due to these fractures. The lateralmost part of the acromion is fractured. The glenoid cavity is completely preserved. The distalmost part of the coracoid process shows a squashed appearance, probably due to a post-depositional process, as indicated by the slight displacement of its most ventral portion.

Morphology

The glenoid cavity has a proximodistal length of 33.8 mm, and an anteroposterior width of 21.8 mm. It is piriform in shape with a marked notch located proximally on the anterior margin. The outline of the posterior margin fits within an arc, while the anterior margin fits within two arcs. The cavity is slightly concave both anteroposteriorly and proximodistally, the maximum of its curvature being at the level of the notch. The cavity also presents a marked retroversion.

The supraglenoid tubercle is not pronounced. The infraglenoid tubercle forms a slightly rounded bulge on the posterodistal edge of the glenoid cavity. The coracoid process is approximately 39.7 mm long and well developed. With a base relatively thin, it projects anteriorly from the supraglenoid tubercle. In lateral view, it forms an obtuse angle with the long axis of the glenoid cavity, and then an angle oriented proximomedially to distolaterally to its base. The coracoid notch is well marked and forms a wide arc.

The acromion is robust, wide, and projects anteriorly (width ML = 19.6 mm, depth AP = 48.1 mm). Its lower surface is concave, and its upper surface is convex. In lateral view, the end of the acromion forms a right angle and adopts a strong curvature towards the glenoid cavity.

OMO VE 3-10063c – acromial half of the right clavicle

Preservation

The preserved lateral portion of the clavicle OMO VE 3-10063c is 89.5 mm long. The specimen consists of four well-preserved and refitting fragments, three of which are portions of the shaft (measuring respectively 12.5; 15.9; and 7.0 mm). The last one, of much larger length (54.0 mm), is a portion of the acromial end. The clavicle is light beige and the acromial end is covered with manganese spots. The shaft is fractured on the sagittal side, shortly after the point of inflection of the internal curvature. The medullary cavity is infilled with matrix. The acromial end of the fragment is missing, leaving the trabecular bone visible. In comparison with clavicles of *Homo sapiens*, between 10 to 20 mm of the acromial end is missing.

Morphology

The clavicle has an estimated length of 141.4+/- 1.9 mm. At the point of inflection of its internal curvature, the specimen has a minimum diameter of 10.0 mm, and a maximum diameter of 14.4 mm. In superior view, the external curvature is weak, almost non-existent, while the internal curvature is well pronounced. In posterior view, a slight inferior curvature is present at the acromial margin and extends to the sternalmost end of the fragment. The specimen does not exhibit an upper curvature in its preserved portion. Overall, the clavicle has a rather horizontal orientation. The *m. deltoideus* origin is marked by the sharp ridge formed by the anterior margin of the clavicle, and, further posteriorly, by the presence of a slight depression bordered by a very poorly developed bulge on the upper surface of the clavicle.

On the lower surface, the groove of *m. subclavius* is shallow and only visible in its lateral portion, at the level of the internal coronal curvature of the clavicle.

The *m. trapezius* insertion is not visible on the posterosuperior border. The conoid tubercle forms a slight, smooth, rounded prominence on the postero-inferior margin of the specimen. The maximum diameter at the conoid tubercle is 18.6 mm, and the minimum diameter is 8.1 mm. The preserved part of the acromial end of the specimen is flattened, with a sharp anterior edge and a broader, flat posterior edge. In the section, the clavicle adopts a profile successively flattened at its acromial end, rounded at mid-length, and elliptical at its most sternal end, with a main axis oriented posteroproximally to distoanteriorly.

OMO VE 3-10063d – vertebral neural arch and spinous process

Preservation

The specimen consists of two refitting neural arch fragments, 49.0 mm long from the distal end of the spinous process to the most preserved posterior point. Both fragments are largely covered with manganese spots. The spinous process is well preserved, although a little eroded on its posterior end. A fracture, located at the base of the lamina on the left lateral side of the vertebra (in caudal view), separates one of the transverse processes, the superior articular surface, and the pedicle from the rest of the neural arch. Both the transverse process and the superior articular surface present on this fragment are eroded. Still, on this fragment, the pedicle is eroded distally but is well preserved proximally and medially. The transverse process is also mostly eroded on the right lateral side of the vertebra. At least half of the superior articular surface is preserved. A mediolateral crack runs at the base of the pedicle. The latter lacks cortical bone laterally but is well preserved for the rest.

Morphology

The overall shape of the spinous process is elliptical in section, slightly more expanded mediolaterally than craniocaudally, which is reflected by a spinous process terminus index (spinous process terminus transverse width/spinous process terminus craniocaudal height*100) of 129.6, which contrasts with the blade-like shape of the process of the last thoracic and lumbar vertebrae. In lateral view, the spinous process is 32.6 mm long, non-bifid, and slightly distally inclined relative to the vertebral pillars. All the above-mentioned characters indicate most probably a C7 or T1. The spinal epiphysis is fused to the process, indicating that this vertebra is from an adult. The laminae are relatively thick (5.8 mm) and flattened craniocaudally (12.3 mm). In cranial view, the laminae form a rounded arch. The preserved portion of the superior articular surface is well-developed. Distal to the articular surface, the lamina is flat, and there is no ridge that would indicate the presence of a laterally projecting transverse process, such as in a thoracic vertebra. Thus, the specimen is most probably a C7. In this section, the pedicles are ovoid. The vertebral foramen should have expanded more mediolaterally (21.1 mm) than dorsoventrally.

OMO VE 3-10063e – vertebral body

Preservation

The specimen consists of a mostly complete vertebral centrum with maximal dimensions of 24.0 mm mediolaterally, 15.5 mm dorsoventrally, and 14.4 mm craniocaudally. The specimen is covered with manganese spots, mostly on the superior and anterior articular surfaces. The articular surfaces are eroded. The left side is largely lacking, such as the root of the transverse tubercle and the left uncinate process, which are not preserved. The right side is superficially eroded and

may still comprise the root of the pedicle. Both anterior and posterior faces are well-preserved. This specimen is non-fitting with the vertebral arch since the root of the right pedicle is conserved on both.

Morphology
In the posterior view, the two nutrient foramina typical of vertebral bodies are present. In cranial view, the posterior rim of the vertebral centrum is rectilinear, and the anterior rim is convex, resulting in a non-heart-shaped body. The vertebral body is then more likely a cervical (C3 to C7) or a first thoracic (T1; Cunningham *et al.* 2016). The centrum is more expanded mediolaterally than dorsoventrally, which confirms the attribution to the vertebra to the upper spine. The vertebral body is quite thick craniocaudally relatively to the dorsoventral and mediolateral dimensions that would exclude the first cervical vertebrae (C3-C5). In lateral view, the anterior edge is rectilinear and slightly inclined such as the inferior rim is more anteriorly projecting than the superior rim. The superior articular surface is dorsally eccentric whereas the inferior articular surface is ventrally eccentric. The caudal and cranial epiphyses are both fused to centrum indicating that this overall vertebral body was from an adult (Cunningham *et al.* 2016). The remaining uncinate process is shallow. In lateral view, on the right side, the root of a pedicle and of a transverse tubercle seems preserved, which suggests a cervical vertebra. All the above-mentioned characters suggest that it is most probably a C6 or C7 than T1.

OMO VE 3-10063F – RIGHT (6TH-9TH?) RIB
Preservation
The specimen consists of three refitting fragments of approximately 172 mm long. Neither of the two ends is preserved. While the head and the neck are lacking, the slight external-to-internal expansion of the shaft near an extremity of the specimen suggests the vicinity of the costal angle. In taphonomic terms, what would be the ventralmost fragment of the rib is not aligned with the two other fragments due to postdepositional alteration, which affects the longitudinal curvature of the specimen. Besides, no biostratinomic effects are discernible, but numerous spots of manganese cover the rib, as with the other associated specimens from OMO VE 3.

Morphology
Both caudal and cranial edges that provide attachment areas for intercostal muscles are visible, although variably preserved. The cranial edge is eroded throughout the specimen, except for a small portion located 70 to 90 mm from the proximal end, displaying a rounded aspect. The caudal edge is also eroded along the proximal half of the specimen. The craniocaudal diameter (measurable 70 to 90 mm from the proximalmost end of the specimen) is 13.6 mm, and the external-internal diameter is 7.8 mm long at its maximum, and 6.8 mm at its minimum at the level of the distalmost end. These dimensions illustrate an oval shape of the shaft in cross-section. The preserved shaft of this rib only shows little torsion.

The costal groove that houses the intercostal artery, vein, and nerve is unambiguously identifiable on the internal-caudal edge of the rib. This groove is well pronounced and expands throughout the specimen, smoothing toward the sternal end. This configuration, as well as the inferred costal angle, conjointly shows that this rib is from the right side. When seen from the internal view, the costal groove covers approximately the third of the craniocaudal diameter of the rib at its maximum degree of expression. In extant humans, such a development of the costal groove generally features at least the 5th to 7th ribs (White & Folkens 2005), but the relatively high degree of curvature would also support an attribution to the 6th or 9th.

Appendix 2. — Stratigraphic position of the OMO VE 3-10063 remains. The individual was found in Member H, Unit H-4 of the Shungura Formation (Ethiopia), in the OMO VE 3 locality. The **red flags** represent the position of the three humeral elements (a-1, a-2, and a-3) and the scapula (b).

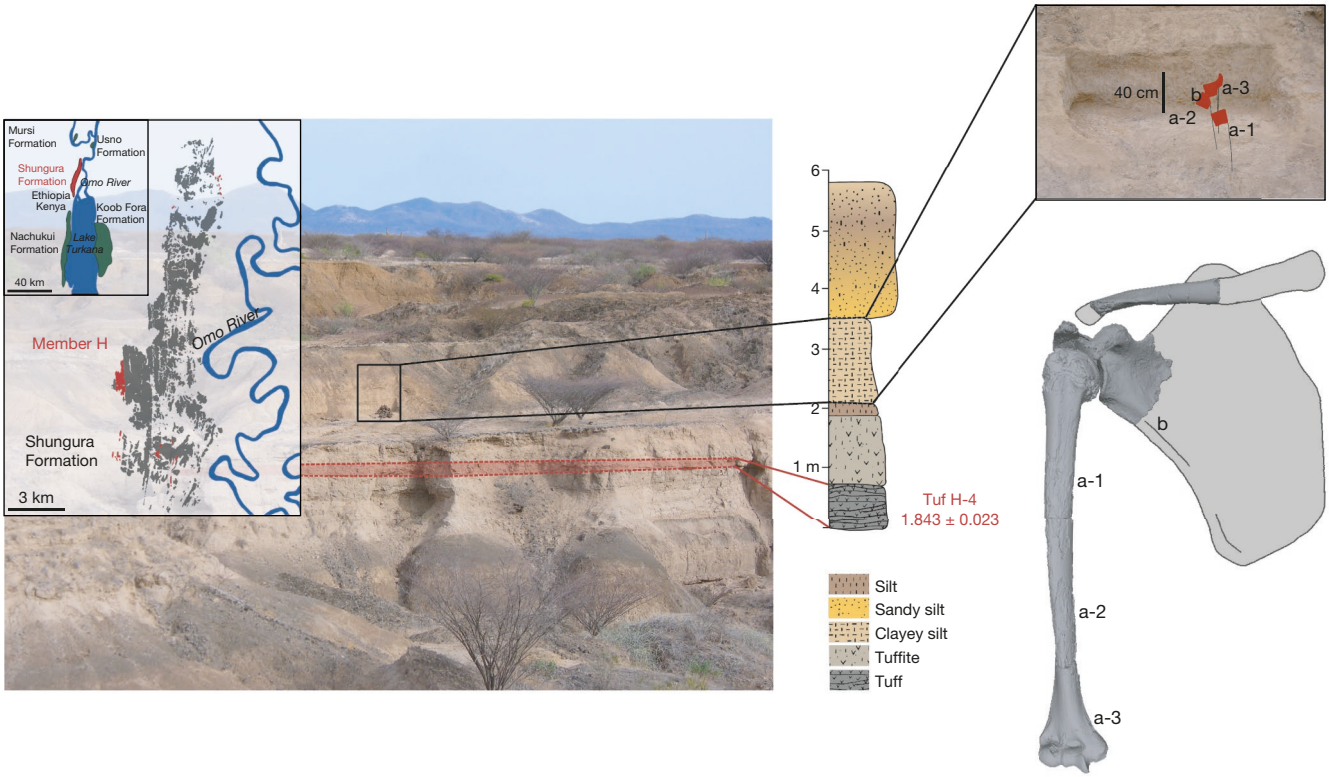

Appendix 3. — Linear measurements of OMO VE 3-10063. Linear measurements were taken on the numerical model of OMO VE 3-10063 with Geomagic.

Bones	Measurements	Definition	Values (mm)
Clavicle	Minimum diameter	Diameter taken at the inflection point of the internal curvature (Carretero *et al.* 1997)	10.0
Clavicle	Maximum diameter	Diameter taken at the inflection point of the internal curvature (Carretero *et al.* 1997)	14.4
Clavicle	Conoid tubercle mininum diameter	Diameters taken at the maximum projection of the conoid tubercle (Vandermeersh 1995)	8.1
Clavicle	Conoid tubercle maximum diameter	Diameters taken at the maximum projection of the conoid tubercle (Vandermeersh 1995)	18.6
Scapula	Glenoid cavity length	Linear distance from the most cranial point on the outer edge of the articular surface to the most caudal point (Green 2013; Green *et al.* 2018)	33.8
Scapula	Glenoid cavity width	Largest width perpendicular to the length, measured at the lateral edges of the articular surface (Green 2013; Green *et al.* 2018)	24.3
Scapula	Coracoid process length	Linear distance between the end of the process and the root of the process (Martin 1957)	39.7
Scapula	Scapular neck breadth	Minimum width of the infraspinous fossa at the neck of the scapula, i.e., minimum distance between the base of the spine and the axillary border (Larson 1995)	28.1
Scapula	Acromion depth	Linear distance from the most caudal point of the posterior part of the acromion to its most cranial point (Martin 1957)	48.1
Scapula	Acromion width	Larger width perpendicular to the depth (Martin 1957)	19.6
Humerus	Maximum length	Linear distance from the most proximal point of the head to the most distal point of the trochlea (Martin 1957)	338.8
Humerus	Physiological length	Linear distance from the most proximal point of the head to the most distal point of the capitulum (Martin 1957)	337.1
Humerus	Sagittal diameter of the head	Distance between the highest and lowest points on the median plane of the head, taken perpendicular to the transverse diameter	43.1
Humerus	Transversal diameter of the head	Distance between the most prominent points of the head edge, taken perpendicular to the sagittal diameter (Dwight 1905)	40.5
Humerus	Bicipital groove width	Distance between the internal crests of the tubercles (Corruccini & Ciochon 1976)	15.5
Humerus	Diaphysis minimal diameter	Diameter taken at mid-length of the diaphysis (Hrdlička 1920)	17.1
Humerus	Diaphysis maximal diameter	Diameter taken at mid-length of the diaphysis (Hrdlička 1920)	22.1
Humerus	Biepicondylar width	Distance between the most lateral point of the lateral epicondyle and the corresponding point on the medial epicondyle (Martin 1957)	59.6
Humerus	Articular surface width	Distance between the lateral edge of the capitulum and the medial edge of the trochlea. Measurement taken in the same direction as the trochlear axis (Martin 1957)	43.6
Humerus	Maximum projection of the lateral epicondyle	Distance between the proximal edge of the lateral epicondyle and the most distal point of the groove between the capitulum and the trochlea (Patterson & Howells 1967)	29.8
Humerus	Maximum projection of the medial epicondyle	Distance from the proximal edge of the medial epicondyle to the most distal point on the lateral crest of the trochlea (Patterson & Howells 1967)	42.1
Humerus	Medial epicondyle thickness	Anteroposterior diameter of the medial epicondyle taken perpendicular to the long axis of the epicondyle (McHenry & Corruccini 1975)	12.1
Humerus	Capitulum diameter	Linear distance between the most lateral point of the capitulum and the groove between the capitulum and the trochlea. Measurement taken in the mediolateral axis of the capitulum (Martin 1957)	17.7
Humerus	Capitulum height	Distance between the anteroproximal and posterodistal edges of the capitulum, along a proximodistal line through the middle of the capitulum (McHenry & Corruccini 1975)	19.4
Humerus	Radial fossa width	Distance between the most lateral and the most medial point of the fossa, measured perpendicular to the axis of the diaphysis	19.2
Humerus	Coronoid fossa width	Distance between the most lateral and the most medial point of the fossa, measured perpendicular to the axis of the diaphysis	16.8
Humerus	Trochlear width	Distance between the medial ridge and the lateral ridge of the trochlea (McHenry & Corruccini 1975)	23.7
Humerus	Trochlear diameter	Distance between the anterior and posterior surfaces of the trochlea. Measurement taken perpendicular to the axis of the diaphysis (Martin 1957)	15.1
Humerus	Lateral crest diameter	Distance between the most anterior point on the groove separating the capitulum and the trochlea and the most posterior point on the lateral crest of the trochlea. Measurement taken perpendicular to the diaphysis (McHenry & Corruccini 1975)	21.0
Humerus	Medial crest diameter	Distance from the most anterior to the most posterior point of the medial crest of the trochlea (Martin 1957)	23.2
Humerus	Medial crest height	Distance from the most proximal to the most distal point of the medial crest of the trochlea (Carretero *et al.* 1997)	17.9
Humerus	Olecranon fossa depth	Distance from the deepest point of the pit to the line joining the extreme medial-lateral edges of the fossa (Martin 1957)	7.4
Humerus	Olecranon fossa width	Maximum medial-lateral distance of the olecranon fossa. Measurement taken perpendicular to the axis of the diaphysis (Martin 1957)	24.5
Humerus	Medial pillar width	Minimum distance between the medial edge of the diaphysis and the medial edge of the olecranon fossa. Measurement taken perpendicular to the axis of the pillar (McHenry & Corruccini 1975)	10.8
Humerus	Lateral pillar width	Minimum distance between the lateral edge of the diaphysis and the lateral edge of the olecranon fossa. Measurement taken perpendicular to the axis of the pillar (McHenry & Corruccini 1975)	17.9

Appendix 3. — Continuation.

Bones	Measurements	Definition	Values (mm)
Vertebral neural arch and spinous process	Length of the spinous process	Distance between the extremity of the distal end of the spinous process and the internal margin of the spinal canal in cranial view	32.6
Vertebral neural arch and spinous process	Neural canal transverse width	Distance between the lateral-most points of the spinal canal in cranial view	21.2
Vertebral body	Anterior vertical diameter	Distance between the superior and the inferior surfaces of the vertebral body measured in the sagittal median plane on the ventral surface of the body (Martin 1957)	11.8
Vertebral body	Posterior vertical diameter	Distance between the superior and the inferior surfaces of the vertebral body measured in the sagittal median plane on the dorsal surface of the body (Martin 1957)	12.9
Vertebral body	Cranial sagittal diameter	Distance between the ventral and dorsal points of the median sagittal planes on the cranial surface of the vertebral body (Martin 1957)	14.4
Vertebral body	Caudal sagittal diameter	Distance between the ventral and dorsal points of the median sagittal planes on the caudal surface of the vertebral body (Martin 1957)	15.5

Appendix 4. — Extant comparative sample of hominoids used for the humeral diaphysis cross-sectional shape analysis, glenoid shape analysis and distal trochlear angle. Abbreviations: **Ad**, adult (bone completely fused); **F**, female; **L**, left; **M**, male; **MfN**, Museum für Naturkunde (Berlin, Germany); **MNHN**, Musée de l'Homme, Paris (France); **MRAC**, Musée Royal d'Afrique Centrale, Tervuren (Belgium); **NMNH**, Smithonian National Museum of Natural History, New York (United-States); **R**, right; **RD Congo**, Democratic Republic of Congo; **Sub**, subadult (partially unfused); **UP**, Université de Poitiers, UMR 7262 laboratoire PALEVOPRIM, Poitiers (France). [a], last erupted tooth when known; [b], collector Tiphaine Brusse.

Collection number	Taxonomy	Locality	Sex	Age	Side (R/L)	Cross-sectional shape of the distal humeral diaphysis	Glenoid shape analysis	Distal trochlear angle	Institutions
USNM397351	*Gorilla beringei*	Mount Mahavura, Above Saddle Between Mt. Mahavura And Mt. M'Gahingo, Rwanda, Africa	M	Ad	L	X	–	–	NMNH
2260	*Gorilla beringei*	Virunga N.O. du Mikeno, 2300-2400 env.	M	(M3[a])	R	X	X	–	MRAC
2263	*Gorilla beringei*	Virunga N.O. du Mikeno, 2300-2400 env.	F	(M3[a])	R+L	X	X	–	MRAC
2257	*Gorilla beringei*	Virunga N.O. du Mikeno, 2300-2400 env.	M	Ad (M3[a])	R+L	X	–	–	MRAC
USNM 395636	*Gorilla beringei*	Virunga Mountains, Mount Viroke, Rwanda, Africa	M	–	R+L	X	–	X	NMNH
USNM 396935	*Gorilla beringei*	Tsundura, Rwanda, Africa	F	Ad	R+L	X	–	X	NMNH
USNM 396937	*Gorilla beringei*	Mount Karisimbi, China Tembo, Rwanda, Africa	F	Ad	R+L	X	–	X	NMNH
USNM 396942	*Gorilla beringei*	Mount Sabinyo, Congo Side Of, Rwanda, Africa	M	Ad	R+L	X	–	–	NMNH
USNM 397351	*Gorilla beringei*	Mount Mahavura, Above Saddle Between Mt. Mahavura And Mt. M'Gahingo, Rwanda, Africa	M	Ad	R	X	–	X	NMNH
USNM 396934	*Gorilla beringei*	Tsundura, Rwanda, Africa	M	?	R+L	–	–	X	NMNH
994	*Gorilla beringei*	Baraka (forest Sibatwa), RD Congo	M	Ad	R	–	X	–	MRAC
995	*Gorilla beringei*	Baraka (forest Sibatwa), RD Congo	F	Ad	R	–	X	–	MRAC
998	*Gorilla beringei*	Baraka (forest Sibatwa), RD Congo	M	Ad	L	–	X	–	MRAC
999	*Gorilla beringei*	Baraka (forest Sibatwa), RD Congo	M	Ad	R	–	X	–	MRAC
1000	*Gorilla beringei*	Baraka (forest Sibatwa), RD Congo	M	Ad	R	–	X	–	MRAC
1001	*Gorilla beringei*	Baraka (forest Sibatwa), RD Congo	M	Ad	R	–	X	–	MRAC
2258	*Gorilla beringei*	Virunga, Rwanda	F	Ad	L	–	X	–	MRAC
8607	*Gorilla beringei*	Mount Karissimbi, Rwanda	F	Ad	R	–	X	–	MRAC
9581	*Gorilla beringei*	Ituri Kilimamensa, Rwanda	M	Ad	R	–	X	–	MRAC
10051	*Gorilla beringei*	10 km from Pinga, RD Congo	M	Ad	R	–	X	–	MRAC
15290	*Gorilla beringei*	Nbayo, Mount Kahuzi, RD Congo	F	Ad	R	–	X	–	MRAC
18739	*Gorilla beringei*	Terr. Lubero, RD Congo	M	Ad	R	–	X	–	MRAC
20085	*Gorilla beringei*	Butembo, RD Congo	M	Ad	R	–	X	–	MRAC
20086	*Gorilla beringei*	Butembo, RD Congo	M	Ad	L	–	X	–	MRAC
27755	*Gorilla beringei*	Itebero-Utu (terr. Walikale), RD Congo	F	Ad	R	–	X	–	MRAC
27756	*Gorilla beringei*	Itebero-Utu (terr. Walikale), RD Congo	F	Ad	R	–	X	–	MRAC
27839	*Gorilla beringei*	Chamaka, RD Congo	F	Ad	R	–	X	–	MRAC
9291	*Gorilla gorilla*	Sangha, Republic of the Congo	M	Ad	R	–	X	–	MRAC
458	*Pan troglodytes*	Stanley Falls	F	?	R+L	X	–	X	MRAC
30676	*Pan troglodytes*	Zoo Antwerpen	M	?	R+L	X	–	X	MRAC
9931	*Pan troglodytes*	Ubangi	F	?	R+L	X	–	X	MRAC
3430	*Pan troglodytes*	Zoo Antwerpen	–	?	R+L	X	–	X	MRAC
11363	*Pan troglodytes*	Moba (St-Louis)	M	?	R+L	X	X	X	MRAC
4188	*Pan troglodytes*	Poko	–	?	R+L	X	–	X	MRAC
15350	*Pan troglodytes*	Ekwangatana	–	?	R+L	X	–	X	MRAC
5891	*Pan troglodytes*	?	F	?	L	X	X	X	MRAC
153	*Pan troglodytes*	Mayumbe, Gabon	F	Ad	R	–	X	–	MRAC
179	*Pan troglodytes*	Ibina forest	M	Ad	R	–	X	–	MRAC
545	*Pan troglodytes*	Stanley Falls, RD Congo	F	Sub	R	–	X	–	MRAC
730	*Pan troglodytes*	Uelé, RD Congo	M	Ad	R	–	X	–	MRAC
1048	*Pan troglodytes*	Romée River, RD Congo	M	Ad	R	–	X	–	MRAC
1554	*Pan troglodytes*	?	M	Ad	R	–	X	–	MRAC
5892	*Pan troglodytes*	Moba, RD Congo	F	Ad	R	–	X	–	MRAC
11362	*Pan troglodytes*	Moba, RD Congo	M	Ad	R	–	X	–	MRAC
19534	*Pan troglodytes*	Mwabi (terr. Mwenga), RD Congo	?	Ad	R	–	X	–	MRAC
22925	*Pan troglodytes*	Utu (Walikale), RD Congo	M	Ad	R	–	X	–	MRAC
29073	*Pan troglodytes*	Utu (Walikale), RD Congo	F	Ad	R	–	X	–	MRAC
29074	*Pan troglodytes*	Confl. Kabakule-Kabika, RD Congo	F	Ad	R	–	X	–	MRAC
37663	*Pan troglodytes*	Bipindi, Cameroon	F	Ad	R	–	X	–	MRAC
ZMB_MAM_11640	*Pan troglodytes*	Sangmelima, Cameroon	F	Ad	R	–	X	–	MfN
ZMB_MAM_19071	*Pan troglodytes*	Ayos Heights, Cameroon	M	Ad	R	–	X	–	MfN
ZMB_MAM_30755	*Pan troglodytes*	Genoa, Cameroon	M	Ad	R	–	X	–	MfN
ZMB_MAM_83610	*Pan troglodytes*	Bipindi, Cameroon	M	Ad	R	–	X	–	MfN

Appendix 4. — Continuation.

Collection number	Taxonomy	Locality	Sex	Age	Side (R/L)	Cross-sectional shape of the distal humeral diaphysis	Glenoid shape analysis	Distal trochlear angle	Institutions
ZMB_MAM_83646	*Pan troglodytes*	?	F	Ad	R	–	X	–	MfN
27696	*Pan paniscus*	Ponthierville, leftbank Congo (Walengolas)	M	Ad (M3[a])	R+L	X	–	–	MRAC
15294	*Pan paniscus*	Stanleyville, 25 km S. terr. Stanleyville (leftbank)	M	Ad (M3[a])	R+L	X	X	–	MRAC
15295	*Pan paniscus*	Stanleyville, 25 km S. terr. Stanleyville (leftbank)	F	Ad (M3[a])	R+L	X	X	–	MRAC
15296	*Pan paniscus*	Stanleyville, 25 km S. terr. Stanleyville (leftbank)	F	Ad (M3[a])	R+L	X	X	–	MRAC
20529	*Pan paniscus*	Zoo Antwerpen	F	Subad	R+L	X	–	X	MRAC
15293	*Pan paniscus*	Stanleyville (terr. Stanleyville), RD Congo	F	Ad	R	–	X	–	MRAC
29035	*Pan paniscus*	Djolu, RD Congo	F	Ad	R	–	X	–	MRAC
29040	*Pan paniscus*	Wamba (terr. Basankusu), RD Congo	F	Ad	R	–	X	–	MRAC
29042	*Pan paniscus*	Wamba (terr. Basankusu), RD Congo	F	Ad	R	–	X	–	MRAC
29044	*Pan paniscus*	Dongo, RD Congo	M	Ad	R	–	X	–	MRAC
29045	*Pan paniscus*	Dongo, RD Congo	F	Ad	R	–	X	–	MRAC
29047	*Pan paniscus*	Dongo, RD Congo	M	Ad	R	–	X	–	MRAC
29052	*Pan paniscus*	Batiakayandja, RD Congo	M	Ad	R	–	X	–	MRAC
29060	*Pan paniscus*	Dongo (Kasai), RD Congo	F	Ad	R	–	X	–	MRAC
29063	*Pan paniscus*	Bolobo, RD Congo	M	Ad	R	–	X	–	MRAC
USNM 143586	*Pongo abelii*	Aru Bay, Indonesia, Asia	M	Sub	R+L	X	–	X	NMNH
USNM 143596	*Pongo abelii*	Aru Bay, Indonesia, Asia	F	Ad	R+L	X	–	X	NMNH
USNM 143593	*Pongo abelii*	Aru Bay, Indonesia, Asia	M	Ad	R+L	X	–	X	NMNH
USNM 143588	*Pongo abelii*	Aru Bay, Indonesia, Asia	M	Ad	R+L	X	–		NMNH
USNM 143595	*Pongo abelii*	Aru Bay, Indonesia, Asia	M	Sub	R+L	X	–	X	NMNH
USNM 143587	*Pongo abelii*	Aru Bay, Indonesia, Asia	M	Ad	R+L	X	–	X	NMNH
USNM 143590	*Pongo abelii*	Aru Bay, Indonesia, Asia	M	Ad	R+L	–	–	X	NMNH
USNM 143594	*Pongo abelii*	Aru Bay, Indonesia, Asia	M	Ad	R+L	X	–	X	NMNH
ZMB_MAM_6947	*Pongo pygmaeus*	Moalang, Borneo	M	Sub	R	–	X	–	MfN
ZMB_MAM_6948	*Pongo pygmaeus*	Kelungen, Borneo	F	Ad	R	–	X	–	MfN
ZMB_MAM_10481	*Pongo pygmaeus*	Sumatra, Indonesia	?	Ad	R	–	X	–	MfN
ZMB_MAM_11647	*Pongo pygmaeus*	North-west Borneo	?	Ad	R	–	X	–	MfN
ZMB_MAM_65360	*Pongo pygmaeus*	Sumatra, Indonesia	M	Ad	R	–	X	–	MfN
ZMB_MAM_83213	*Pongo pygmaeus*	Sumatra, Indonesia	F	Ad	R	–	X	–	MfN
ZMB_MAM_83497	*Pongo pygmaeus*	Borneo, Malaysia/Indonesia/Brunei	M	Ad	R	–	X	–	MfN
ZMB_MAM_83499	*Pongo pygmaeus*	Borneo, Malaysia/Indonesia/Brunei	F	Ad	R	–	X	–	MfN
ZMB_MAM_87090	*Pongo pygmaeus*	Sagama river, Borneo, Malaysia	?	Ad	R	–	X	–	MfN
ZMB_MAM_87091	*Pongo pygmaeus*	Sagama river, Borneo, Malaysia	?	Ad	R	–	X	–	MfN
ZMB_MAM_87092	*Pongo pygmaeus*	La Datu, Borneo, Malaysia	?	Sub	R	–	X	–	MfN
ZMB_MAM_87093	*Pongo pygmaeus*	Sumatra, Indonesia	?	Ad	R	–	X	–	MfN
ZMB_MAM_87094	*Pongo pygmaeus*	Sumatra, Indonesia	?	Ad	R	–	X	–	MfN
IPCR73	*Homo sapiens*	Modern Age population	?	Ad	R	X	–	–	UP
IPCR73TA	*Homo sapiens*	Modern Age population	?	Ad	R	X	–	–	UP
VL[b]	*Homo sapiens*	Modern Age population	?	Ad	R	X	–	X	UP
VL3[b]	*Homo sapiens*	Modern Age population	?	Ad	R	X	–	X	UP
VL17[b]	*Homo sapiens*	Modern Age population	?	Ad	R	X	–	X	UP
VLC	*Homo sapiens*	Modern Age population	?	Ad	R	X	–	–	UP
VLF	*Homo sapiens*	Modern Age population	?	Ad	R	X	–	–	UP
VLX	*Homo sapiens*	Modern Age population	?	Ad	R	X	–	X	UP
X	*Homo sapiens*	Modern Age population (Poitiers, France)	?	Ad	R	–	–	X	UP
PA-PO-74-10-F27[b]	*Homo sapiens*	Modern Age population (Poitiers, France)	?	Ad	R	X	–	X	UP

Appendix 4. — Continuation.

Collection number	Taxonomy	Locality	Sex	Age	Side (R/L)	Cross-sectional shape of the distal humeral diaphysis	Glenoid shape analysis	Distal trochlear angle	Institutions
PA-PO-74-08-D23[b]	*Homo sapiens*	Modern Age population (Poitiers, France)	?	Ad	R	X	–	X	UP
PA-PO-74-07-H30[b]	*Homo sapiens*	Modern Age population (Poitiers, France)	?	Ad	R	X	–	X	UP
PA-PO-74-11-B27[b]	*Homo sapiens*	Modern Age population (Poitiers, France)	?	Ad	R	X	–	X	UP
PA-PO-74-12	*Homo sapiens*	Modern Age population (Poitiers, France)	?	Ad	R	X	–	–	UP
PA-PO-74-25-Q13[b]	*Homo sapiens*	Modern Age population (Poitiers, France)	?	Ad	R	X	–	X	UP
PA-PO-74-28-U17[b]	*Homo sapiens*	Modern Age population (Poitiers, France)	?	Ad	R	X	–	X	UP
PA-PO-74-83-D83[b]	*Homo sapiens*	Modern Age population (Poitiers, France)	?	Ad	R	–	–	X	UP
PA-PO-130-X1[b]	*Homo sapiens*	Modern Age population (Poitiers, France)	?	Ad	R	–	–	X	UP
PA-PO-130-X5[b]	*Homo sapiens*	Modern Age population (Poitiers, France)	?	Ad	R	–	–	X	UP
PA-PO-130-X8[b]	*Homo sapiens*	Modern Age population (Poitiers, France)	?	Ad	R	–	–	X	UP
9758	*Homo sapiens*	Hermosa, Luçon, Philippines	?	Ad	R	–	X	–	MNHN
10253	*Homo sapiens*	Santa Cruz, California, USA	F	Ad	R	–	X	–	MNHN
10289	*Homo sapiens*	Hoste-Navarin, Tierra del Fuego, Chile	M	Ad	R	–	X	–	MNHN
11246	*Homo sapiens*	Arguineguin, Gran Canaria, Canary Islands	?	Ad	R	–	X	–	MNHN
12262	*Homo sapiens*	Primavera Angostura, Patagonia, Argentina	?	Ad	R	–	X	–	MNHN
17721	*Homo sapiens*	Djougou, Benin	?	Ad	R	–	X	–	MNHN
17947	*Homo sapiens*	Haut Ituri, RD Congo	M	Ad	R	–	X	–	MNHN
17978	*Homo sapiens*	Casamance, Sénégal	?	Ad	R	–	X	–	MNHN
19849	*Homo sapiens*	Ancon, Lima, Peru	F ?	Ad	R	–	X	–	MNHN
19850	*Homo sapiens*	Ancon, Lima, Peru	?	Ad	R	–	X	–	MNHN
19851	*Homo sapiens*	Ancon, Lima, Peru	?	Ad	R	–	X	–	MNHN
20828	*Homo sapiens*	Tamba, Awaji, Japan	?	Ad	R	–	X	–	MNHN
23876	*Homo sapiens*	Santa Barbara, California, United States	?	Ad	R	–	X	–	MNHN
23881	*Homo sapiens*	San Nicola, California, United States	?	Ad	R	–	X	–	MNHN
23943	*Homo sapiens*	Ancon, Lima, Peru	?	Ad	R	–	X	–	MNHN
24091	*Homo sapiens*	La Sardina, Gran Canaria, Canary Islands	?	Ad	R	–	X	–	MNHN
25561	*Homo sapiens*	Tierra del Fuego	?	Ad	R	–	X	–	MNHN
35579	*Homo sapiens*	Cambodia	?	Ad	R	–	X	–	MNHN
35602	*Homo sapiens*	India	?	Ad	R	–	X	–	MNHN
35603	*Homo sapiens*	India	?	Ad	R	–	X	–	MNHN

Appendix 5. — Fossil hominin material used for each measurement. Values are either taken from the literature (**X italic**) or measured in this study (**X bold font**). [1], collector Guillaume Daver. Abbreviations: **Ad**, adult; **A.org**, Africanfossils.org; **Ch.**, Chamber; **Dik.**, Dikika; **Krom.**, Kromdraai; **NE3D**, NextEngine 3D scanner Ultra HD (NextEngine, United States); **Mb.**, Member; **M.org**, Morphosource.org; **R**, right; **SI**, Smithsonian Institution online collection; **SSC-CT**, Siemens Sensation Cardiac CT scanner (Medsystem); **Sub**, subadult; **Swart.**, Swartkrans; **Sterk.**, Sterkfontein; **W.-Mille**, Woranso-Mille. References: [a], Granger *et al.* 2015; [b], Carlson *et al.* 2021; [c], McDougall & Brown 2008; [d], Granger *et al.* 2022; [e], Green *et al.* 2018; [f], Green & Alemseged 2012; [g], Larson 1996; [h], Haile-Selassie *et al.* 2010; [i], Taylor *et al.* 2024; [j], Alemseged *et al.* 2006; [k], Campisano & Feibel 2008; [l], Stern & Susman 1983; [m], Dirks *et al.* 2010; [n], Churchill *et al.* 2013; [o], Churchill *et al.* 2018; [p], Braga *et al.* 2022; [q], McDougall & Brown 2006; [r], Lague *et al.* 2019; [s], Lague 2019; [t], Richmond *et al.* 2020; [u], McHenry 2012; [v], Feibel *et al.* 1989; [w], Gibbon *et al.* 2014; [x], McDougall *et al.* 2012; [y], Lordkipanidze *et al.* 2007; [z], Morgan *et al.* 2012; [aa], Dirks *et al.* 2017; [ab], Feuerriegel *et al.* 2017; [ac], Feuerriegel *et al.* 2019.

							Quantitative approach						
Taxonomy	**Specimen**	**Site / Formation / Locality / Strat.**	**Repository / Acquisition**	**Age (Ma)**	**Developmental stage**	**Qualitative approach**	**Cross-sectional shape of the distal humeral diaphysis**	**Glenoid shape analysis**	**Scapular neck breadth**	**Pillar-glenoid angle**	**Distal trochlear angle**	**Humeral torsion**	**Clavicle curvature and length estimate**
A. prometheus	StW 573	Sterk./ Mb. 2	–	3.51-3.83[a]	Ad	**X**	–	–	–	*X*[b]	–	*X*[b]	–
A. anamensis	KNM-KP 271	Kanapoi	A.org	4.195-4.108[c]	Ad	–	–	–	–	–	X	–	–
A. africanus	Sts 7	Sterk./ Mb. 4	NE3D	3.49-3.41[d]	?	**X**	–	**X**	*X*[e]	*X*[f]	–	*X*[g]	–
A. africanus	StW 162	Sterk./ Mb. 4	–	3.49-3.41[d]	?	–	–	–	*X*[e]	*X*[f]	–	–	–
A. africanus	StW 431[1]	Sterk./ Mb. 4	NE3D	3.49-3.41[d]	Ad	**X**	**X**	–	–	–	X	–	–
A. afarensis	KSD-VP 1/1	W.-Mille/ Korsi Dora	–	3.6-3.58[h]	Ad	**X**	–	X	*X*[e]	*X*[h]	–	–	*X*[i]
A. afarensis	DIK 1-1	Dik./ Mb. Sidi Hakoma	–	3.35-3.31[j]	Sub	–	–	–	–	*X*[f]	–	–	–
A. afarensis	A.L. 137-48[1]	Hadar/ Mb. SH-2	NE3D	3.42-3.33 [k]	Ad	**X**	X	–	–	–	X	–	–
A. afarensis	A.L. 137-50	Hadar/ Mb. SH-1	NE3D	3.42-3.33 [k]	–	–	X	–	–	–	–	–	–
A. afarensis	A.L. 223-23	Hadar/ Mb. SH-3	NE3D	3.42-3.30[k]	–	–	X	–	–	–	–	–	–
A. afarensis	A.L. 288-1	Hadar/ Mb. KH-1	NE3D	3.22-3.11[k]	Ad	**X**	**X**	**X**	*X*[e]	*X*[l]	**X**	*X*[g]	–
A. afarensis	A.L. 322-1[1]	Hadar/ Mb. SH-4/DD-1	NE3D	3.33-3.22[k]	?	**X**	**X**	–	–	–	X	–	–
A. afarensis	A.L. 333-29	Hadar/ Mb. DD-2	–	3.22-3.11[k]	–	X	–	–	–	–	–	–	–
A. afarensis	A.L. 333-87	Hadar/ Mb. DD-2	–	3.22-3.11[k]	–	X	–	–	–	–	–	–	–
A. afarensis	A.L. 333-106	Hadar/ Mb. DD-2	–	3.22-3.11[k]	–	X	–	–	–	–	–	–	–
A. afarensis	A.L. 333-107	Hadar/ Mb. DD-2	–	3.22-3.11[k]	–	X	–	–	–	–	–	–	–
A. afarensis	A.L. 333x-6/9	Hadar/ Mb. DD-2	–	3.22-3.11[k]	–	X	–	–	–	–	–	–	–
A. sediba	U.W. 88-88 (MH1)	Malapa	–	1.95-1.78[m]	Sub	–	–	–	–	–	–	*X*[n]	–
A. sediba	U.W. 88-38 (MH2)[1]	Malapa	–	1.95-1.78[m]	Ad	**X**	–	–	–	–	–	–	–
A. sediba	U.W. 88-56 (MH2)[1]	Malapa	M.org	1.95-1.78[m]	Ad	**X**	–	**X**	*X*[e]	*X*[o]	–	–	–
A. sediba	U.W. 88-57 (MH2)[1]	Malapa	M.org	1.95-1.78[m]	Ad	**X**	X	–	–	–	X	X	–
A. sediba	U.W. 88-101 (MH2)[1]	Malapa	–	1.95-1.78[m]	Ad	**X**	–	–	–	–	–	–	–
			–	–			–	–	–	–	–	–	–
A. sediba	U.W. 88-45, 46, 47, 48, 59, 60, 61 (MH2)	Malapa	–	1.95-1.78[m]	Ad	**X**	–	–	–	–	–	–	–
P. robustus	TM 1517g[1]	Krom./ Possibly Mb. 5-6(*34*)	NE3D	<1.95[p]	Ad	**X**	**X**	–	–	–	X	–	–
P. boisei	KNM-ER 739[1]	Koobi Fora/ Mb. Okote	NE3D	1.60-1.38[q]	Ad	**X**	X	–	–	–	**X**	*X*[g]	–
P. boisei	KNM-ER1504[1]	Koobi Fora/ Mb. KBS(*35*)	NE3D	1.87-1.61[q]	Ad	**X**	**X**	–	–	–	X	–	–
P. boisei	KNM-ER 1591	Koobi Fora/ Mb. KBS	–	1.87-1.60[q]	–	–	–	–	–	–	*X*[r]	–	–
P. boisei	KNM-ER 45510	Koobi Fora/ Mb. Upper Burgi	NE3D	1.9[s]	–	–	X	–	–	–	X	–	–
P. boisei	KNM-ER 6020[1]	Koobi Fora/ Mb. KBS	NE3D	1.87-1.60[q]	Ad	**X**	**X**	–	–	–	X	–	–
P. boisei	KNM-ER 47000	Koobi Fora/ FwJj14E	–	1.53-1.51[t]	Ad	*X*	–	–	*X*[e]	*X*[e]	*X*[r]	–	–
H. habilis	OH 48	Olduvai/ Upper Bed I	–	1.85-1.79[u]	–	X	–	–	–	–	–	–	*X*[i]
H. habilis	KNM-ER 3735	Koobi Fora/ Mb. Upper Burgi	NE3D	1.91-1.88[v]	–	X	X	–	–	–	–	–	–
H. habilis	SK 24600	Swart./ Member 1 LB	NE3D	1.89-1.71[w]	–	–	X	–	–	–	X	–	–
H. erectus	KNM-WT 15000[1]	Nachukui/ Nariokotome III	NE3D	1.5-1.44[x]	Sub	**X**	**X**	**X**	*X*[e]	*X*[f]	**X**	**X**	*X*[i]
H. erectus	D2680	Dmanisi	SSC-CT	*c.* 1.77[y]	Sub	**X**	–	–	–	–	–	*X*[y]	–
H. erectus	D2715	Dmanisi	SSC-CT	*c.* 1.77[y]	Sub	**X**	–	–	–	–	–	–	–
H. erectus	D2724	Dmanisi	–	*c.* 1.77[y]	Sub	–	–	–	–	–	–	–	–
H. erectus	D4161	Dmanisi	–	*c.* 1.77[y]	Ad	**X**	–	–	–	–	–	–	–
H. erectus	D4161	Dmanisi	–	*c.* 1.77[y]	Ad	**X**	–	–	–	–	–	–	–
H. erectus	D4162	Dmanisi	–	*c.* 1.77[y]	Ad	**X**	–	–	–	–	–	–	–
H. erectus	D4166	Dmanisi	–	*c.* 1.77[y]	Ad	**X**	–	–	–	–	–	–	–
H. erectus	D4507[1]	Dmanisi	SSC-CT	*c.* 1.77[y]	Ad	**X**	–	–	–	–	X	–	–

Appendix 5. — Continuation.

Taxonomy	Specimen	Site / Formation / Locality / Strat.	Repository / Acquisition	Age (Ma)	Developmental stage	Qualitative approach	Quantitative approach						
							Cross-sectional shape of the distal humeral diaphysis	Glenoid shape analysis	Scapular neck breadth	Pillar-glenoid angle	Distal trochlear angle	Humeral torsion	Clavicle curvature and length estimate
H. erectus	SKX 10924[1]	Swart./ Mb. 3	NE3D	1.05-0.87[w]	–	–	–	–	–	–	X	–	–
H. erectus	IB 7594[1]	Melka Kunture/ Gom. I	NE3D	>1.39[z]	Ad	**X**	**X**	–	–	–	X	–	–
H. erectus	KNM-ER 1808	Koobi Fora/ Upper Mb.	–	*c.* 1.5	Ad	–	–	–	–	–	–	–	*X*[i]
H. naledi	U.W. 101-283	Rising Star/ Dinaledi Ch.	SI	0.335-0.236[aa]	Ad	–	X	–	–	–	–	*X*[ab]	–
H. naledi	U.W. 101-466	Rising Star/ Dinaledi Ch.	SI	0.335-0.236[aa]	Ad	–	X	–	–	–	–	–	–
H. naledi	U.W. 101-948	Rising Star/ Dinaledi Ch.	SI	0.335-0.236 [aa]	Sub	–	X	–	–	–	–	*X*[ab]	–
H. naledi	U.W. 101-1301	Rising Star/ Dinaledi Ch.	–	0.335-0.236 [aa]	?		–	–	–	*X*[ab]	–	–	–
H. naledi	U.W. 102a-257	Rising Star/ Lesedi Ch.	–	?	Ad		–	–	–	–	–	*X*[ac]	–
Indet.	OH 89	Olduvai/ Upper Bed I	–	*c.* 1.8[i]	Ad		–	–	–	–	–	–	*X*[i]

Appendix 6. — Comparison of the morphology of OMO VE 3-10063 with that of selected hominins and *Pan troglodytes*. Abbreviations: **AP**, anteroposterior; **NA**, not available; **SI**, superoinferior. Notes: **a**, as represented by D4161, D4162, KNM-WT 15000 C and D (clavicle); D4166, KNM-WT 15000 E (scapula); KNM-WT 15000 F, D2715, D2680, D4507 (proximal humerus); KNM-WT 15000 F, D2715, D2680, D4507, IB 7594 (distal humerus); KNM-WT 15000 R (spinous process of the vertebra); KNM-WT 15000 CB, AP, AU, AO, BD-BE-BJ, AK, AL, AM, AS (rib); **b**, as represented by OH 48 (clavicle); KNM-ER 3735 (distal humerus); **c**, as represented by KNM-ER 47000 (scapula); KNM-ER 739, KNM-ER 1504, KNM-ER 6020, KNM-ER 45510, TM 1517, SK 24600 (distal humerus); **d**, as represented by U.W. 88-1, U.W. 88-38, A.L. 333x6/9, KSD-VP 1/1, StW 431, StW 573 (clavicle), KSD-VP 1/1 only for the relative sternal curvature; U.W. 88-56, A.L. 288-1, KSD-VP 1/1, StW 431, Sts 7, StW 573 (scapula); Sts7, U.W. 88-101, U.W. 88-57, A.L. 288-1r, A.L. 288-1m, A.L. 333-87, A.L. 333-107 (proximal humerus); A.L. 288-1, A.L. 137-48a, A.L. 322-1, A.L. 333-29 (distal humerus); U.W. 88-09 (spinous process of the vertebra); A.L. 333-106, KSD-VP 1/1 (vertebral body); A.L. 288-1, KSD-VP 1/1, U.W. 88-45, 46, 47, 48, 59, 60, 61 (rib); **e**, KNM-WT 15000 only; **f**, StW 573 only; **g**, in lateral view; **h**, the character coding was based on the information and images published in Green *et al.* 2018, as we did not have access to scans of KNM-ER 47000; **i**, concern A. sediba only because of a poorly preserved fossil record for other *Australopithecus* species; **j**, defined as the length of the radius of sternal curvature relative to the radius of acromial curvature (cf. Methods); **k**, transverse width relative to the SI height; **l**, SI height relative to transverse breadth.

Bones	Characters	*H. sapiens*	OMO VE 3-10063	*H. erectus*[a]	*H. habilis*[b]	*Paranthropus*[c]	*Australopithecus*[d]	*P. troglodytes*
Humerus	Bicipital groove	Shallow	Shallow	Shallow	NA	NA	Shallow to deep	Deep
	Lateral supracondylar ridge	Faint	Faint	Faint to prominent	Prominent	Prominent	Prominent	Prominent
	Shape of the distal cross-section	Rounded	Rounded	Rounded to elliptical	Elliptical	Elliptical	Elliptical	Elliptical
	Distal trochlear angle	Intermediate to high	High	High	NA	Low to intermediate	Intermediate to high	Low to intermediate
	Humeral torsion	High	Low	Low	NA	Low	Low to intermediate	High
Scapula	Ventral bar	Weak	Weak	Weak to strong	NA	Weak	Strong	Weak
	Development of the glenoid notch	Weak to strong	Strong	Weak to strong	NA	Weak	Weak	Weak
	Spine origin in lateral view	Intermediate to high	High	High	NA	Intermediate	Intermediate to high	Low to intermediate
	Pillar-glenoid angle	High	Intermediate	High	NA	NA	Low	Low
	Scapular neck breadth	Broad	Broad	Broad	NA	Narrow	Narrow to broad	Narrow
	Coracoid process end shape	Rounded	Rounded	Rounded[e]	NA	NA	Rounded[f]	Rounded
	Glenoid outline[g]	Oval	Oval	Intermediate	NA	Oval[h]	Intermediate to oval	Rounded
	Glenoid ventral border[g]	Concave	Concave	Convex to concave	NA	Concave[h]	Convex to intermediate	Convex
Clavicle	Conoid tubercle	Weak	Weak	Weak	Weak	NA	Strong[i]	Strong
	Groove of the subclavius	Present	Present	Present	Absent	NA	Variable	Absent
	Orientation of the clavicle in the transverse plane	Horizontally-set	Horizontally-set	Horizontally-set	NA	NA	Obliquely-set	Obliquely-set
	Relative sternal curvature [j]	Intermediate	Intermediate	Intermediate	Intermediate	NA	Intermediate	Intermediate to long
	Relative centrum height[l]	Low	Low	Low	NA	NA	Low to high	High
	Relative centrum height[l]	Low	Low	Low	NA	NA	Low to high	High
	Slope of the uncinate process	Oblique	Oblique	Oblique	NA	NA	Oblique to vertical	Vertical
Rib (5th-9th)	Shape of the cross-section	Flat	Oval	Oval	NA	NA	Oval	Round

Appendix 7. — Anatomical comparison of OMO VE 3-10063 with extant and fossil hominoid taxa. Images were taken from three-dimensional surface scans, except for KNM-ER 47000 (modified from Green *et al.* (2018): **A**, anterior view of the humerus. The specimens are oriented such that the axis passing through the condyles is aligned horizontally. Oblique **black arrows** show the bicipital groove; **B**, scapula in ventral view. **White arrows** point to the ventral bar; **C**, scapula in lateral view. The specimens are oriented such that the glenoid is facing the viewing plane. White arrows show the glenoid notch and white dashed lines show the position of the origin of the scapular spine; **D**, coracoid process of the scapula. Specimens are oriented such that the coracoid processes are horizontally-aligned. The low band shows the largest breadth of the distal end of the process and the blue band shows the narrowest breadth; **E**, clavicle in dorsal view. The specimens are oriented such that the acromial end is in the transverse plane showing the orientation of the clavicular shaft. White arrows highlight the conoid tubercle (the tubercle is eroded on KSD-VP 1/1); **F**, vertebra in dorsal view. **Dashed lines** show the transverse expansion of the terminus of the spinous process; **G**, vertebra in ventral view. **White dashed lines** show the relative craniocaudal expansion of the vertebral body. **Yellow dashed lines** highlight the slope of the uncinate process.

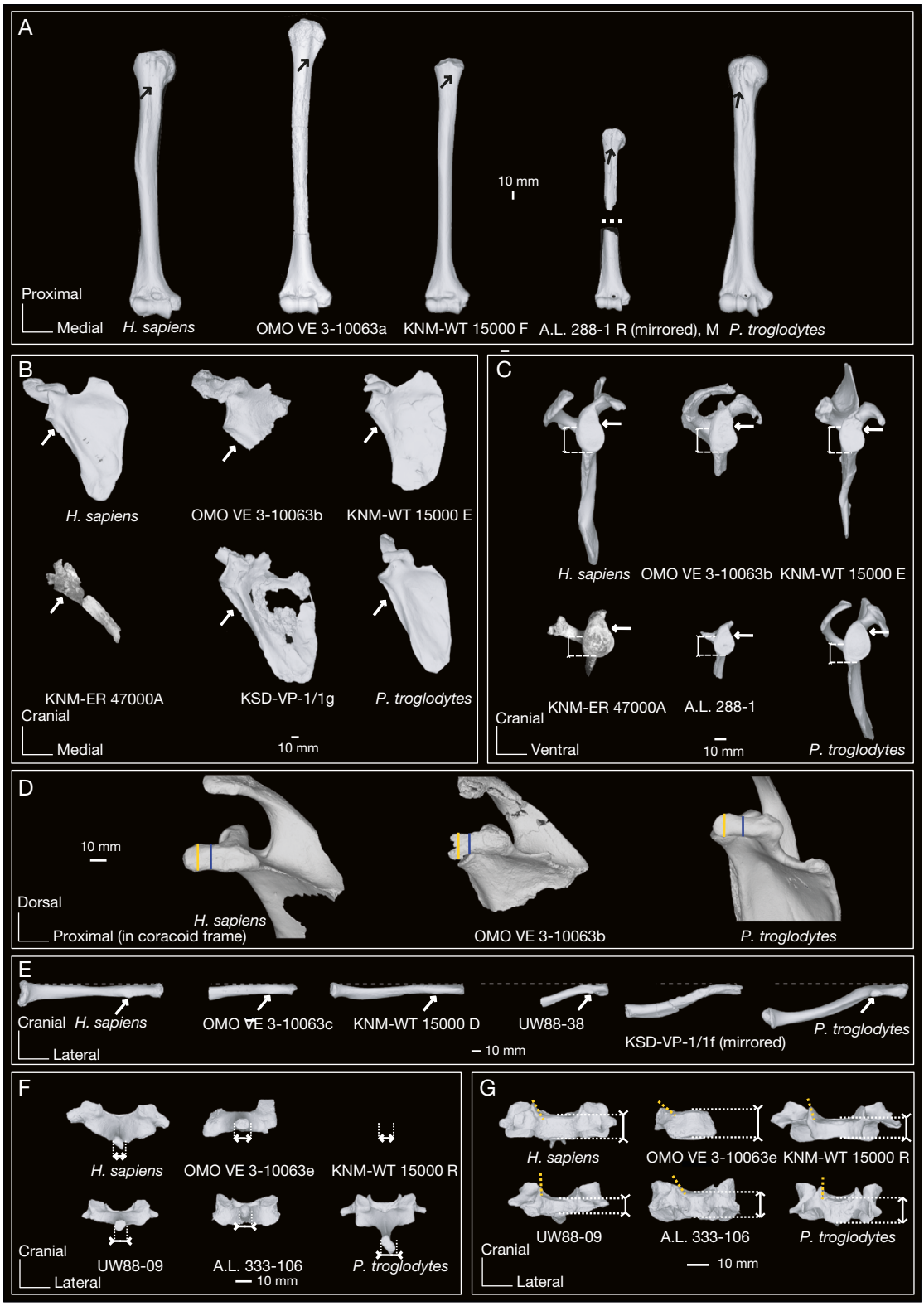

Appendix 8. — **A**, General morphology of the anterior edge of the coracoid process of extant hominoids with *Homo sapiens* (n = 29), *Gorilla* sp. (n = 38), *Pongo pygmaeus* (n = 24), *Pan troglodytes* (n = 30), and *Pan paniscus* (n = 19). Values are from Voisin (2000); **B**, absolute length of the coracoid process in extant hominoids and OMO VE 3-10063. The coracoid process of OMO VE 3-10063 lacks its most terminal part. Thus, two values are given for OMO VE 3-10063: the lowest measurement represents the preserved length, and the highest measurement is the preserved length plus 5 mm to estimate the length of the complete process; **C**, relative length of the coracoid process in extant hominoids and OMO VE 3-10063, calculated as [(length of the process/height of the glenoid cavity)x100]. The two values for OMO VE 3-10063 are the indices calculated with the raw length and with the corrected value.

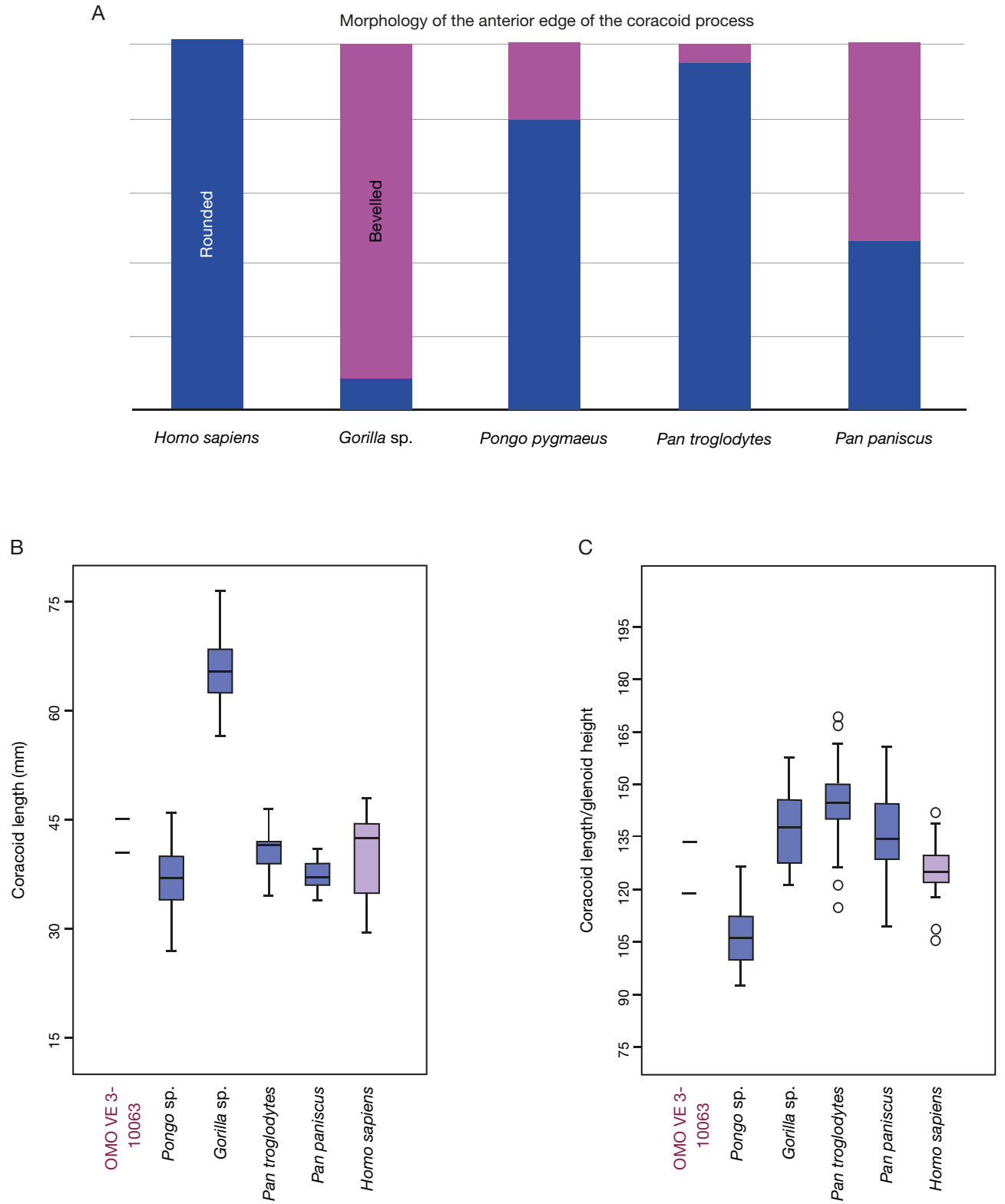

Appendix 9. — Frequency of the presence of the subclavian sulcus (in %) on the clavicle of extant hominoids with *Homo sapiens* (n = 31), *Gorilla* sp. (n = 33), *Pongo pygmaeus* (n = 23), *Pan troglodytes* (n = 24), and *Pan paniscus* (n = 19). Values are from Feuerriegel *et al.* (2019).

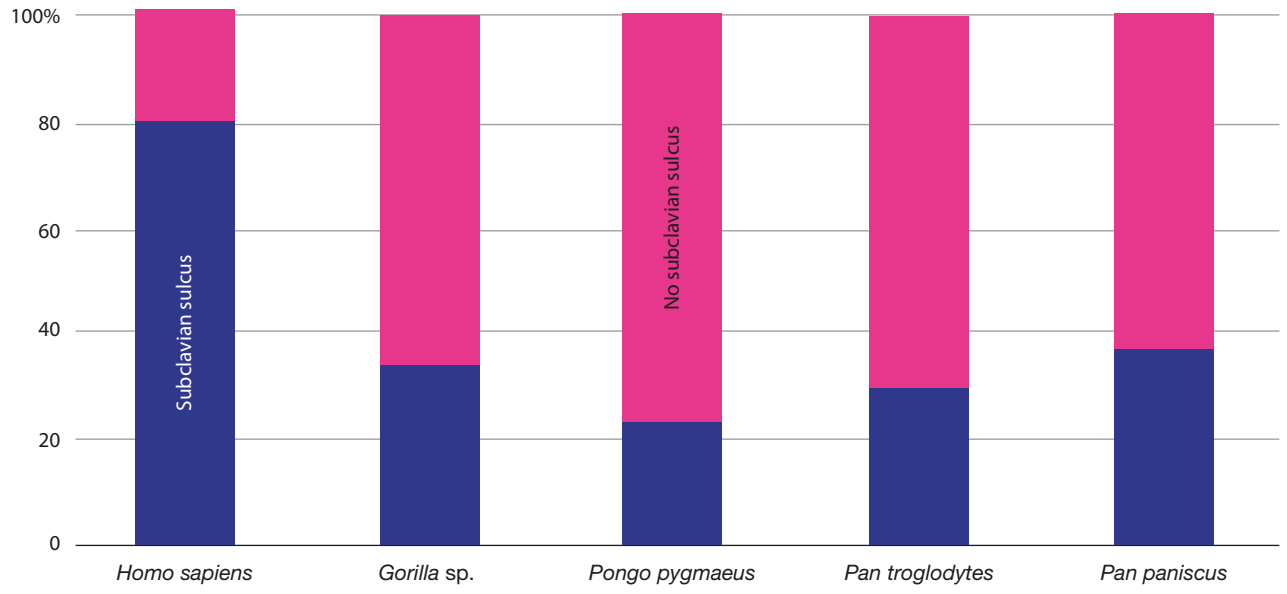

Appendix 10. — Ordinary least squares regression on clavicle midshaft size using four subsamples from Taylor *et al.* (2024). The clavicle midshaft size is defined differently than in Taylor *et al.* (2024), here as [√ anteroposterior width x superoinferior height] according to data availability (see Methods). The oblique black line is the regression equation: clavicle maximum length = b + a x clavicle midshaft size: **A**, the regression is performed on the complete sample, i.e., with male and female *Gorilla gorilla*, male and female *Homo sapiens*, and male and female *Pan troglodytes*. Note that the coefficient of determination (R2) is lower in this case than in Taylor *et al.* (2024) with the same sample; **B**, the regression is performed on a subsample that excludes male *Gorilla gorilla*; **C**, the regression is performed on a subsample that excludes male and female *Gorilla gorilla*; **D**, the regression is performed on a subsample that excludes male and female *Gorilla gorilla* and *Pan troglodytes*. Data are from Taylor *et al.* 2024.

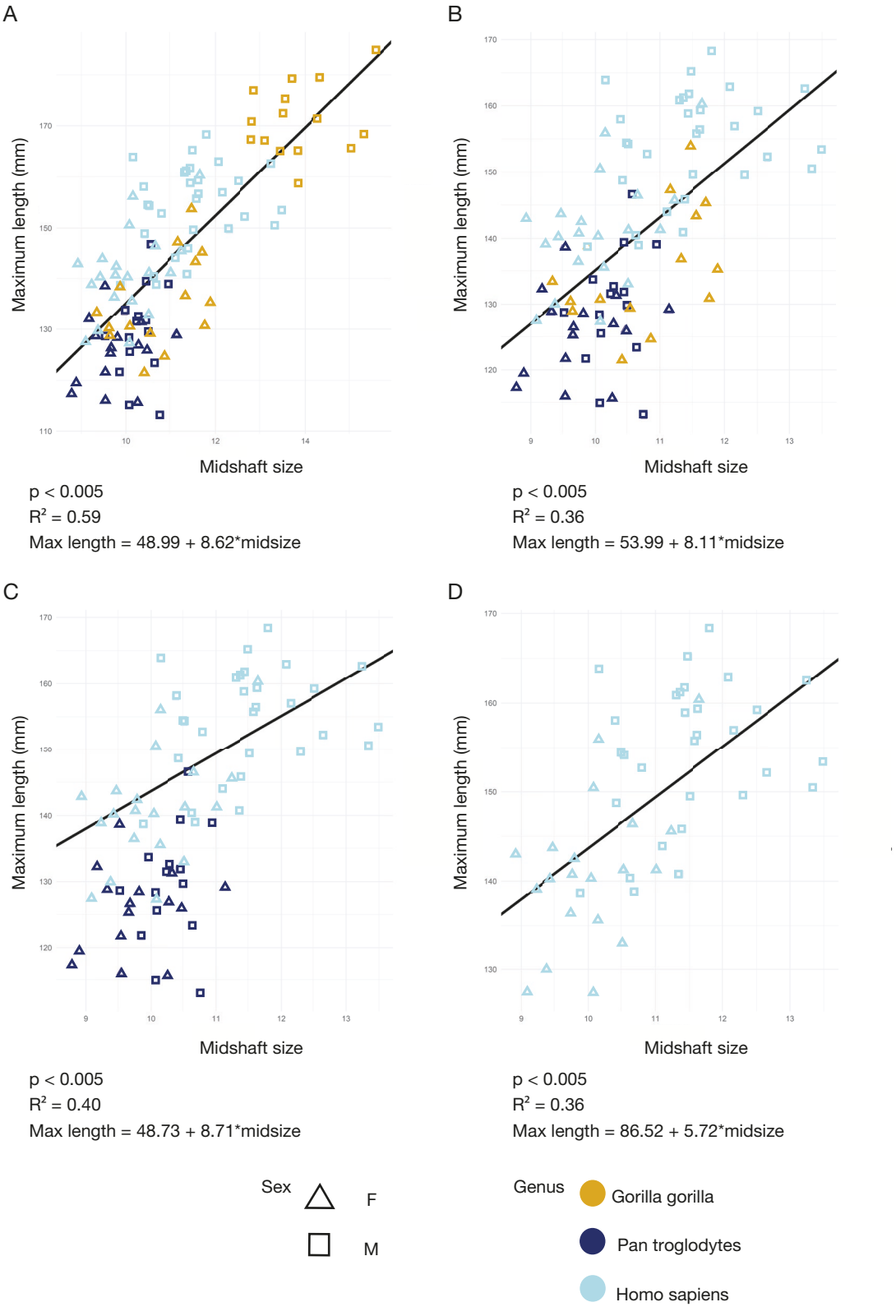

APPENDIX 11. — Distance matrix of the complete comparative sample.

Name	OMO VE 3-10063	*H. erectus*	*H. habilis*	*Paranthropus*	*Australopithecus*	*H. sapiens*	*P. troglodytes*
OMO VE 3-10063	0	3.055806	8.625595	6.193205	6.49391	3.050953	9.065907
H. erectus	3.055806	0	8.020089	6.013162	5.311078	3.842658	8.120722
H. habilis	8.625595	8.020089	0	3.81208	5.758654	8.591467	5.090213
Paranthropus	6.193205	6.013162	3.81208	0	5.033505	6.574307	6.997651
Australopithecus	6.49391	5.311078	5.758654	5.033505	0	6.687073	5.486457
H. sapiens	3.050953	3.842658	8.591467	6.574307	6.687073	0	8.779254
P. troglodytes	9.065907	8.120722	5.090213	6.997651	5.486457	8.779254	0

APPENDIX 12. — Hierarchical clustering of postcranial morphology on a reduced comparative sample: **A**, heat map of the 21 postcranial characters used in the cluster analysis (columns; see Appendix 6) for OMO VE 3-10063 and the comparative taxa without *Homo habilis* and *Paranthropus* to avoid taxa with missing values (**rows**). Different colors indicate discrete character states. The dendrogram to the right shows Ward's hierarchical clustering based on Euclidean distances of log-transformed, z-standardized characters; **B**, constellation plot of the same clustering. Points are colored by genus (**red**, *Homo*; **orange**, *Australopithecus*; **green**, **Pan**), and the connecting lines reproduce the hierarchical relationships from panel A. OMO VE 3-10063 (**circled**) falls within the *Homo* cluster; **C**, clustering history showing distance between clusters.

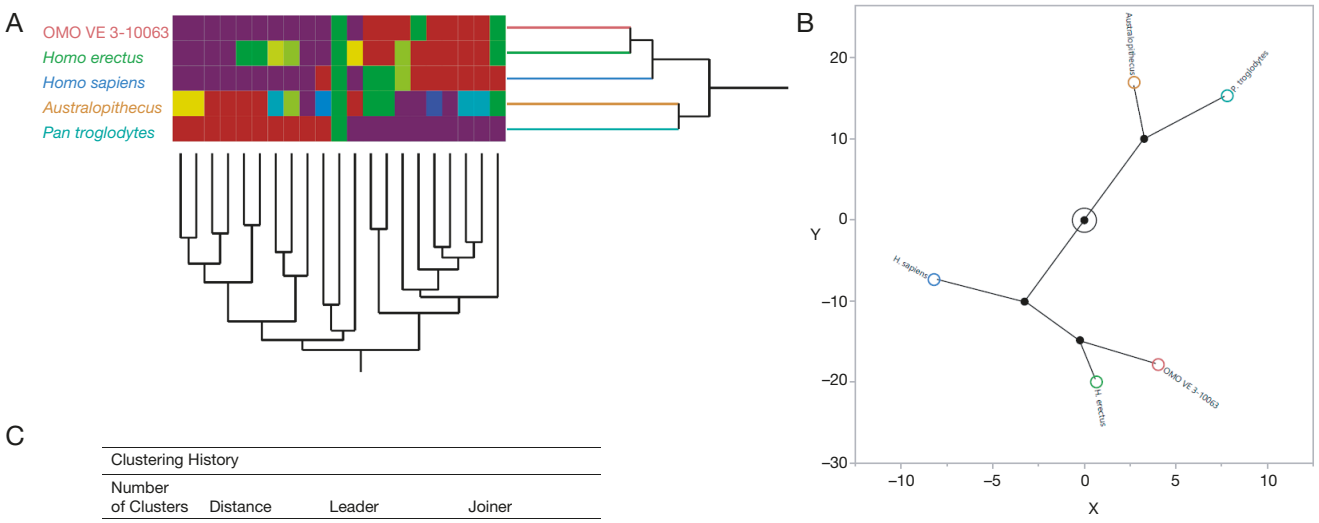

C

Clustering History			
Number of Clusters	Distance	Leader	Joiner
4	2.065879266	OMO VE 3-10063	*Homo erectus*
3	2.486870284	OMO VE 3-10063	*Homo sapiens*
2	3.832897436	*Australopithecus*	*Pan troglodytes*
1	7.406518500	OMO VE 3-10063	*Australopithecus*

APPENDIX 13. — Distance matrix of the reduced comparative sample.

Name	OMO VE 3-10063	*H. erectus*	*Australopithecus*	*H. sapiens*	*P. troglodytes*
OMO VE 3-10063	0	2.921594	6.359233	3.093773	9.11937
H. erectus	2.921594	0	5.289193	3.640055	8.279841
Australopithecus	6.359233	5.289193	0	6.459533	5.420536
H. sapiens	3.093773	3.640055	6.459533	0	8.797784
P. troglodytes	9.11937	8.279841	5.420536	8.797784	0